DISSERTATION

PROTOPORPHYRINOGEN OXIDASE: ORIGINS, FUNCTIONS, AND IMPORTANCE AS AN HERBICIDE TARGET SITE

Submitted by

Abigail Barker

Department of Agricultural Biology

In partial fulfillment of the requirements

For the Degree of Doctor of Philosophy

Colorado State University

Fort Collins, Colorado

Fall 2021

Doctoral Committee:

Advisor: Franck Dayan

Christopher Snow
Marinus Pilon
Todd Gaines

ABSTRACT

PROTOPORPHYRINOGEN OXIDASE: ORIGINS, FUNCTIONS, AND IMPORTANCE AS AN HERBICIDE TARGET SITE

Protoporphyrinogen IX oxidase (PPO)-inhibiting herbicides are effective tools to control a broad spectrum of weeds, including those that have evolved resistance to glyphosate. Their utility is being threatened by the appearance of biotypes that are resistant to PPO inhibitors. While the chloroplastic PPO1 isoform is thought to be the primary target of PPO herbicides, evolved resistance mechanisms elucidated to date are associated with changes to the mitochondrial PPO2 isoform, suggesting that the importance of PPO2 has been underestimated. Our investigation of the evolutionary and structural biology of plant PPOs provides some insight into the potential reasons why PPO2 is the preferred target for evolution of resistance. The most common target-site mutation imparting resistance involved the deletion of a key glycine codon. The genetic environment that facilitates this deletion is apparently only present in the gene encoding PPO2 in a few species. Additionally, both species with this mutation (*Amaranthus tuberculatus* and *Amaranthus palmeri*) have dual targeting of PPO2 to both the chloroplast and the mitochondria, which might be a prerequisite to impart herbicide resistance. The most recent target-site mutations have substituted a key arginine residue involved in stabilizing the substrate in the catalytic domain of PPO2. This arginine is highly conserved across all plant PPOs, suggesting that its substitution could be equally likely on PPO1 and PPO2, yet it has only occurred on PPO2, underscoring the importance of this isoform for the evolution of herbicide resistance.

As glyphosate resistance becomes widespread, weed control turns to older mechanisms of action with less resistance. Protoporphyrinogen oxidase (PPO) inhibitors are a versatile class of herbicides that have been used since the 1960's, with active ingredients that work in pre-emergent and post-emergent applications. Differential efficacy of PPO inhibitors applied pre-emergent, early post-emergent and late post-emergent has been observed in multiple species and settings. Understanding the cause of higher efficacy in younger plants could preserve these important weed control tools. To understand the differing efficacies elements that affect the mechanism of action of PPO inhibitors were analyzed over the course of plant growth including target site transcript levels and protein levels, herbicide uptake, antioxidant capacity, and indicators of flux through the pathway. Data show levels of PPO do not explain differential efficacy. Increases of glutamate, the pathway precursor, do increase damage due to PPO inhibitor treatment, but increased levels are not observed in younger plants. Differential efficacy is likely due to a combination of increase in antioxidant capacity and a decrease in herbicide uptake. Other possible factors such as metabolism will need to be measured in future work.

Protoporphyrinogen oxidase (PPO) is a critical enzyme across life as the last common step in the synthesis of many metalloporphyrins. The reaction mechanism of PPO was assessed *in silico* and the unstructured loop near the binding pocket was investigated. The substrate, intermediates, and product were docked in the catalytic domain of PPO using a modified Autodock method, introducing flexibility in the macrocycles. Sixteen PPO protein sequences across phyla were aligned and analyzed with Phyre2 and ProteinPredict to study the unstructured loop from residue 204–210 in the *H. sapiens* structure. Docking of the substrate, intermediates, and product all resulted in negative binding energies, though the substrate had a lower energy than the others by 40%. The α-H of C10 was found to be 1.4 angstroms closer to FAD than the

β-H, explaining previous reports of the reaction occurring on the *meso* face of the substrate. A lack of homology in sequence or length in the unstructured loop indicates a lack of function for the protein reaction. This docking study supports a reaction mechanism proposed previously whereby all hydride abstractions occur on the C10 of the tetrapyrrole followed by tautomeric rearrangement to prepare the intermediate for the next reaction.

Weed control is essential in modern agriculture, though it becomes more difficult with increasing resistance levels to current herbicides and a slow process to register a new mechanisms of action because of safety concerns and current methods. Agrematch provides a new method to identify possible herbicide candidates using an artificial intelligence algorithm that takes into effect biological parameters with the goal of reducing R&D time on new herbicides. Herein we describe the discovery of 4-chloro-2-pentenamides as novel inhibitors of protoporphyrinogen oxidase, a known herbicide target site, by the Agrematch AI. The herbicidal activity is confirmed in greenhouse assays, with the highest performing AGR001 showing good activity pre-emergent at 150 g/ha and post emergent as low as 50 g/ha on the troublesome weed palmer amaranth (*Amaranthus palmeri*). A lack of activity is shown on PPO resistant palmer amaranth carrying the ΔG210 deletion mutation. The mechanism of action is confirmed by the herbicide dependent accumulation of protoporphyrin IX, subsequent light dependent loss of membrane integrity, and direct inhibition of protoporphyrinogen oxidase in an *in vitro* assay. Modeling of the docking of these inhibitors in the active site of protoporphyrinogen oxidase confirms the target.

ACKNOWLEDGEMENTS

First I have to thank my wonderful friends, family and partner who were endlessly supportive through the roller coaster that is graduate school. Though many changes I always had someone to talk to, lean on, or remind me to eat occasionally.

Secondly I must thank my advisor, Dr. Franck Dayan, who took me on as his first student and gave me the opportunities to develop skills that most graduate students would not have the chance to, such as fixing an LCMS and managing a lab. I admire those things he does that are above and beyond many advisors—creating an environment where students feel safe and prioritizing well-being.

I must thirdly thank my committee member Dr Todd Gaines first of all for the introduction to weed science as an undergraduate researcher and secondly for his advice and assistance during my graduate career.

Next, my thanks to Dr. Marinus Pilon and Dr. Christopher Snow for serving on my committee and dispensing useful advice on my degree, it would not have been possible without your involvement.

Finally, all the sources that funded my graduate career including: Valent USA and Sumitomo, The Foundation for Food and agricultural research, Western Sugar Co-op, Cotton Inc. Agrematch Ltd and the USDA National Institute of Food and Agriculture.

TABLE OF CONTENTS

LIST OF TABLES

LIST OF FIGURES

CHAPTER 1: ORIGINS AND STRUCTURE OF CHLOROPLASTIC AND MITOCHONDRIAL PLANT PROTOPORPHYRINOGEN OXIDASES: IMPLICATIONS FOR EVOLUTION OF HERBICIDE RESISTANCE [1]

INTRODUCTION

Importance of the porphyrin pathway

Porphyrins are ring-shaped molecules consisting of the circular assembly of 4 pyrrole units. These molecules are ubiquitous in the entire tree of life, their origins being traced back to very early organisms. Their universality is rooted in the critical roles they play in many foundational biochemical processes necessary to sustain life [1]. A key feature of porphyrins is their ability to chelate metal dications (e.g, Mg2+, Fe2+, Ni2+, and Co2+). Metalloporphyrins are designed to catalyze highly specific reactions requiring electron transport such as chlorophylls in photosynthesis, heme in aerobic and coenzyme F430 in anaerobic respiration, vitamin B12, and a host of other functions. Porphyrins are often referred to as the "colors of life" because they have highly conjugated chromophores that interact with light to produce with a range of colorful pigments (e.g., green, red, and oranges) [2]. The pathways leading to porphyrin synthesis are highly regulated because any disruption has remarkably negative consequences on organisms [3]. In plants, disruption of porphyrin metabolism is lethal [4, 5] and that characteristic has led to the development of herbicides that target porphyrin synthesis in plants [6, 7].

The primary target of herbicides that interfere with porphyrin synthesis is protoporphyrinogen oxidase (PPO). This enzyme catalyzes the sequential FAD-driven oxidation

[1] This chapter contains published work from: Dayan, F. E.; Barker, A.; Tranel, P. J. Origins and structure of chloroplastic and mitochondrial plant protoporphyrinogen oxidases: implications for the evolution of herbicide resistance. Pest Management Science 2018, 74, 2226-2234. DOI: 10.1002/ps.4744.

of protoporphyrinogen IX (protogen) to form protoporphyrin IX (proto) [2]. In plants, this enzyme is involved in the synthesis of both chlorophylls and hemes. Two nuclear encoded genes (*PPX1* and *PPX2*) produce isoforms of this enzyme, PPO1 compartmentalized in the chloroplast and PPO2 compartmentalized in the mitochondria (Fig. 1.1). This latter one is sometimes dual-targeted to both the mitochondria and the chloroplast [8], which may be important in the evolution of resistance to PPO-inhibiting herbicides.

Discovery and development of PPO herbicides

A number of groups developed novel chemistry independently from each other that ultimately were commercialized as herbicides many years before it was known that they shared a common target site. For example, nitrofen was first synthesized at Iowa State University in 1930 [9] and introduced as a herbicide by Rohm and Haas in 1963 [10], oxadiazon was introduced in 1968 by Rhône-Poulenc [11], and chlorophthalim was introduced in 1972 by Mitsubishi [12]. These herbicides belong to structurally distinct chemical groups (diphenyl ethers, oxadiazoles and phenyl imides, respectively), and no one would have predicted that these diverse chemistries would all target PPO. By now, more than 100,000 PPO inhibitors have been synthesized and protected by more than 5000 patents.

While PPO-inhibiting herbicides have been commercialized for a long time, their mechanism of action (MOA) eluded scientist for many years. Early studies rapidly recognized that the MOA of these compounds was light-dependent but its link to porphyrin synthesis was reported in the late 1980s [13-15]. With the understanding that proto accumulated in plants treated with these herbicides, a significant effort ensued to identify the target site downstream from the step resulting in proto synthesis. A French group was the first to report the unusual aspect of the mechanism of action of PPO inhibitors, in that proto, the catalytic product of PPO, the enzyme

being inhibited, accumulates [16, 17]. Proto is a highly photodynamic pigment that induces membrane peroxidation in the presence of light and molecular oxygen [13, 18].

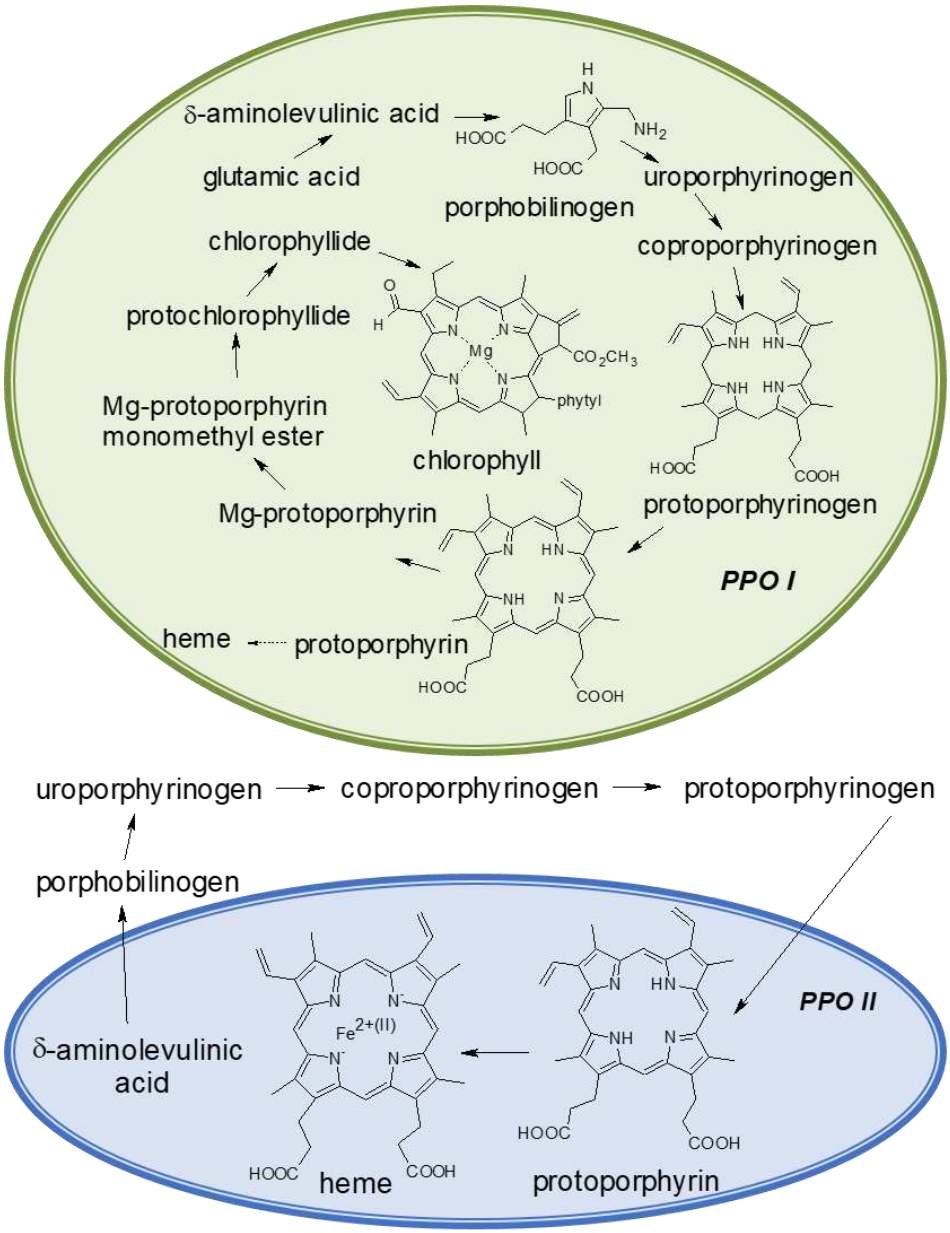

Figure 1.1 Tetrapyrrole pathways in higher plants. Chlorophyll biosynthesis occurs exclusively in chloroplasts (green) whereas heme synthesis occurs in both the mitochondria (blue) and chloroplasts. The first committed step is the formation of the pyrrole-containing porphobilinogen. Bold italics denote the target site of commercial herbicides [protoporphyrinogen oxidase 1 (PPO1) and protoporphyrinogen oxidase 2 (PPO2)]. This is the last step in common between chlorophyll and heme synthesis.

Use of PPO herbicides

As mentioned above, PPO-inhibiting herbicides have been commercialized for more than 50 years. At the peak of their use, they represented more than 10% of the global herbicide market [7] and were a key component of weed management in soybean fields. Consequently, these herbicides are applied primarily in the Midwest and southern regions of the USA (Fig. 1.2A). The use of PPO herbicides remained steady for many years but suffered a dramatic decline after the introduction of transgenic glyphosate-resistant soybean in 1996 (Fig. 1.2B), and these herbicides accounted for only 1.3% of the total herbicide output in the United States in 2006 [19]. However, interest in PPO-inhibiting herbicides has surged in recent years (2013) (Fig. 1.2B), as they have proved to be excellent tools to control problematic weeds that have evolved resistance to glyphosate. However, this renewed interest has faced some setback associated with a few species that have evolved resistance to PPO-inhibiting herbicides (see below).

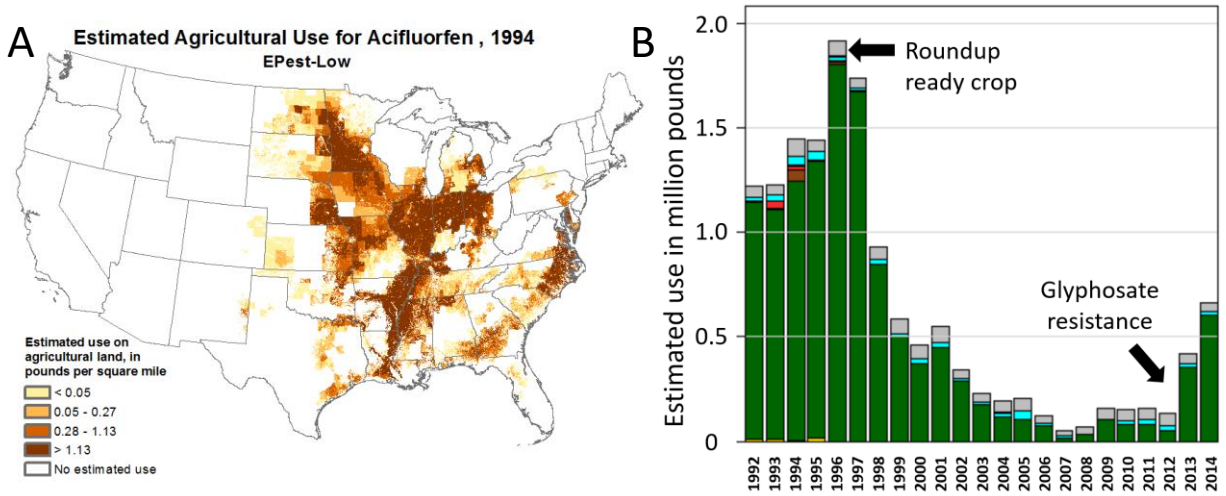

Figure 1.2 (A) Geographical distribution of use of the PPO-inhibiting diphenyl ether herbicide acifluorfen in the lower 48 US states in 1994 highlighting the concentrated use of the herbicide in the midwestern and the southern regions. (B) Amount of acifluorfen used in the USA from 1992 to 2014.19 The profile is similar to that of other PPO

Table 1.1 Weeds with evolved resistance to PPO inhibitors

Species[a]	Common name	Country	First year	Mechanism
Amaranthus tuberculatus (Moq.) J.D. Sauer	Tall waterhemp	United States	2001	PPO2 Gly210 deletion [23]
Euphorbia heterophylla L.	Wild poinsettia	Brazil	2004	ND
Amaranthus hybridus L.	Smooth pigweed	Bolivia	2005	ND
Ambrosia artemisiifolia L.	Common ragweed	United States	2005	PPO2 Arg98 substitution[31]
Acalypha australis L.	Asian copperleaf	China	2011	ND[b]
Amaranthus palmeri S. Watson	Palmer amaranth	United States	2011	PPO2 Gly210 deletion [30]; PPO2 Arg98 substitution [32]
Descurainia sophia (L.) Webb ex Prantl	Flixweed	China	2011	ND
Amaranthus retroflexus L.	Redroot pigweed	Brazil	2014	ND
Senecio vernalis Waldst. & Kit.	Eastern groundsel	Israel	2014	ND
Avena fatua L.	Wild oat	Canada	2015	ND
Eleusine indica (L.) Gaertn.	Goosegrass	USA	2015	ND

[a]data from www.weedscience.org (accessed April 2017)

[b]ND=not determined

Current state of resistance to PPO inhibitors

To date, 11 weed species have been reported resistant to PPO inhibitors (Table 1.1). The list of PPO-inhibitor-resistant weeds includes four Amaranthus species and two grass species. The list is short, relative to many other herbicide groups, despite the long and widespread use of PPO inhibitors.

Resistance to PPO inhibitors is best characterized in *Amaranthus tuberculatus*, the first weed to evolve such resistance [20]. The first PPO-inhibitor-resistant *A. tuberculatus* population was observed in a Kansas, USA field with a long history of continuous soybean production and repeated selection by acifluorfen. Additional reports of PPO-inhibitor resistance in *A. tuberculatus* followed from throughout the Midwest USA [21, 22]. Resistance to PPO inhibitors is now common and widespread in *A. tuberculatus*; in Illinois, USA, for example, *A. tuberculatus* populations resistant to PPO inhibitors have been confirmed from most counties (Fig. 1.3A).

Described in more detail in following sections, a deletion of an amino acid (termed ΔG210) in the PPO2 enzyme conferred resistance to PPO inhibitors in *A. tuberculatus* [23]. Subsequent surveys demonstrated that the ΔG210 mutation was ubiquitous among PPO-inhibitor-resistant *A. tuberculatus* populations [24-26]. The ΔG210 mutation confers broad cross resistance to most PPO inhibitors [20, 21, 27]. The highest resistance magnitude was reported to lactofen, with resistance:sensitive (R/S) ratios ranging from about 20 to 80, whereas resistances to most other PPO inhibitors were more modest and generally under 10-fold. The stage of growth at the time of application has a pronounced effect on the level of resistance [28]. With a typical herbicide application timing—to plants 10- to 15-cm in height—resistant biotypes exhibit injury symptoms typical of PPO inhibitors shortly after application, but this initial injury is followed

within a couple days by healthy new growth from the meristem (Fig. 1.3B). If the herbicide is applied when plants are very small (e.g., 5-cm in height), resistant biotypes are not always able to recover.

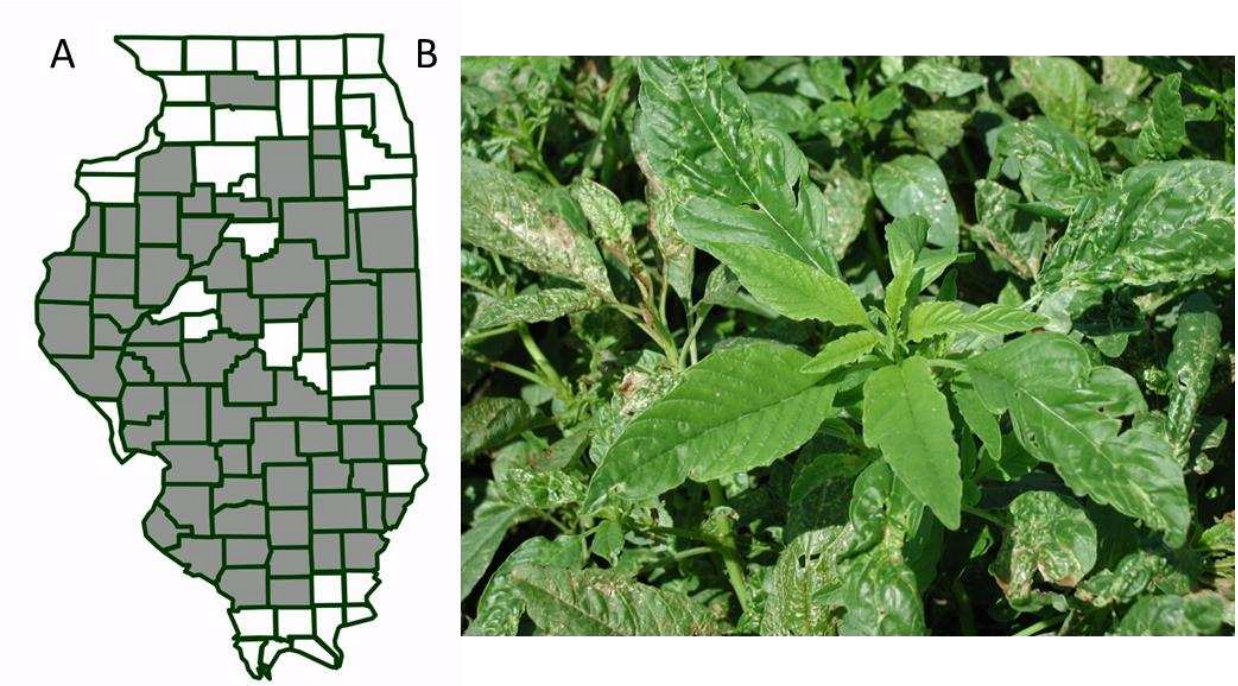

Figure 1.3 Resistance to PPO inhibitors in *Amaranthus tuberculatus* is a common and widespread problem in the midwestern USA. (A) Resistant populations have been confirmed in most counties in Illinois (shaded in gray) (Tranel PJ et al., unpublished). (B) Typical phenotypic response of *A. tuberculatus* resistant to PPO-inhibiting herbicides. Older tissues exhibit typical bronzing and burning associated with the light-dependent damage resulting from proto accumulation. However, newer tissues emerging from the meristematic region are not injured.

The efficacy of PPO inhibitors is age and size dependent, consequently, younger seedlings of PPO-inhibitor-resistant A. tuberculatus are still controlled by pre-emergence (PRE) applications of these herbicides.27, 28 Nevertheless, it is incorrect to state that resistance to PPO-inhibitors in *A. tuberculatus* only applies to postemergence (POST) and not to PRE applications. Wuerffel et al. [29] demonstrated that the length of residual control of resistant individuals will be shorter, since they are able to tolerate higher concentrations of PPO inhibitors in the soil during germination/emergence.

Much less is known about resistance to PPO inhibitors in weed species other than *A. tuberculatus*, both in regards to mechanisms of resistance and distribution/impact of resistant populations. However, resistance mechanisms have been reported for two other PPO-inhibitor-resistant weed species, *Ambrosia artemisiifolia* and *Amaranthus palmeri* [30-32]. These mechanisms, which also involve target-site changes, are described below. Additionally, some mechanistic work has been reported for *Euphorbia heterophylla*, the second weed species identified with resistance to PPO inhibitors (Table 1). As is the case with *A. tuberculatus*, PPO-inhibitor resistance in *E. heterophylla* exhibits broad cross resistance and is conferred by a single, (partially) dominant, nuclear gene [33, 34]. Trezzi et al. [35] suggested resistance could be due to differential leaf absorption, but this has yet to be confirmed.

There are at least a couple cases in which resistance to PPO inhibitors likely occurred as a result of selection by herbicides with different target sites. A population of *Avena fatua* recently was reported resistant to the PPO inhibitor sulfentrazone applied PRE, despite not having been previously exposed to this herbicide [36]. The authors suggested sulfentrazone resistance could be conferred by increased endogenous gibberellin content (allowing for more rapid germination and emergence), or enhanced cytochrome P450 activity, both of which were selected by exposure to other herbicides (triallate and ALS/ACCase inhibitors, respectively). A second example involves an *A. tuberculatus* population initially identified as being resistant to HPPD-inhibiting herbicides [37]. This population was shown to be resistant to saflufenacil, but not to lactofen. It was hypothesized that enhanced oxidative metabolism, which conferred resistance to HPPD inhibitors, was also responsible for the saflufenacil resistance. To date, this is the only confirmed case of *A. tuberculatus* with resistance to PPO inhibitors not due to the ΔG210 mutation.

In terms of economic impact, PPO-inhibitor resistance in *A. palmeri*, although only recently reported [30], is likely to rapidly become significant. As was the case with *A. tuberculatus*, PPO inhibitors became heavily depended upon to control glyphosate-resistant biotypes. Widespread resistance to PPO inhibitors, along with widespread resistance to glyphosate and ALS inhibitors, leaves few options for POST control of these two Amaranthus species, particularly in soybean and cotton.

Target site resistance to PPO inhibitors

In their 1997 review of PPO inhibitors, Dayan and Duke [6] specified numerous potential resistance mechanisms for these herbicides. In addition to typical resistance mechanisms (target site changes, reduced uptake/translocation, and enhanced metabolism), they speculated upon other mechanisms that could arise due to the unique mode of action of these herbicides. It is also noteworthy that natural tolerance to PPO inhibitors in crops (as well as in some weed species) often is due to enhanced herbicide metabolism (reviewed in Dayan et al. [38]), indicating that enzymes for metabolism of these herbicides exist. Nevertheless, based on what we know thus far, target-site changes seem to offer the best evolutionary pathway for resistance to PPO inhibitors.

Before target-site resistance to PPO-inhibitors was observed in weeds, it was used as a basis for developing PPO-inhibitor-resistant crops (reviewed by Li and Nicholl [39]). Interestingly, however, is that efforts with crops focused more on PPO1 than on PPO2, whereas, in weeds, known cases of target-site resistance have all involved PPO2.

As briefly mentioned above, the first identified resistance to PPO inhibitors was the result of an unusual mutation, in which three nucleotides were deleted from the PPX2 gene (which encodes PPO2), resulting in the deletion of glycine at position 210 of the protein [23]. This

glycine caps the α-8 helix of the enzyme; its loss leads to a shortening of the helix and, consequently, to about a 50% increase in the size of the active-site cavity [40]. Although the structural changes to the enzyme decrease its catalytic rate, they make the enzyme 100- to 500-fold less sensitive to diphenyl ether herbicides, explaining, enzymatically, why an unusual deletion mutation was selected. Genetically, selection for the codon deletion can be explained by the nucleotide sequence within and adjacent to the G210 codon [23, 41]. Specifically, this region contained bi-repeats of three-nucleotide sequences, which can be considered as short microsatellites. Due to DNA slippage during replication, the number of repeats within a microsatellite often increases or decreases. Thus, the *A. tuberculatus* PPO2 was predisposed for the G210 deletion due to the specific nucleotide pattern in the corresponding region of the gene. Analysis of several other Amaranthus species found that most were not predisposed to the same mutation; *A. palmeri*, however contained the same microsatellite, leading Riggins and Tranel [42] to predict that this species would evolve resistance to PPO inhibitors via the same ΔG210 mutation. Four years later, therefore, it was not surprising when *A. palmeri* plants resistant to PPO inhibitors were had this mutation [30].

The second evolved target-site mutation for PPO-inhibitor resistance was the more traditional point mutation, found in *A. artemisiifolia* [31]. This mutation, also in PPX2, conferred an arginine-to-leucine substitution at position 98 (R98L) of the PPO2 enzyme. Like the *A. tuberculatus* ΔG210 mutation, the R98L mutation confers broad cross resistance to PPO inhibitors. In general, the magnitudes of resistance are also similar but, whereas *A. tuberculatus* exhibited the greatest resistance to lactofen, *A. artemisiifolia* exhibited the greatest resistance to fomesafen.

After initial identification of the ΔG210 mutation in *A. palmeri*, it was observed that this mutation did not account for all cases of PPO-inhibitor resistance in the species. Sequencing of PPX2 from fomesafen-resistant *A. palmeri* individuals lacking the ΔG210 led to the identification of two new substitutions at the R98 position, glycine (R98G) and methionine (R98M), that likely are sufficient for resistance [32]. Although these latter two mutations have yet to be fully characterized, it is now apparent that a range of substitutions are possible at the R98 position, despite its very high conservation across multiple plant species (described below).

Resistance has been artificially produced in laboratory settings. The tobacco line YZI-1S was concurrently selected for resistance by increasing doses of S231 [42,43] and later characterized as resistant via overexpression of PPO2 [44]. A soybean line stepwise- selected with oxyfluorfen showed resistance through a similar overexpression of PPO2, although a point mutation was not investigated [45]. A transgenic tobacco line overexpressing the *Myxococcus xanthus* PPO, which dually targeted this microbial enzyme to the chloroplast and the mitochondria, also showed resistance to oxyfluorfen [46].

As target-site resistance to PPO herbicides predominantly involve mutations (overexpression, codon deletion of Gly210 or amino acid mutations of Arg98 [23, 33, 44-46]) in PPO2, it is clear that this isoform of PPO contributes significantly to the survival of plants in the presence of herbicides. The importance of PPO2 in conferring evolved resistance might stem from its dual-targeted nature in at least some species. Consequently, the origins, targeting, and structures of plant chloroplastic and mitochondrial PPOs may determine whether evolution of resistance may be more prone in some species relative to others.

ORIGINS OF PROTOPORPHYRINOGEN OXIDASE

Early evolution

As described above tetrapyrroles, including heme and chlorophyll, are important for life across the phyla. These two molecules in particular are responsible for the processes of oxygenation, respiration, and photosynthesis. PPO is the last common step in the pathway leading to both heme and chlorophyll, and most forms of life have at least one PPO gene. There have been three classes of PPO genes identified: HemG, HemJ, and HemY. HemG is found in mostly γ-proteobacteria. HemJ most likely originated in α-proteobacteria and is also found in other proteobacteria and cyanobacteria. HemY is the only class of PPO found in prokaryotes and eukaryotes. Therefore all PPO from eukaryotes are likely derived from similar ancestry. Some organisms do not contain any PPO proteins—those that lack the entire heme synthesis pathway and rely on an external supply and those that use a pathway not involving conversion of uroporphyrinogen III [47]. As with much of the tetrapyrrole pathway, the origin of PPO into eukaryotes is postulated to have coincided with the endosymbiotic events that originated the eukaryotes [48]. Within the HemY family, green plants possess two divergent isoforms of PPO, and it is yet unclear whether the two isoforms of PPO were caused by separate endosymbiotic events or by a gene duplication within an ancestral green plant. These nuclear-encoded genes are PPX1 and PPX2, which produce the chloroplast PPO1 and mitochondrial PPO2 enzymes, respectively.

Plant protoporphyrinogen oxidases

There are two distinct isoforms of PPO in plants, as described above. Both are derived from a common HemY ancestor. Despite the common ancestry and identical functionality, the two isoforms carry <30% identity at the protein level. Both carry <30% identity to mammalian

PPO proteins as well, although PPO1 and PPO2 carry approximately 70% identity to their counterparts in other plants [49]. The two isoforms separate into two branches on a phylogenetic tree generated from a homolog search for the tobacco (*Nicotiana tabacum*) PPO1 and PPO2 protein sequences (Fig. 1.4). The isoforms are separated clearly by phylum. Both monocots and eudicots are separated into the same branch of the tree for each isoform. The ability to mutate and gain resistance to PPO-inhibiting herbicides has been identified at two different regions. The blue squares in Fig. 1.4 indicate the only organisms that do not have the Arg98 in the active site. All plant species investigated maintained the arginine in both PPO1 and PPO2. All conserved residues of the active site, including the Arg98, are shown in Table 1.2. The tandem repeat facilitating the Gly210 deletion is only found in PPO2 in some plant species, identified by red triangles in Fig. 1.4. As previously mentioned, *A. tuberculatus* and *A. palmeri* have evolved resistance to PPO-inhibiting herbicides via this deletion. Our sequence analysis identified *Kochia scoparia* as another problematic weed possessing this tandem repeat [50, 51]. As the soybean market expands north and west in the USA, it will be interesting to see if *K. scoparia* evolves resistance to PPO inhibitors via this same deletion mutation. Other short tandem repeats in this region could also lead to the deletion of the same codon encoding other amino acid residues (green triangles in Fig. 1.4) , but there is no evidence that this has occurred in resistant biotypes.

Compartmentalization and importance of dual target transit peptide

The compartmentalization of chlorophyll and heme production is necessary due to the toxic intermediates involved. It has been suggested that PPO directly interacts with the proteins directly before and after it in the pathway, which would keep the intermediates from having any chance of causing cellular damage [52]. As discussed earlier, PPO1 is targeted to the chloroplast while PPO2 is generally accepted to be targeted to the mitochondria. In some cases PPO2 is dual

targeted to both the mitochondria and the chloroplast.8 Within the chloroplast PPO1 is located in the thylakoid membrane, on the stromal side [53]. PPO2 in the mitochondria is located on the inner mitochondrial membrane and when it is found in the chloroplast it is located in the chloroplastic membrane [8].

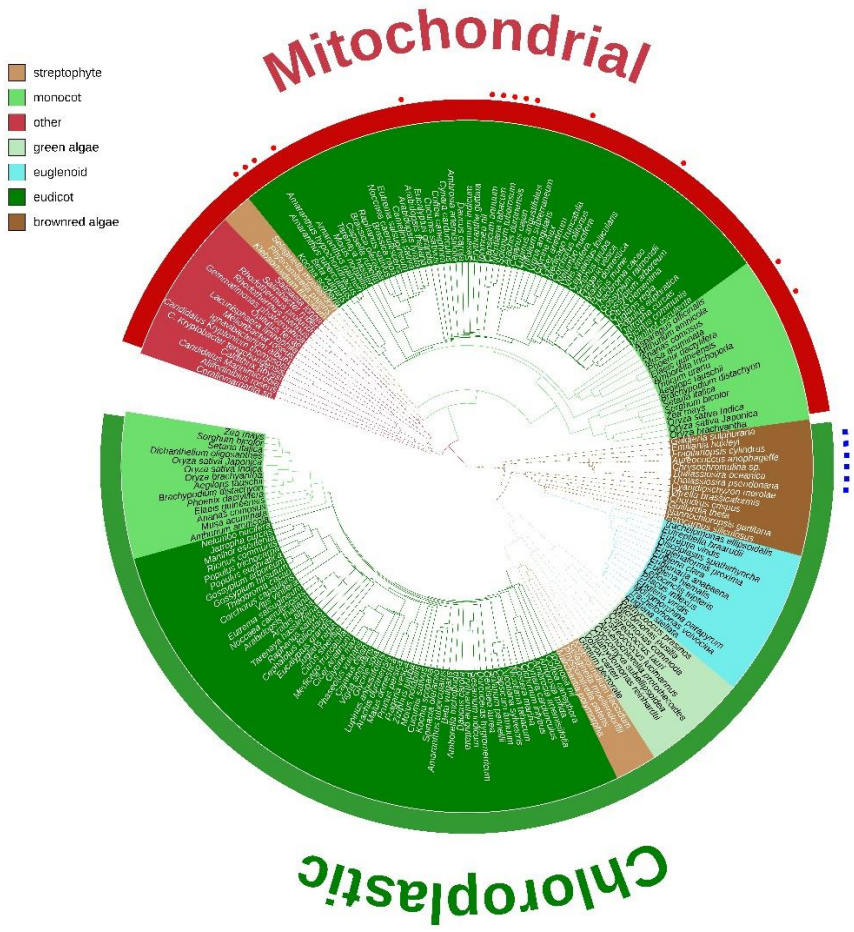

Figure 1.4 Phylogenetic relationship of PPO. This figure was generated by blasting the protein sequences of chloroplastic and mitochondrial PPO from *Nicotiana tabacum* in NCBI and selecting sequences with at least 70% coverage. Non-redundant sequences were identified with h-CD-hit set at 98.5% sequence identity 64, 65. The phylogenetic relationship was obtained by aligning the sequences with MAFFT (v6.864) 66 using blosum 62 and generating an output in phylip format. The image was generated with the interactive tree of life 67. Red dots identify sequences with tandem repeats associated with Gly201 deletion leading to herbicide resistance. Blue squares identify sequences with a Pro instead of Arg at position 98 associated with amino acid substitutions leading to herbicide resistance.

Table 1.2 Conserved regions involved in substrate binding and thought to interact with herbicides [58,63]

Organism	Arg98 region	Phe353-Leu356 region
	NKRYI	EGFGVLVP
Mitochondrial		
Higher plants	***	:*** *:*
Others	*:.	:*** * *
Chloroplastic		
Higher plants	*::	:*** * .
Euglenids	*::	*** *:*
Green algae	*::	*** * *
Brown algae	:	*** * *
Moss	*::	*** * *

Consensus symbols from Clustal W mean the following: an asterisk (*****) indicates positions that have a single, fully conserved residue; a colon (**:**) indicates conservation between groups of strongly similar properties; a period (**.**) indicates conservation between groups of weakly similar properties; the blue box indicates the unique proline residue at this position in brown algae.

Recent research has found that resistance mechanisms to PPO-inhibiting herbicides have only been due to mutations on PPO2. This indicates that it has a greater role in the mechanism of action of the PPO-inhibiting herbicides than previously assumed. Since dual targeting of the *A. tuberculatus* PPO2 is an important aspect of the mechanism of resistance to PPO-inhibiting herbicides, it is likely an aspect of similar resistance in other species. Dual targeting in plants is more common than previously assumed, and is generally conserved through evolution [54]. Due to this dual targeting of PPO2 may be much more prevalent than has been previously suggested. Proteins can achieve dual targeting thorough many mechanisms including competing target signals, ambiguous signals that are recognized by receptors on multiple compartments, signals that are only exposed in some folding states, or by transport out of a compartment after signal cleavage [55]. The dual targeting of PPO2 is proposed to be caused by the use of two in-frame start codons that create two different length proteins, identical to the mechanism found in spinach (*Spinacia oleracea*) [8, 23]. The approximately 30 amino acid extension resulting from a translation initiation at the first start codon encodes a chloropolastic targeting sequence, resulting in a larger protein being targeted into the chloroplast than that targeted to the mitochondria. *A. tuberculatus* had a similar upstream start codon, and the sequence following was identified as a chloroplastic targeting peptide [23]. Upon alignment and analysis of homologs to PPX2 from the NCBI database very few sequences had a second start codon around 90bp upstream or downstream from the identified start codon. This may be a result of incomplete sequence data. Targeting signals are often predicted based on specific amino acid sequences within the N-terminal sequence [56]. Dual targeting is difficult to predict even with computational tools—the best are only up to 75% accurate [57].

STRUCTURE OF PROTOPORPHYRINOGEN OXIDASE

Our current knowledge of the structure of plant PPO is based on a single publication reporting the X-ray crystallography analysis of the mitochondrial PPO2 from tobacco (*N. tabacum*) [58]. Each monomer of this dimeric enzyme consists of approximately 500 amino acids with a molecular mass of 55 kDa. Structurally, PPO is a compact protein arranged in 17 α-helices and 17 β-sheets to form three main domains, namely a FAD-binding domain, a substrate-binding domain and a membrane-binding domain (Fig. 1.5).

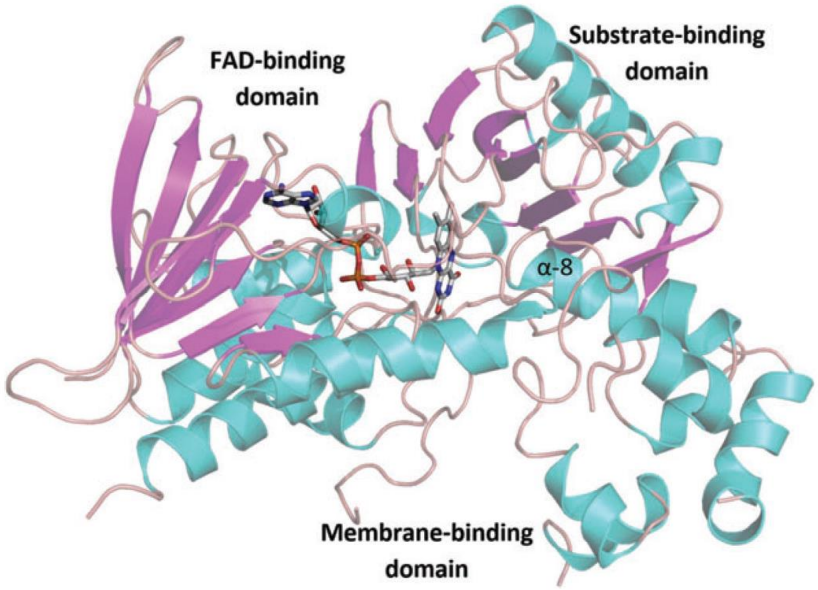

Figure 1.5 *Nicotiana tabacum* mitochondrial PPO monomer and its key structural features. The coordinates published by Koch et al. [58] were obtained from the crystal structure of 1SEZ.pdb available from the protein data bank [68].

This mitochondrial PPO has distinct Rossmann-fold topology common to many oxidase enzymes [59]. Analysis of its sequence with Cofactory [60] identified a 42-amino acid region with a beta-alpha-beta fold signature of dinucleotide binding sites favoring FAD-binding over other cofactors such as NAD and NADP, with 0.946, 0.211, and 0.066 neural network scores, respectively (Figs. 1.6A and B) [59]. Cofactory scores >0.5 indicate that the domain is predicted to be specific for the particular cofactor. Although the structure of the chloroplastic PPO from

tobacco is not known, a 42-amino acid sequence with a signature for FAD binding was also found, with neural network scores of 0.932 0.157 0.092 for FAD, NAD and NADP, respectively.

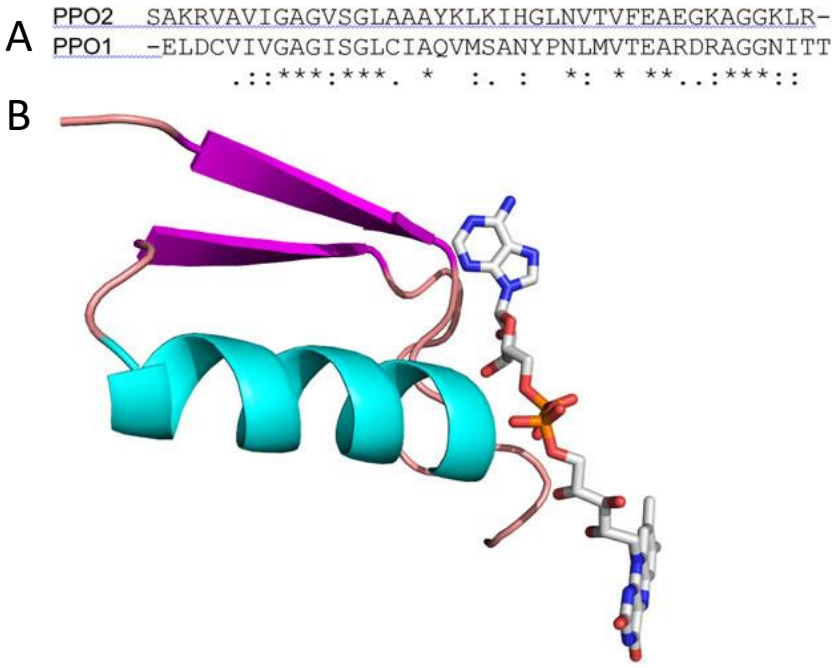

Figure 1.6 Rossmann fold identified by Cofactory analysis of the sequences of tobacco PPO1 and PPO2. (A) Alignment of the 42-amino acid stretches showing the key FAD-binding signature of a Rossmann fold. (B) Location of the Rossmann fold with respect of the binding of FAD from the crystal structure of tobacco PPO2 [58].

The substrate-binding domain is positioned within a relatively large recess to accommodate the movement of the protogen substrate in the catalytic domain and the transport of the proto product via a channel between PPO and the chelatase catalyzing the next step in heme synthesis. PPO2 is tightly bound to the inner mitochondrial membrane via interaction of lipophilic amino acids, including the conserved sequence regions from residue 112 to 136 and from 150 to 213, exposed on the outer shell of the protein [58].

Features of the catalytic domain

The catalytic domain of all plant PPOs consists of the following features: a flavin ring of the FAD prosthetic group forms the roof and a Gly175 opposite the flavin ring serves as a pivot

for the tetrapyrrole ring at the bottom of the pocket (Fig. 1.7). A Gly178 (often referred to as Gly210 based on the sequence of *A. tuberculatus* PPO2) is associated with the stabilization of the capping region of α-8 helix. Deletion of this amino acid leads to herbicide resistance in the mitochondrial PPO. The highly conserved Arg98 (Fig. 1.4; Table 1.2) is involved in the positioning of the tetrapyrrole ring via ionic interactions with the propionate side chains of ring C of proto(gen) (Fig. 1.7). Amino acid substitutions of Arg98 to Leu, Met or Gly are associated with PPO herbicide resistance.32 Finally, Phe353 and Leu356 are highly conserved residues that are thought to interact with the D-ring of the substrate (Table 1.2 and Fig. 1.7). These amino acids may also be involved in the binding of the herbicides, accounting for the competitive reversible inhibition exerted by PPO inhibitors [16, 17, 40, 61, 62].

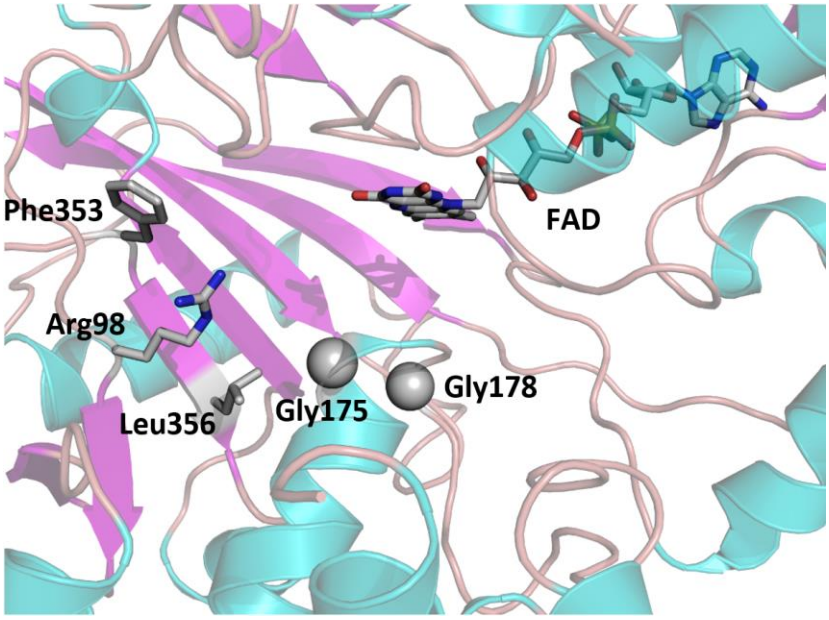

Figure 1.7 Catalytic domain of *Nicotiana tabacum* mitochondrial PPO showing FAD forming the roof of the pocket and Gly175 at the terminal end of the α-8 helix serving as a pivot for the tetrapyrrole ring at the bottom of the pocket. Gly178 indicates the site of a codon deletion leading to herbicide resistance on the mitochondrial PPO. Arg98 is involved in the positioning of the tetrapyrrole ring via ionic interactions of the carboxylic side chain of the substrate. Arg98 to Met or Val mutations on the mitochondrial enzyme are associated with PPO-herbicide resistance. The highly conserved Phe353 and Leu356 residues interact with the D-ring of the substrate and are thought to be involved in the binding of the herbicide.

CONCLUSIONS

PPO-inhibiting herbicides were important tools to manage a broad spectrum of weeds prior to the introduction of glyphosate-resistant (GR) transgenic crops. This class of chemistry appeared to be obsolete in the USA after widespread adoption of glyphosate-resistant crops. However, the tremendous selection pressure imparted by the widespread application of glyphosate has led to the emergence of glyphosate-resistant weeds, with *A. palmeri* and *A. tuberculatus* being particularly problematic. This has led to a resurgence of interest in PPO-inhibiting herbicides. However, their utility is now threatened by resistant biotypes. To date, resistance to PPO inhibitors in nearly all known cases has been associated with mutations and/or deletions in the mitochondrial PPO2 isoform, even though the chloroplastic PPO1 isoform is thought to be the primary target of these herbicides. The evolutionary and structural biology of plant PPOs confirms that the genetic environment that facilitates the deletion of a key glycine residue involved in herbicide resistance is only present in a few PPXII genes. To date, the only species with this mutation (*A. tuberculatus* and *A. palmeri*) are predicted to have dual targeting of PPO2 to both the chloroplast and the mitochondria, which may be required to impart sufficient herbicide resistance to whole plants. The most recent target site mutation involves a key arginine residue involved in stabilizing the substrate in the catalytic domain. This arginine is highly conserved across all plant PPOs, suggesting that this mutation could be equally likely in PPO1 and PPO2, yet it has only occurred in PPO2, underscoring the importance of this isoform for evolution of herbicide resistance.

REFERENCES

1. Heinemann, I. U.; Jahn, M.; Jahn, D., The biochemistry of heme biosynthesis. Arch. Biochem. Biophys. 2008, 474, 238-251.
2. Dayan, F. E.; Dayan, E., Porphyrins: One ring in the colors of life. Amer. Sci. 2011, 99, 236-243.
3. Anderson, K. E.; Kappas, A., The porphyrias. Endo-Metab 2010, doi 10.2310/7900.1162.
4. Hu, G.; Yalpani, N.; Briggs, S. P.; Johal, G. S., A porphyrin pathway impairment is responsible for the phenotype of a dominant disease lesion mimic mutant of maize. Plant Cell 1998, 10, 1095-1106.
5. Taylor, C. B., Vampire plants? Plant Cell 1998, 10, 1071-1074.
6. Dayan, F. E.; Duke, S. O., Phytotoxicity of protoporphyrinogen oxidase inhibitors: Phenomenology, mode of action and mechanisms of resistance. In Herbicide Activity: Toxicology, Biochemistry and Molecular Biology, Roe, R. M.; Burton, J. D.; Kuhr, R. J., Eds. IOS Press: Amsterdam, Netherland, 1997; pp 11-35.
7. Dayan, F. E.; Duke, S. O., Protoporphyrinogen oxidase-inhibiting herbicides. In Haye's Handbook of Pesticide Toxicology, 3rd ed.; Krieger, R.; Doull, J.; Hodgson, E.; Maibach, H.; Reiter, L.; Ritter, L.; Ross, J.; Slikker, W. J.; Van Hemmen, J., Eds. Academic Press, Elsevier: San Diego, CA, 2010; Vol. 2, pp 1733-1751.
8. Watanabe, N.; Che, F.-S.; Iwano, M.; Takayama, S.; Yoshida, S., Dual targeting of spinach protoporphyrinogen oxidase II to mitochondria and chloroplasts by alternative use of two in-frame initiation codons. J. Biol. Chem. 2001, 276, 20474-20481.
9. Raiford, L. C.; Thiessen, G.; Wernert, I., Some derivatives of diphenyl ether. J. Am. Chem. Soc. 1930, 52, 1205-1209.
10. Senseman, S. A., Herbicide Handbook. 9th ed.; Weed Science Society of America: Lawrence, KS, 2007; p 458.
11. Rhone-Poulenc, S. Oxadiazolinone compounds and herbicidal compositions. GB Patent 1,110,500, 1968.
12. Matsui, K.; Kasugai, H.; Matsuya, K.; Aizawa, H. N-Substituted-Δ1-tetrahydrophthalimide herbicides. FR2119703A5, 1972.
13. Becerril, J. M.; Duke, S. O., Protoporphyrin IX content correlates with activity of photobleaching herbicides. Plant Physiol. 1989, 90, 1175-1181.
14. Lydon, J.; Duke, S. O., Porphyrin synthesis is required for photobleaching activity of the p-nitrosubstituted diphenyl ether herbicides. Pestic. Biochem. Physiol. 1988, 31, 74-83.
15. Matringe, M.; Scalla, R., Effects of acifluorfen-methyl on cucumber cotyledons: Porphyrin accumulation. Pestic. Biochem. Physiol. 1988, 32, 164-172.
16. Matringe, M.; Camadro, J.-M.; Labbe, P.; Scalla, R., Protoporphyrinogen oxidase inhibition by three peroxidizing herbicides: oxadiazon, LS 82-556 and M&B 39279. FEBS Lett. 1989, 245, 35-38.
17. Matringe, M.; Camadro, J.-M.; Labbe, P.; Scalla, R., Protoporphyrinogen oxidase as a molecular target for diphenyl ether herbicides. Biochem. J. 1989, 260, 231-235.
18. Cox, G. S.; Krieg, M.; Whitten, D. G., Self-sensitized photooxidation of protoporphyrin IX derivatives in aqueous surfactants solutions: Product and mechanistic studies. J. Am. Chem. Soc. 1982, 104, 6930-6937.

19. USDA-NASS U.S. Department of Agriculture, National Agricultural Statistics Service www.nass.usda.gov (April 2017),
20. Shoup, D. E.; Al-Khatib, K.; Peterson, D. E., Common waterhemp (Amaranthus rudis) resistance to protoporphyrinogen oxidase-inhibiting herbicides. Weed Sci. 2003, 51, 145-150.
21. Patzoldt, W. L.; Tranel, P. J.; Hager, A. G., A waterhemp (Amaranthus tuberculatus) biotype with multiple resistance across three herbicide sites of action. Weed Sci. 2005, 53, 30-36.
22. Legleiter, T. R.; Bradley, K. W., Glyphosate and multiple herbicide resistance in common waterhemp (Amaranthus rudis) populations from Missouri. Weed Sci. 2008, 56, 582-587.
23. Patzoldt, W. L.; Hager, A. G.; McCormick, J. S.; Tranel, P. J., A codon deletion confers resistance to herbicides inhibiting protoporphyrinogen oxidase. Proc. Nat. Acad. Sci. USA 2006, 103, 12329-12334.
24. Schultz, J. L.; Chatham, L. A.; Riggins, C. W.; Tranel, P. J.; Bradley, K. W., Distribution of herbicide resistances and molecular mechanisms conferring resistance in Missouri waterhemp (Amaranthus rudis Sauer) populations. Weed Sci. 2015, 63, 336-345.
25. Thinglum, K. A.; Riggins, C. W.; Davis, A. S.; Bradley, K. W.; Al-Khatib, K.; Tranel, P. J., Wide distribution of the waterhemp (Amaranthus tuberculatus) ΔG210 PPX2 mutation, which confers resistance to PPO-Inhibiting herbicides. Weed Sci. 2011, 59, 22-27.
26. Wuerffel, R. J.; Young, J. M.; Lee, R. M.; Tranel, P. J.; Lightfoot, D. A.; Young, B. G., Distribution of the ΔG210 protoporphyrinogen oxidase mutation in Illinois waterhemp (Amaranthus tuberculatus) and an improved molecular method for detection. Weed Sci. 2015, 63, 839-845.
27. Wuerffel, R. J.; Young, J. M.; Matthews, J. L.; Young, B. G., Characterization of PPO-inhibitor–resistant waterhemp (Amaranthus tuberculatus) response to soil-applied PPO-inhibiting herbicides. Weed Sci. 2015, 63, 511-521.
28. Falk, J. S.; Shoup, D. E.; Al-Khatib, K.; Peterson, D. E., Protox-resistant common waterhemp (Amaranthus rudis) response to herbicides applied at different growth stages. Weed Sci. 2006, 54, 793-799.
29. Wuerffel, R. J.; Young, J. M.; Tranel, P. J.; Young, B. G., Soil-residual protoporphyrinogen oxidase–inhibiting herbicides influence the frequency of associated resistance in waterhemp (Amaranthus tuberculatus). Weed Sci. 2015, 63, 529-538.
30. Salas, R. A.; Burgos, N. R.; Tranel, P.; Singh, S.; Glasgow, L.; Scott, R. C.; Nichols, R. L., Resistance to PPO-inhibiting herbicide in Palmer amaranth from Arkansas, USA. Pest Manage. Sci. 2016, 72, 864–869.
31. Rousonelos, S. L.; Lee, R. M.; Moreira, M. S.; VanGessel, M. J.; Tranel, P. J., Characterization of a common ragweed (Ambrosia artemisiifolia) population resistant to ALS- and PPO-inhibiting herbicides. Weed Sci. 2012, 60, 335-344.
32. Giacomini, D. A.; Umphres, A. M.; Nie, H.; Mueller, T. C.; Steckel, L. E.; Young, B. G.; Scott, R. C.; Tranel, P. J., Two new PPX2 mutations associated with resistance to PPO-inhibiting herbicides in Amaranthus palmeri. Pest Manage. Sci. 2017, 73, 1559-1563.
33. Trezzi, M. M.; Felippi, C. L.; Mattei, D.; Silva, H. L.; Nunes, A. L.; Debastiani, C.; Vidal, R. A.; Marques, A., Multiple resistance of acetolactate synthase and protoporphyrinogen oxidase inhibitors in Euphorbia heterophylla biotypes. J. Environ. Sci. Health. Part B 2005, 40, 101-109.

34. Brusamarello, A. P.; Oliveira, P. H.; Trezzi, M. M.; Xavier, E.; Dalosto, E. D., Inheritance of resistance to protoporphyrinogen oxidase inhibitor herbicides in wild poinsettia. Planta Daninha 2016, 34, 575-580.
35. Trezzi, M. M.; Vidal, R. A.; Kruse, N. D.; Silva, R. P.; Gustmann, M. S.; Franchin, E., Fomesafen absorption site as a mechanism of resistance in an Euphorbia heterophylla biotype resistant to PROTOX inhibitors. Planta Daninha 2009, 27, 139-148.
36. Mangin, A. R.; Hall, L. M.; Beckie, H. J., Triallate-resistant wild oat (Avena fatua L.): unexpected resistance to pyroxasulfone and sulfentrazone. Can. J. Plant Sci. 2016, 97, 20-25.
37. Riechers, D. E.; O'Brien, S. R.; Ma, R.; Lygin, A. V. In Characterization of resistance to saflufenacil applied postemergence in Amaranthus tuberculatus, Weed Science Society of America, San Juan, Puerto Rico, 2016; San Juan, Puerto Rico, 2016; p 426.
38. Dayan, F. E.; Owens, D. K.; Tranel, P. J.; Preston, C.; Duke, S. O., Evolution of resistance to phytoene desaturase and protoporphyrinogen oxidase inhibitors – state of knowledge. Pest Manage. Sci. 2014, 70, 1358-1366.
39. Li, X.; Nicholl, D., Development of PPO inhibitor-resistant cultures and crops. Pest Manage. Sci. 2005, 61, 277-285.
40. Dayan, F. E.; Daga, P. R.; Duke, S. O.; Lee, R. M.; Tranel, P. J.; Doerksen, R. J., Biochemical and structural consequences of a glycine deletion in the α-8 helix of protoporphyrinogen oxidase. Biochim. Biophys. Acta - Prot. Proteom. 2010, 1804, 1548-1556.
41. Gressel, J.; Levy, A. A., Agriculture: The selector of improbable mutations. Proc. Natl. Acad. Sci. USA 2006, 103, 12215-12216.
42. Riggins, C. W.; Tranel, P. J., Will the resistance mechanism to PPO-inhibiting herbicides evolve in other Amaranthus species? Internat. J. Agron. 2012, 2012, doi:10.1155/2012/305764.
43. Ichinose, K.; Che, F.-S.; Kimura, Y.; Matsunobu, A.; Sato, F.; Yoshida, S., Selection and characterization of protoporphyrinogen oxidase inhibiting herbicide (S23142) resistant photomixotrophic cultured cells of Nicotiana tabacum. J. Plant Physiol. 1995, 146, 693-698.
44. Watanabe, N.; Takayama, S.; Yoshida, S.; Isogai, A.; Che, F.-S., Resistance to protoporphyrinogen oxidase-inhibiting compound S23142 from overproduction of mitochondrial protoporphyrinogen oxidase by gene amplification in photomixotrophic tobacco cells. Bioscience, Biotechnology, and Biochemistry 2002, 66, 1799-1805.
45. Warabi, E.; Usui, K.; Tanaka, Y.; Matsumoto, H., Resistance of a soybean cell line to oxyfluorfen by overproduction of mitochondrial protoporphyrinogen oxidase. Pest Manage. Sci. 2001, 57, 743-748.
46. Jung, S.; Lee, Y.; Yang, K.; Lee, S. B.; Jang, S. M.; Ha, S. B.; Back, K., Dual targeting of Myxococcus xanthus protoporphyrinogen oxidase into chloroplasts and mitochondria and high level oxyfluorfen resistance. Plant Cell Environ. 2004, 27, 1436-1446.
47. Kobayashi, K.; Masuda, T.; Tajima, N.; Wada, H.; Sato, N., Molecular phylogeny and intricate evolutionary history of the three isofunctional enzymes involved in the oxidation of protoporphyrinogen IX. Genome Biol. Evol. 2014, 6, 2141-2155.
48. Oborník, M.; Green, B. R., Mosaic Origin of the Heme Biosynthesis Pathway in Photosynthetic Eukaryotes. Molecular Biology and Evolution 2005, 22, 2343-2353.
49. Lermontova, I.; Kruse, E.; Mock, H. P.; Grimm, B., Cloning and characterization of a plastidal and a mitochondrial isoform of tobacco protoporphyrinogen IX oxidase. Proc. Natl. Acad. Sci. USA 1997, 94, 8895-8900.
50. Heap, I., Herbicide Resistant Weeds. In Integrated Pest Management: Pesticide Problems, Pimentel, D.; Peshin, R., Eds. Springer Netherlands: Dordrecht, 2014; Vol. 3, pp 281-301.

51. Varanasi, V. K.; Godar, A. S.; Currie, R. S.; Dille, A. J.; Thompson, C. R.; Stahlman, P. W.; Jugulam, M., Field-evolved resistance to four modes of action of herbicides in a single kochia (Kochia scoparia L. Schrad.) population. Pest Manage. Sci. 2015, 71, 1207-1212.
52. Medlock, A. E.; Shiferaw, M. T.; Marcero, J. R.; Vashisht, A. A.; Wohlschlegel, J. A.; Phillips, J. D.; Dailey, H. A., Identification of the mitochondrial heme metabolism complex. PLoS ONE 2015, 10, 1-20.
53. Che, F. S.; Watanabe, N.; Iwano, M.; Inokuchi, H.; Takayama, S.; Yoshida, S.; Isogai, A., Molecular characterization and subcellular localization of protoporphyrinogen oxidase in spinach chloroplasts. Plant physiology 2000, 124, 59-70.
54. Xu, L.; Carrie, C.; Law, S. R.; Murcha, M. W.; Whelan, J., Acquisition, conservation, and loss of dual-targeted proteins in land plants. Plant Physiol. 2013, 161, 644-662.
55. Karniely, S.; Pines, O., Single translation—dual destination: mechanisms of dual protein targeting in eukaryotes. EMBO Rep. 2005, 6, 420-425.
56. Sunderland, P. A.; West, C. E.; Waterworth, W. M.; Bray, C. M., An evolutionarily conserved translation initiation mechanism regulates nuclear or mitochondrial targeting of DNA ligase 1 in Arabidopsis thaliana. Plant J. 2006, 47, 356-367.
57. Höglund, A.; Dönnes, P.; Blum, T.; Adolph, H.-W.; Kohlbacher, O., MultiLoc: prediction of protein subcellular localization using N-terminal targeting sequences, sequence motifs and amino acid composition. In Oxford Univ Press: 2006.
58. Koch, M.; Breithaupt, C.; Kiefersauer, R.; Freigang, J.; Huber, R.; Messerschmidt, A., Crystal structure of protoporphyrinogen IX oxidase: a key enzyme in haem and chlorophyll biosynthesis. EMBO J. 2004, 23, 1720-1728.
59. Hanukoglu, I., Proteopedia: Rossmann fold: A beta-alpha-beta fold at dinucleotide binding sites. Biochem. Mol. Biol. Ed. 2015, 43, 206-209.
60. Geertz-Hansen, H. M.; Blom, N.; Feist, A. M.; Brunak, S.; Petersen, T. N., Cofactory: Sequence-based prediction of cofactor specificity of Rossmann folds. Proteins Struct. Funct. Bioinform. 2014, 82, 1819-1828.
61. Dayan, F. E.; Weete, J. D.; Duke, S. O.; Hancock, H. G., Soybean (Glycine max) cultivar differences in response to sulfentrazone. Weed Sci. 1997, 45, 634-641.
62. Dayan, F. E.; Duke, S. O.; Weete, J. D.; Hancock, H. G., Selectivity and mode of action of carfentrazone-ethyl, a novel phenyl triazolinone herbicide. Pestic. Sci. 1997, 51, 65-73.
63. Heinemann, I. U.; Diekmann, N.; Masoumi, A.; Koch, M.; Messerschmidt, A.; Jahn, M.; Jahn, D., Functional definition of the tobacco protoporphyrinogen IX oxidase substrate-binding site. Biochem. J. 2007, 402, 575-580.
64. Li, W.; Godzik, A., Cd-hit: a fast program for clustering and comparing large sets of protein or nucleotide sequences. Bioinformatics 2006, 22, 1658-1659.
65. Huang, Y.; Niu, B.; Gao, Y.; Fu, L.; Li, W., CD-HIT Suite: a web server for clustering and comparing biological sequences. Bioinformatics 2010, 26, 680-682.
66. Katoh, K.; Kuma, K.-i.; Toh, H.; Miyata, T., MAFFT version 5: improvement in accuracy of multiple sequence alignment. Nucleic Acids Res. 2005, 33, 511-518.
67. Letunic, I.; Bork, P., Interactive Tree Of Life v2: online annotation and display of phylogenetic trees made easy. Nucleic Acids Res. 2011, 39, W475-W478.
68. Berman, H. M.; Westbrook, J.; Feng, Z.; Gilliland, G.; Bhat, T. N.; Weissig, H.; Shindyalov, I. N.; Bourne, P. E., The Protein Data Bank. Nucleic Acids Res. 2000, 28, 235-242.

ADDENDUM TO CHAPTER 1: CURRENT UPDATE ON PPO INHIBITORS

INTRODUCTION

Protoporphyrinogen oxidase (PPO) is the penultimate enzyme in heme synthesis, as well as a common enzyme to chlorophyll, siroheme and phytochromobilin in plants [1]. These colorful tetrapyrroles with covalent metal bonds are used across life with their high affinity to electron excitement being utilized in photosynthesis, protein active sites, light signaling and respiration. In humans the protein is well characterized due to the hundreds of mutations in PPO which can cause variegate porphyria by partial or total loss of enzyme function [2]. In agriculture PPO is highly studied due to the class of herbicides targeting both isoforms of the protein found in plants, leading to historically good control of broadleaf weeds. These herbicides showed an increase in use as glyphosate (the most common herbicide) resistance cases became commonplace and use rates have plateaued in the last five years (Fig. 1.8).

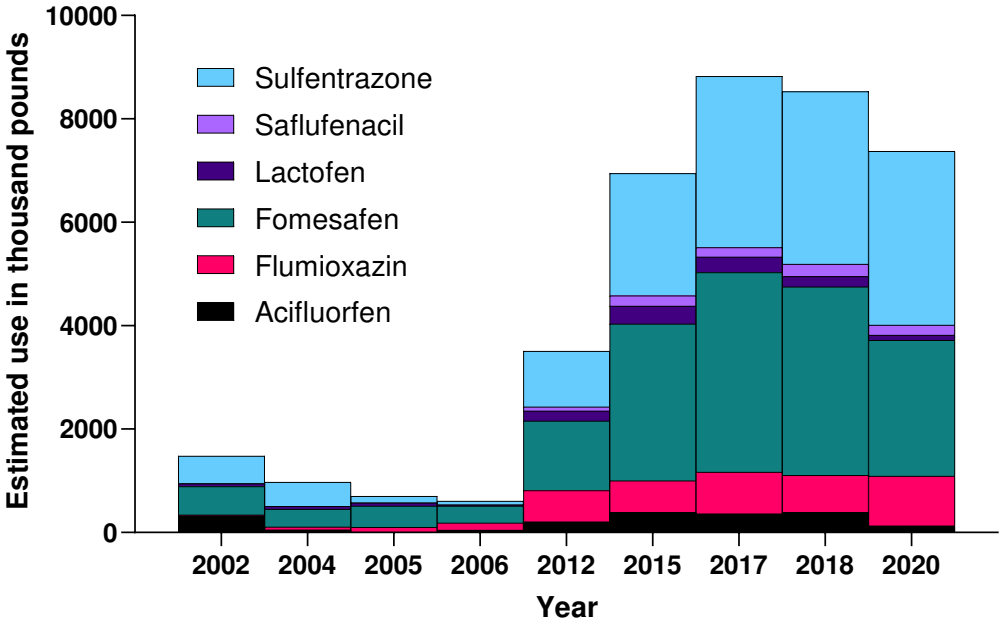

Figure 1.8 PPO inhibitor use in soybeans from 2002 to 2020 from the NASS (https://www.nass.usda.gov/)

As herbicide resistance issues have been increasing in recent years, and new herbicide sites of action are slow to develop, older chemistries with relatively few resistance reports are becoming critical tools for agriculture. The goal of this review is to compile information on the currently active chemicals in this class of herbicides. There are many published reviews on the subject [3-10], but most focus on the mechanism of action which is well characterized and none cover the last ten years of insight due to resistance

CHEMICAL CLASSES

Diphenyl ethers are the oldest commercial PPO inhibitors, released in the 1960's. Much of the initial mechanism of action (MoA) work was done on acifluorfen or its methyl ester and oxyfluorfen. While these oldest chemicals are still in use (acifluorfen, oxyfluorfen, fomesafen, bifenox, and lactofen) more chemical classes that also inhibit PPO were discovered and commercialized. Per the newest version of the HRAC herbicide classification poster from 2020 there are 21 registered PPO inhibitors which fall into five groups: Diphenyl ethers, *N*-phenyl-imides, *N*-phenyl-triazolinones, *N*-phenyl-oxadiazolones, and two which do not fall into any of these categories (Table 1.3) (https://hracglobal.com/).

All currently registered inhibitors of PPO show similar structures (Fig. 1.9), including rigid, multicyclic regions that mimic the structure of the endogenous substrate, protoporphyrinogen (protogen). This similarity allows the inhibitors to bind to the active site similarly to protogen and many of the same conserved residues are used to stabilize the inhibitors (i.e., Arg98, Phe353 and Leu356).

Table 1.3 Currently registered PPO-inhibiting herbicides separated by chemical structure groups

Diphenyl ethers	Lactofen Bifenox Acifluorfen Fomesafen Oxyfluorfen
N-phenyl-imides	Butafenacil Flumiclorac-pentyl Flumioxazin Cinidon-ethyl Fluthiacet-methyl Pentoxazone Saflufenacil Tiafenacil Trifludimoxazin
N-phenyl-triazolinones	Azafenidin Carfentrazone-ethyl Sulfentrazone
N-phenyl-oxadiazolones	Oxadiargyl Oxadiazon
Others	Pyraflufen-ethyl Pyraclonil

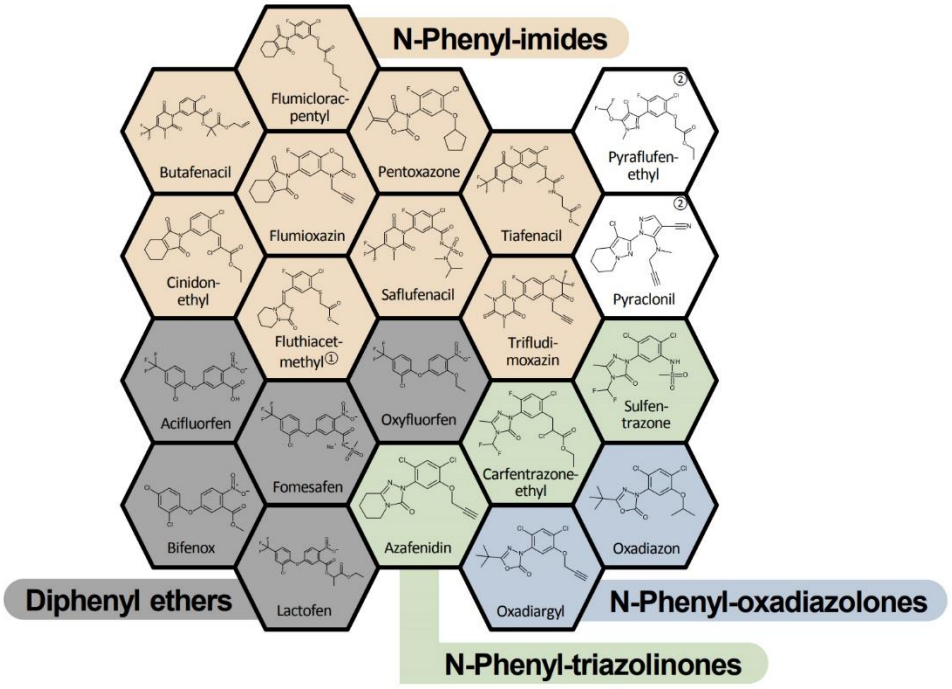

Figure 1.9 Structures of the currently registered PPO-inhibiting herbicides from HRAC (https://hracglobal.com/)

PROPERTIES

Most PPO inhibiting molecules have some xylem mobility, though this is generally not physiologically relevant in foliar application (postemergence) due to the rapid action of PPO inhibitors. Tissue which has absorbed the herbicide is often dead before mobilization can occur. The increased xylem mobility of some, such as sulfentrazone, does explain soil and pre-emergent activity vs less mobile compounds like lactofen which are effective post-emergent [11]. For a comprehensive list of post- vs pre- emergent applications see the most recent edition of the Weed Science Society of America Herbicide Handbook [12].

PPO inhibiting herbicides are considered to have low environmental impacts with a few exceptions. Volatilization is low or non-existent in all labelled PPO inhibitors. Most foliar applied compounds have a half-life of a few days in soil, largely due to microbe degradation, and many are either water insoluble or degrade rapidly in aqueous solutions. Exceptions to the rule are in the long-lasting soil applied compounds such as sulfentrazone and fomesafen which have a half-life in soil over 100 days and show some moderate leaching as a result [11]. The requirement of light for damage from PPO inhibitors and selectivity for the plant enzymes means that there are few off target effects. One of note per the label for Cobra herbicide (formulated lactofen), applications on soybean can suppress white mold (https://www.agrian.com/pdfs/current/Cobrar_Herbicide_Label1y.pdf).

PPO AS A PROTEIN

PPO is an essential protein for most forms of life, though the protein that performs the oxidation of protoporphyrinogen to protoporphyrin IX shows very little conservation of sequence (Table 1.4). Even more closely related species, such as mammals or plants, show only around a

50-60% homology of related proteins. Plants in general have two isoforms of PPO, commonly referred to as the mitochondrial (PPO2) and chloroplastic (PPO1) forms. Non-photosynthetic organisms have one form of PPO which is in the family of PPO2. Rather uniquely *Chlamydamonas reinhartdii,* a photosynthetic algae, only encodes one isoform which is more closely related to PPO1. Despite the naming conventions the PPO2 in species such as *Drosophila melanogaster* and *Homo sapiens* show the same conservation of sequence (25-30%) with both the plant isoforms.

Despite greatly differing sequences, PPO proteins across phyla fold in very similar patterns. Comparisons of crystal structures from *Nicotiana tabacum* [13] and *H. sapiens* PPO2 [14] proteins shows an RMSD of only 1.779 Angstroms despite the 24.55% sequence identity. Similar structural similarities are true between crystal structures of PPO1 and PPO2 in *N. tabacum* (Lerchl, J personal correspondence)

Table 1.4 Percent identity matrix of PPO proteins selected from across phyla, compared at an amino acid sequence level by Clustal Omega [15]

		1	2	3	4	5	6	7	8	9	10	11	12	13	14	15	16
1	PPO C. elegans	100	12.96	12.7	13.19	13.35	14.91	14.95	13.71	13.82	15.25	17.7	10.66	11.85	12.89	13.84	14.29
2	PPO Saccharomyces cerevisiae	12.96	100	27.33	22.88	24.58	26.11	24.09	24.09	19.87	20.73	20.26	21.88	19.26	21.7	21.67	20.35
3	PPO2 Drosophila melanogaster	12.7	27.33	100	36.01	40.43	37.96	38.48	38.04	25.56	25.11	24.72	22.81	29.48	22.37	23.94	22.65
4	PPO Trichoplax sp. H2	13.19	22.88	36.01	100	39.66	40.64	40.17	39.74	27.88	28.32	26.83	27.42	28.76	24.89	25.22	26.55
5	PPO2 Danio Rerio	13.35	24.58	40.43	39.66	100	57.89	52.85	50.74	24.16	25.28	25.11	27.15	31	25.84	23.73	24.72
6	PPO2 Anolis carolinensis	14.91	26.11	37.96	40.64	57.89	100	58.02	57.17	25.28	24.83	26.01	28.73	32.35	24.05	25.5	24.28
7	PPO2 Homo sapiens	14.95	24.09	38.48	40.17	52.85	58.02	100	88.68	24.94	26.06	24.55	25.96	30.86	25.94	27.15	25.5
8	PPO2 Mus musculus	13.71	24.09	38.04	39.74	50.74	57.17	88.68	100	24.94	24.72	25	25.96	31.08	26.39	26.93	25.72
9	PPO2 Oryza sativa japonica	13.82	19.87	25.56	27.88	24.16	25.28	24.94	24.94	100	57.75	57.26	22.3	27.45	26.57	26.85	27.29
10	PPO2 Arabidopsis thaliana	15.25	20.73	25.11	28.32	25.28	24.83	26.06	24.72	57.75	100	66.53	24.12	26.95	27.29	26.57	27
11	PPO2 Nicotiana tabacum	17.7	20.26	24.72	26.83	25.11	26.01	24.55	25	57.26	66.53	100	23.5	26.33	27.94	26.79	27.97
12	PPO Bacillus subtilis	10.66	21.88	22.81	27.42	27.15	28.73	25.96	25.96	22.3	24.12	23.5	100	27.68	27.25	30.33	29.71
13	PPO Myxococcus Xanthus	11.85	19.26	29.48	28.76	31	32.35	30.86	31.08	27.45	26.95	26.33	27.68	100	29.51	29.36	30.04
14	PPO Chlamydamonas reinhardtii	12.89	21.7	22.37	24.89	25.84	24.05	25.94	26.39	26.57	27.29	27.94	27.25	29.51	100	56.32	57.76
15	PPO1 Arabidopsis thaliana	13.84	21.67	23.94	25.22	23.73	25.5	27.15	26.93	26.85	26.57	26.79	30.33	29.36	56.32	100	75.99
16	PPO1 Nicotiana tabacum	14.29	20.35	22.65	26.55	24.72	24.28	25.5	25.72	27.29	27	27.97	29.71	30.04	57.76	75.99	100

MECHANISM OF ACTION

To date the mechanism of action of PPO inhibiting herbicides has been well classified. The inhibition of PPO leads to a buildup of protoporphyrinogen (protogen), which then leaks into the cytoplasm where it becomes oxidized. The method of oxidization here is still contested: either by a membrane bound general peroxidase enzyme or by the auto-oxidative ability of the molecule itself. Regardless this causes a rapid buildup of protoporphyrin IX (proto), a highly light reactive molecule which, upon excitement, reacts with endogenous oxygen carrying molecules to make reactive oxygen species which lead to lipid peroxidation and rapid death compared to many other herbicides [5].

Recently, due to observations of resistance mechanisms, new investigations into the mechanism of action of PPO inhibitors have been started. The importance of the two isoforms has been thrown into question. In photosynthetic tissue, the target of these herbicides, most of the tetrapyrrole pathway output is leading to chlorophyll and therefore associated with PPO1. This makes the observation that most resistance occurs due to mutations on PPO2 puzzling, and leads to questions of the specific activity of herbicides on each of the proteins as well as the specific contribution of PPO1 and PPO2 in the plant. Another curious observation of differing efficacy of pre- and post- emergent applications on resistant populations has led to further questions about application timing [16]. A third interesting development is the interaction and synergy of PPO inhibitors with glufosinate, an inhibitor of glutamine synthetase. Applications of low levels of glufosinate along with PPO inhibitors greatly increases the damage to plants, and could be used as a tool to overcome resistance [17].

TOLERANCE AND RESISTANCE IN WEEDS

Few weed species have natural tolerance to PPO inhibitors. Common chickweed is one which shows higher tolerance, likely due to sequestration of the herbicide which leads to less contact with the target proteins [18]. Beyond natural tolerance, the first cases of resistance in field populations were reported in common waterhemp (*Amaranthus tuberculatus*) in 2006. This population was classified as resistant due to a codon deletion at position 210 of PPO2 [19]. Since then, target site resistance has been confirmed in many species with four main mutations (Table 1.5). Of note is that only one monocot species has developed resistance via a mutation of PPO1, while the remaining species are dicots which have developed resistance through mutations of PPO2. Palmer and waterhemp are particularly troublesome with how many different mutations they have developed. Each of these mutations shows different resistance profiles for the classes of herbicides: G399A mutations seem to confer resistance across classes, G210 deletions and R128 mutations do not confer as high of a resistance to *N*-phenyl-imides or oxadiazolones [20].

Table 1.5 Current verified target site resistance mechanisms to PPO inhibitors

Protein	Mutation	Species	Reference
PPO2	ΔG210	*Amaranthus tuberculatus, Amaranthus palmeri*	Patzoldt et al. [21], Salas et al. [22]
PPO2	R128G, I, L, M,	*Amaranthus tuberculatus, Amaranthus palmeri, Amaranthus retroflexus, Ambrosia artemisiifolia, Euphorbia heterophylla*	Rousonelos et al. [23], Giacomini et al. [24], Nie et al. [25], Mendes et al. [26], Huang et al. [27]
PPO2	G399A	*Amaranthus palmeri*	Rangani et al. [20]
PPO1	A212T	*Elusine indica*	Bi et al. [28]

TOLERANCE AND RESISTANCE IN CROPS

No GM PPO-resistant crops have been released to the public, though many species already have natureal tolerance to PPO inhibitors. This tolerance is largely based on metabolism of the PPO inhibiting molecule after uptake into the crop. Soybean, for example, cleaves the ether bridges common in the diphenyl ethers which allows the phenyl rings to be conjugated and detoxified. For inhibitors without the ether bridge, soybean performs oxidative degradation followed by a similar conjugation [29-31]. Despite the ability to metabolize these molecules, the rapid action still often leads to transient crop injury after application, though plants grow out of the injury [32].

Though none have been released, there is still potential for more robust PPO-resistance trait through GM technologies. Early on crops were shown to be resistant through overexpression of the PPX1 gene. More recently crops have been shown to be resistant when expressing a bacterial form of PPO, similar to Roundup Ready crop technology with resistance to glyphosate [11]. Though the publications on these resistant crops are from the early 2000s, the pipeline to release GM crop technology can take 15-20 years.

CONCLUSIONS

Despite the age of PPO inhibitor technology, these chemicals are still relevant to our modern agricultural practices. With only 13 troublesome weed species showing resistance to some or all of the herbicides in this group, there is still a great deal of usefulness in a diverse weed control program. Areas of continuing research for PPO inhibitors are the individual contributions of

PPO1 and PPO2 to the activity of these herbicides, the differential activity of PPO inhibitors with application timing, and synergy with the inhibitor of glutamine synthetase.

REFERENCES

1. Tanaka, R., and Tanaka, A. (2007) Tetrapyrrole biosynthesis in higher plants. Annu. Rev. Plant Biol. 58, 321-346
2. Chen, B., Whatley, S., Badminton, M., Aarsand, A. K., Anderson, K. E., Bissell, D. M., Bonkovsky, H. L., Cappellini, M. D., Floderus, Y., Friesema, E. C. H., Gouya, L., Harper, P., Kauppinen, R., Loskove, Y., Martásek, P., Phillips, J. D., Puy, H., Sandberg, S., Schmitt, C., To-Figueras, J., Weiss, Y., Yasuda, M., Deybach, J.-C., and Desnick, R. J. (2019) International Porphyria Molecular Diagnostic Collaborative: an evidence-based database of verified pathogenic and benign variants for the porphyrias. Genet Med 21, 2605-2613
3. Böger, P. (1984) Multiple modes of action of diphenyl ethers. Zeitschrift für Naturforschung C 39, 468-475
4. Gilham, D. J., and Dodge, A. D. (1987) The mode of action of nitrodiphenyl ether herbicides. In "Progress in Pesticide Biochemistry and Physiology"(DH Hutson and TR Roberts, eds.), Vol. 7. Wiley, New York
5. Duke, S. O., Lydon, J., Becerril, J. M., Sherman, T. D., Lehnen Jr, L. P., and Matsumoto, H. (1991) Protoporphyrinogen oxidase-inhibiting herbicides. Weed Science, 465-473
6. Kunert, K. J., Sandmann, G., and Boger, P. (1987) Modes of action of diphenyl ethers. Reviews of weed science (USA)
7. Matsunaka, S. (1976) Diphenyl ethers. Herbicides: chemistry, degradation, and mode of action 2, 709-739
8. Dayan, F., and Duke, S. (1997) Phytotoxicity of protoporphyrinogen oxidase inhibitors: phenomenology, mode of action and mechanisms of resistance. REVIEWS IN TOXICOLOGY 1, 11-36
9. Nandihalli, U. B., and Duke, S. O. (1993) The porphyrin pathway as a herbicide target site.
10. Scalla, R., and Matringe, M. (1994) Inhibitors of protoporphyrinogen oxidase as herbicides: diphenyl ethers and related photobleaching molecules. Reviews of weed science (USA)
11. Dayan, F., and Duke, S. (2010) Protoporphyrinogen oxidase-inhibiting herbicides. Book Chapter 2, 1731-1751
12. Shaner, D. L. (2014) Herbicide Handbook of the Weed Science Society of America. Weed Sci. Soc. of Amer. Lawrence, KA
13. Koch, M., Breithaupt, C., Kiefersauer, R., Freigang, J., Huber, R., and Messerschmidt, A. (2004) Crystal structure of protoporphyrinogen IX oxidase: a key enzyme in haem and chlorophyll biosynthesis. EMBO J. 23, 1720-1728
14. Qin, X., Tan, Y., Wang, L., Wang, Z., Wang, B., Wen, X., Yang, G., Xi, Z., and Shen, Y. (2011) Structural insight into human variegate porphyria disease. FASEB J. 25, 653-664
15. Li, W., Cowley, A., Uludag, M., Gur, T., McWilliam, H., Squizzato, S., Park, Y. M., Buso, N., and Lopez, R. (2015) The EMBL-EBI bioinformatics web and programmatic tools framework. Nucleic Acids Res 43, W580-W584
16. Lillie, K. J., Giacomini, D. A., and Tranel, P. J. (2020) Comparing responses of sensitive and resistant populations of Palmer amaranth (Amaranthus palmeri) and waterhemp (Amaranthus tuberculatus var. rudis) to PPO inhibitors. Weed Technology 34, 140-146

17. Takano, H. K., Beffa, R., Preston, C., Westra, P., and Dayan, F. E. (2020) Glufosinate enhances the activity of protoporphyrinogen oxidase inhibitors. Weed Science 68, 324-332
18. Matsumoto, H., Kashimoto, Y., and Warabi, E. (1999) Basis for common chickweed (Stellaria media) tolerance to oxyfluorfen. Pesticide biochemistry and physiology 64, 47-53
19. Wuerffel, R. J., Young, J. M., Matthews, J. L., and Young, B. G. (2015) Characterization of PPO-Inhibitor–Resistant Waterhemp (Amaranthus tuberculatus) Response to Soil-Applied PPO-Inhibiting Herbicides. Weed Science 63, 511-521
20. Rangani, G., Salas-Perez, R. A., Aponte, R. A., Knapp, M., Craig, I. R., Meitzner, T., Langaro, A. C., Noguera, M. M., and Burgos, N. R. (2019) A novel single-site mutation in the catalytic domain of protoporphyrinogen oxidase IX (PPO) confers resistance to PPO-inhibiting herbicides. Frontiers in plant science 10, 568
21. Patzoldt, W. L., Hager, A. G., McCormick, J. S., and Tranel, P. J. (2006) A codon deletion confers resistance to herbicides inhibiting protoporphyrinogen oxidase. Proceedings of the National Academy of Sciences of the United States of America 103, 12329-12334
22. Salas, R. A., Burgos, N. R., Tranel, P. J., Singh, S., Glasgow, L., Scott, R. C., and Nichols, R. L. (2016) Resistance to PPO-inhibiting herbicide in??Palmer amaranth from Arkansas. Pest Manag. Sci. 72, 864-869
23. Rousonelos, S. L., Lee, R. M., Moreira, M. S., VanGessel, M. J., and Tranel, P. J. (2012) Characterization of a common ragweed (Ambrosia artemisiifolia) population resistant to ALS- and PPO-inhibiting herbicides. Weed science 60, 335-344
24. Giacomini, D. A., Umphres, A. M., Nie, H., Mueller, T. C., Steckel, L. E., Young, B. G., Scott, R. C., and Tranel, P. J. (2017) Two new PPX2 mutations associated with resistance to PPO-inhibiting herbicides in Amaranthus palmeri. Pest Manag. Sci.
25. Nie, H., Mansfield, B. C., Harre, N. T., Young, J. M., Steppig, N. R., and Young, B. G. (2019) Investigating target-site resistance mechanism to the PPO-inhibiting herbicide fomesafen in waterhemp and interspecific hybridization of Amaranthus species using next generation sequencing. Pest Manag. Sci. 75, 3235-3244
26. Mendes, R. R., Takano, H. K., Adegas, F. S., Oliveira Jr, R. S., Gaines, T. A., and Dayan, F. E. (2020) Arg-128-Leu target-site mutation in PPO2 evolves in wild poinsettia (Euphorbia heterophylla) with cross-resistance to PPO-inhibiting herbicides. Weed Science 68, 437-444
27. Huang, Z., Cui, H., Wang, C., Wu, T., Zhang, C., Huang, H., and Wei, S. (2020) Investigation of resistance mechanism to fomesafen in Amaranthus retroflexus L. Pesticide biochemistry and physiology 165, 104560
28. Bi, B., Wang, Q., Coleman, J. J., Porri, A., Peppers, J. M., Patel, J. D., Betz, M., Lerchl, J., and McElroy, J. S. (2020) A novel mutation A212T in chloroplast protoporphyrinogen oxidase (PPO1) confers resistance to PPO inhibitor oxadiazon in Eleusine indica. Pest Manag. Sci. 76, 1786-1794
29. Frear, D. S., Swanson, H. R., and Mansager, E. R. (1983) Acifluorfen metabolism in soybean: diphenylether bond cleavage and the formation of homoglutathione, cysteine, and glucose conjugates. Pesticide Biochemistry and Physiology 20, 299-310
30. Dayan, F. E., Weete, J. D., and Hancock, H. G. (1996) Physiological basis for differential sensitivity to sulfentrazone by sicklepod (Senna obtusifolia) and coffee senna (Cassia occidentalis). Weed Science 44, 12-17
31. Dayan, F. E., Weete, J. D., Duke, S. O., and Hancock, H. G. (1997) Soybean (Glycine max) cultivar differences in response to sulfentrazone. Weed Science 45, 634-641

32. Graham, M. Y. (2005) The diphenylether herbicide lactofen induces cell death and expression of defense-related genes in soybean. Plant physiology 139, 1784-1794

CHAPTER 2: DIFFERENTIAL RESISTANCE TO PPO INHIBITING HERBICIDES IN PRE AND POST EMERGENT APPLICATIONS[2]

INTRODUCTION

Weeds are the most important agricultural pest in terms of potential yield loss,[1] and herbicide-resistant weeds are threatening our ability to control these pests. The widespread issue of glyphosate resistance (GR) has caused a return to conventional weed management practices that relies on older mechanisms of action that still have efficacy on GR weeds.[2] Protoporphyrinogen oxidase (PPO)-inhibiting herbicides (group 14) are important tools for control of GR weed species in soybean, corn and cotton in the US. Members of this large class of herbicides include those used both pre-emergent (i.e., sulfentrazone and flumioxazin) and post-emergent (i.e., acifluorfen and saflufenacil) as well as herbicides labelled for use in both cases (i.e., lactofen). The flexibility in timing of application across different group 14 herbicides makes these inhibitors attractive and effective tools to control species such as common waterhemp (*Amaranthus tuberculatus*) that germinate throughout the growing season.[3]

The tendency of older plants to be less sensitive to PPO inhibiting herbicides than younger plants has been observed since early investigations into the mechanism of action. In some species older plants metabolize the photoactive proto more than younger plants.[4] Lambsquarters and morningglory plants treated with acifluorfen accumulated more of the photoactive proto in 3 week-old tissue than 7 week-old tissue .[5] Finally, Palmer amaranth and

[2] Author information: Abigail Barker†, Dawn Resfell‡, John Pawlak‡ and Franck E. Dayan†

†Agricultural Biology Department, Colorado State University, Fort Collins, CO 80523-1177

‡Valent/Sumitoto, 14571 Arcadia Woods Drive Spring Lake, MI 49456

waterhemp with the gly210 deletion both show less sensitivity to post emergence herbicide application, relative to pre emergence, as well as less control in later post emergent sprays. [6-8] These observations extend across multiple PPO inhibiting herbicides from different families of molecules. Consequently, a better understanding of the role of PPO1 and PPO2 on the efficacy of PPO-inhibiting herbicides as the plants develop is critically needed to make informed decisions on how to most effectively use PPO-inhibiting herbicides.

PPO is a highly effective herbicide target due to inhibition of the tetrapyrrole pathway which produces two extremely important pigments: chlorophyll and heme. The mechanism of action of herbicides targeting PPO is complex.[9] Briefly, PPO inhibition leads to the transient accumulation of its colorless substrate protoporphyrinogen which leaks out of the organelles into the cytosol where it is oxidized to its highly photodynamic product protoporphyrin IX (proto).[10, 11] Photoactivation of proto leads to the accumulation of reactive oxygen species (ROS) which cause lipid peroxidation and subsequent loss of membrane integrity and cell death. There is a strong relationship between the pool of free glutamate/glutamine and the tetrapyrrole pathway.[12] This pathway utilizes 8 glutamate molecules to form the tetrapyrrole ring backbone through a multienzyme process. The first committed step of this process is the condensation of two glutamate into one 5-aminolevulinic acid (ALA), and it is well characterized that exogenous addition of ALA increases flux through the pathway and increases the herbicidal activity of PPO inhibitors.[13]

Plants have two genes encoding for PPO (*PPX1* and *PPX2*). Both of these genes are encoded in the nucleus and their protein products are directed to different subcellular compartments. The *PPX1* gene product, PPO1, is imported to the chloroplast and participates primarily in chlorophyll synthesis. The *PPX2* gene product, PPO2, is imported to the

mitochondria and is involved in heme synthesis (Fig. 2.1). Although this is the commonly accepted paradigm, there have been studies showing significant heme production in the chloroplast[14] and some species "dual target" PPO2 to both the mitochondria and the chloroplasts.[15] From a biological standpoint, most of the porphyrin produced in plants is directed towards chlorophyll synthesis (the most abundant pigment in the world).[16] Historical understanding of the mode of action of herbicides targeting PPO is that the accumulation of proto is derived mostly form the carbon flux channeled toward chlorophyll synthesis in the chloroplasts.

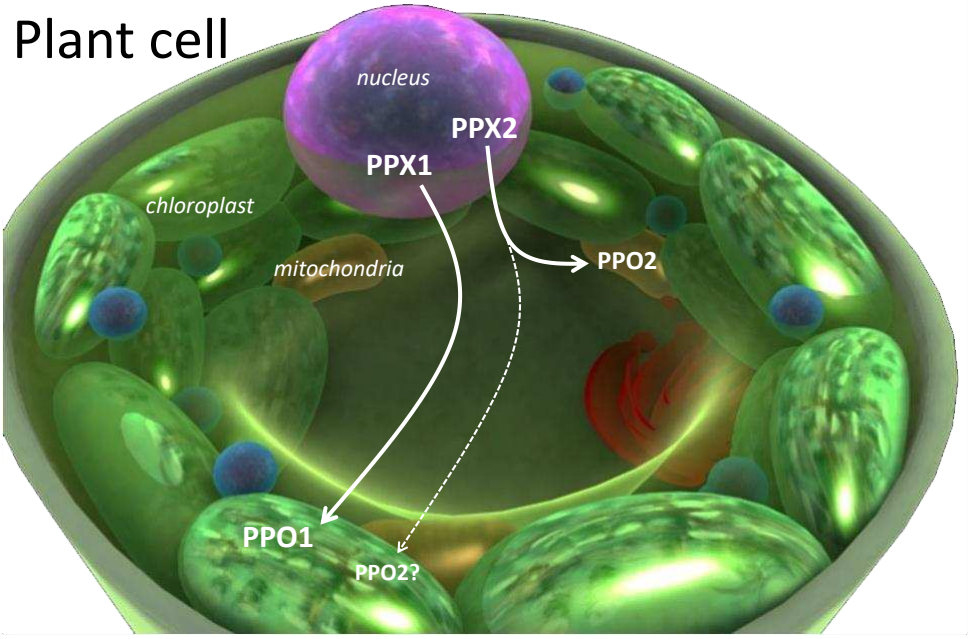

Figure 2.1. Diagram illustrating the location of the PPX1 and PPX2 genes in the nucleus and the ultimate organelle localization of PPO1 and PPO2 in the chloroplast and mitochondria, respectively. The dotted line indicates the possibility that some PPO2 can be dual-targeted toward both the mitochondria and chloroplast.

Herbicide resistance mechanisms can also impart an understanding of natural tolerance to herbicides. Target-site resistance (TSR) mechanisms involve mutations on the proteins targeted by herbicides whereas non-target site resistance (NTSR) mechanisms involve processes reducing

the ability of herbicides to reach their target sites.[17] Thirteen species in 7 countries have been identified with resistance to PPO inhibitors, including some biotypes of common waterhemp (*Amaranthus tuberculatus*), common ragweed (*Ambrosia artemisiifolia*), Palmer amaranth (*Amaranthus palmeri*), and goosegrass (*Elusine indica*).[18] While our biochemical understanding is that inhibition of PPO1 is more deleterious; most target site mutations imparting resistance to PPO inhibitors have evolved on PPO2. Four separate target site mutations have been identified to date: deletion of the codon for glycine at the 210 position (ΔGly210) on PPO2,[19] mutation of the arginine in the active site (Arg98) of PPO2,[20, 21] mutation of the glycine at position 399 in PPO2 to an alanine,[22] and a mutation of alanine 212 on PPO1 to threonine.[23] Other resistance cases have been attributed to metabolism-based non-target site resistance.[24, 25] Because it was the first identified case of resistance to this mechanism of action, research was conducted on a waterhemp line with the ΔGly210 mutation. This deletion makes the catalytic domain of the mitochondrial enzyme slightly larger, which prevents the competitive inhibition of the enzyme by the herbicides.[26]

Some plants naturally tolerate proto accumulation by other means. Plants have natural defenses to ROS production, since normal functions of the mitochondria, chloroplast and peroxisome can lead to the accumulation of ROS. These defense mechanisms include enzyme systems such as catalases, peroxidases, and superoxide dismutases; and antioxidant molecules such as the lipophilic carotenoids and water-soluble ascorbate and glutathione. Weeds increase their levels of ROS scavenging proteins as a response to herbicide treatment, and some non-target site resistance (NTSR) is indicated to be involved with ROS protection.[27] Studies manipulating antioxidant potentials also demonstrate that increasing the ability to quench ROS reduces the toxic effect of these herbicides whereas inhibiting the ability of quench ROS

increases the deleterious effect of these herbicides.[28] In the past a correlation was also indicated between levels of ascorbic acid and tocopherols and tolerance levels to the PPO inhibitor oxyfluorfen.[29] Additionally, some plants may have the ability to prevent or decrease the phytotoxic effect of PPO-inhibiting herbicides by metabolizing the highly photodynamic proto to less toxic chlorins,[30] and ultimately non-photodynamic water-soluble metabolites.[31] This process involves cytosolic peroxidases and requires the presence of thiol-containing substrates such as glutathione and cysteine.

The aim of this study was to investigate the investigate the mechanisms of differential response to pre- and post-emergence application PPO-inhibiting herbicides during plant development. Accordingly, levels of *PPX1* and *PPX2* transcription as well as PPO1 and PPO2 protein were analyzed during plant germination and growth. Uptake of herbicide, antioxidant levels and indicators of flux through the tetrapyrrole pathway were also investigated for possible roles in herbicide efficacy. These findings will help develop weed management strategies that protect and prolong the preemergence efficacy of PPO-inhibiting herbicides.

MATERIALS AND METHODS

Plant growth

Seeds were received from Pat Tranel, a line derived from ACR that is homozygous for the ΔG210 deletion which confers resistance to PPO inhibitors and WUS a universally herbicide sensitive line. Plants were grown in a greenhouse kept at 30 C ± 2 with 16-h days. *Amaranthus tuberculatus* seeds were sterilized via chlorine gas sterilization and then plated on 0.5% agar

plates and kept at 4 C for one week prior to exposure to greenhouse conditions. After germination plants were transplanted into 2-inch pots.

Dose response

When plants were approximately 10 cm tall R and S biotypes were sprayed with lactofen (1× rate 219 gai/ha). Each biotype was treated with 8 rates: 0, 1/128, 1/32, 1/16, 1/8, 1/4, 1 and 2× for the sensitive and 0, 1/4, 1/2, 1, 2, 8 and 16× for the resistant biotypes, respectively. 4 weeks after treatment plants were rated for injury, alive/dead counts, and collected for dry weight.

Plate assay

Pre-emergent dose responses were performed on agar plates. 0.5% agar was dissolved over heat and then autoclaved. When autoclaved media had been cooled to approximately 60 C lactofen was added in a serial dilution to concentrations of 1,000, 100, 10, 0.1, 0.01, 0.001, and 0 μM. Three replicate plates were poured at each concentration and half of each plate was seeded with 50 ACR and the other half seeded with 50 WUS seeds. Plates were then cold treated for 10 d after which they were put under growth lights on a 12-h day at 25C. Data was taken on hypocotyl emergence 7 and 14 d after exposure to light.

Amino acid supplementation experiments

10 cm plants were removed from the greenhouse, the roots were washed of soil and transferred to solutions of 1% MES pH 7.0 containing one of five amino acid treatments: negative control, glutamate, glutamine, aspartate, and asparagine. Plants were left under growth lights at 30 C ± 2 for 24 h, then half of each treatment was sprayed with a pre- determined dose of formulated acifluorfen (Ultra Blazer) that would case approximately 20% damage, 28 g/ha for

the resistant line and 2.8 g/ha for the susceptible line. 15 h after spraying the third expanded leaf was taken from each plant to measure proto accumulation. Damage ratings were measured after 48 h and two weeks, and dry weights were taken after two weeks.

Proto IX measurement

Apical meristem tissue was collected from plants treated with a post-emergent spray of acifluorfen (Ultra Blazer) at a field rate of 280 g/ha at four ages: the 2 true leaf stage, the 4 true leaf stage, the 6 true leaf stage and after the development of secondary stems. Samples collected from the amino acid supplementation experiment were also processed the same way. Plants were kept in the dark until collection to reduce any damage to the tissue. Leaf tissue (~100 mg) was collected 15 h after treatment (HAT) and ground with liquid nitrogen. Proto was extracted by homogenizing the powder in 2 mL of methanol:0.1 M NH4OH (9:1) and centrifuged at 5,000×g for 15 min (Dayan et al. 2015). The supernatants were filtered through a 0.25 μm nylon membrane filter and proto levels were determined by Liquid Chromatography Mass Spectrometry (LC-MS/MS) analysis. The LC-MS/MS system (Shimadzu Scientific Instruments, Columbia, MD 21046) consisted of a Nexera X2 UPLC (2 LC-30 AD pumps), a SIL-30 AC MP autosampler, a DGU-20A5 Prominence degasser, a Kinetex 2.6 μm F5 100 A LC column, and SPD-M30A diode array detector coupled to an 8040 quadrupole mass-spectrometer. The solvent A was 10 mM ammonium acetate (pH 5.6) and solvent B was methanol. The gradient started at 50% B and increased linearly to 70% B until 8 min, followed by a linear gradient to 90% B until 11 min. The mobile phase remained at 90% B until 13 min, then returned to 50% B at 13.5 min and maintained to 50% until the end of the run (15 min). The flow rate was 0.4 mL min^{-1} and 5 μL of the samples were analyzed. Proto levels were quantified based on the external calibration curve (P8293, Sigma-Aldrich, St. Louis, USA).

Amino acid quantification

Apical meristem tissue was collected from plants at five ages: directly after emergence at the cotyledon stage, at the 2 true leaf stage, the 4 true leaf stage, the 6 true leaf stage and after the development of secondary stems. 60 mg of tissue were ground under liquid nitrogen with a tube pestle. 1.5 mL of 25:75 methanol:water solution was added and samples were incubated in an ultrasonic bath for 24 min. Samples were then centrifuged at 16,000×g for 10 min. Supernatant was filtered through 0.2 μm nylon filter for analysis on LCMS. Samples were analyzed via LC-MS/MS on the system described above as described in Takano et al. (2019).[12]

Antioxidant measurement including molecules and proteins

Apical meristem tissue was collected from plants at five ages: directly after emergence at the cotyledon stage, at the 2 true leaf stage, the 4 true leaf stage, the 6 true leaf stage and after the development of secondary stems. Antioxidants were extracted from 100 mg of tissue ground under liquid nitrogen. Samples were extracted in 1 mL phosphate buffered saline, diluted to 1/100× and measured via a commercial kit (Sigma- MAK187, Total Antioxidant Capacity Assay Kit). Samples were assayed according to the manufacturers protocol and extracts were compared to Trolox standards at 570 nm.

Herbicide quantification in tissue

Apical meristem tissue was collected from plants treated with a post-emergent spray of acifluorfen (Ultra Blazer) at a field rate of 280 g/ha at four ages: the 2 true leaf stage, the 4 true leaf stage, the 6 true leaf stage and after the development of secondary stems. Plants were kept in the dark 15 hours until collection to reduce any damage to the tissue. Acifluorfen was extracted using a modified QuEChERS method. Tissue aliquots (150 mg) were flash frozen in liquid

nitrogen and ground in a 2 mL tube using a tube pestle. 600 µL of water was then added and samples vortexed until well suspended. 600 µL of ACN with 0.1% formic acid was added and tubes were vortexed. Samples were then shaken for 10 min at room temperature, then 0.3 g of QuEChERS salts added and immediately vortexed. Once all samples are dissolved, they were centrifuged for 10 min at room temperature at 5,000 x g. Organic phase was then filtered through 0.2 µm PTFE filter into an LC-MS vial and capped.

Samples were then analyzed via LC-MS/MS on the system described above. The solvent A was 3 mM ammonium acetate and solvent B was 3 mM ammonium acetate in Acetonitrile. The gradient started at 15 % B and remained constant until 2 min, followed by a linear gradient to 75 % B until 10 min. The mobile phase remained at 75 % B until 14 min, then returned to 15 % B at 14.5 min and maintained to until the end of the run (15 min). The flow rate was 0.4 mL min^{-1} and 1 µL of the samples were analyzed. Acifluorfen sodium salt levels were quantified based on the external calibration curve (Chem Service, West Chester, PA USA)

mRNA extraction and qPCR

Apical meristem tissue was collected from plants at five ages: directly after emergence at the cotyledon stage, at the 2 true leaf stage, the 4 true leaf stage, the 6 true leaf stage and after the development of secondary stems. mRNA was extracted as described by Yaffe, Buxdorf [32]. Briefly, tissue was ground under liquid nitrogen and then extracted in a buffer of 8 M guanidine hydrochloride, 20 mM MES, and 20 mM EDTA. Ground tissue was sedimented by centrifugation at 4 C on max speed for 20 min, supernatant was diluted 1:1 with 200 proof EtOH and loaded onto a plasmid column (Qiagen cat no. 27115). Column was washed with 3M sodium acetate once, 70% EtOH once, and dried before RNA elution with DEPC water heated to 60 C.

mRNA was then DNase treated with the Turbo DNA-free kit (Thermo Fisher Cat no. AM1907) as per the kit instructions. cDNA was created from 1 ug RNA with the iScript cDNA synthesis kit (BioRad cat no. 1708891) as per the manufacturer instructions. qPCR was performed with SSOAdvanced universal SYBR green mastermix (Bio-Rad, Hercules, CA USA) on the CFX96 Real-Time PCR Detection System (Bio-Rad, Hercules, CA USA). Primers for *PPX1* and *PPX2* transcripts [33] and reference genes *EF1α* and *GADPH* [34] were used as in previous studies. All samples were run with four biological replicates and 3 technical replicates. Expression was calculated by the ΔCt method using the geometric mean of both reference genes.[35] The equation was used as below.

$$2^{(Ct_{unknown} - \text{average } Ct_{reference})}$$

Protein extraction and blotting

Apical meristem tissue was collected from plants at five ages: directly after emergence at the cotyledon stage, at the 2 true leaf stage, the 4 true leaf stage, the 6 true leaf stage and after the development of secondary stems. Tissue was ground finely under liquid nitrogen, then crude protein extracted in potassium phosphate buffer (40 mM potassium phosphate dibasic, 10 mM potassium phosphate monobasic, 0.1% ascorbate, 0.2% Triton-X, 1 mM PMSF, 1 mM DTT) as follows: 400 µL of extraction buffer was added for every 100 mg of tissue, samples were incubated on ice for 30 min before centrifugation at 10,000×g for 10 min. Supernatant was centrifuged again at 10,000×g for another 10 min.

Crude protein was mixed with 4× SDS-PAGE buffer and boiled for 5 min before separation by SDS-PAGE. Protein was then transferred onto nitrocellulose and blotted using monoclonal antibodies grown in rabbits against PPO1 and PPO2 (Agrisera, Vännäs, Sweden).

Imaging was preformed using HRP conjugated secondary antibody and Clarity Western ECL substrate (Bio-Rad Laboratories, Hercules, CA USA)

Statistical analysis

Statistical analysis was performed using the R software (v 4.1.0). Dose responses were fit using the DRC package. [36] Quantitative analyses were analyzed via ANOVA to determine if biotype was a significant factor, if it was not data was combined and multiple t-tests with Tukey adjustment were performed to determine statistical significance.

RESULTS

Dose response curves of lactofen

Waterhemp lines sensitive (WUS) and resistant (ACR) to PPO inhibitors via the ΔG210 deletion were treated in a pre-emergent plate assay and a post-emergent spray dose response (Fig. 2.2). In both assays, ACR was much more resistant to lactofen than WUS. The resistance factor, calculated as the ratio of the dose lethal to 50% (GR_{50}) of the populations, is two orders of magnitude higher in the pre-emergent assay relative to the post-emergent assay: 7,240 vs 76.7. However, the concentration equivalent to field rate in the pre-emergent assay is 2,500 μM whereas the field rate post-emergent is 219 g active ingredient per hectare. The GR_{50} of resistant plants in a pre-emergent assay is 0.86% of a field rate, whereas it is 234% of the post emergent field rate when the plants were sprayed at 6-10 cm (approximately the 6-leaf stage).

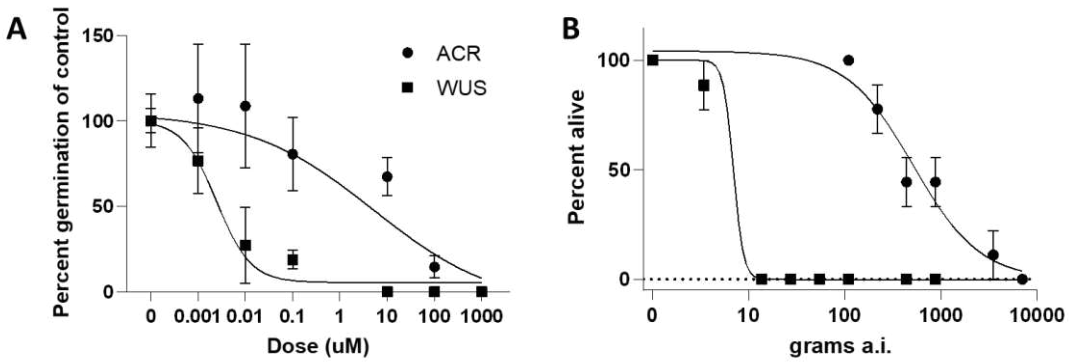

Figure 2.2: Dose response curves of ACR (PPO resistant) and WUS (PPO sensitive) waterhemp treated with lactofen. (A) pre-emergent dose response in percent germination compared to the control dose and (B) post-emergent in percent alive 28 DAT. Regression curves are included from the 4-parameter regression curves, error bars represent standard error.

mRNA and protein levels

Transcript levels and protein levels of both isoforms of PPO were measured through five growth stages of both lines of waterhemp: directly after emergence at the cotyledon stage, at the 2 true leaf stage, the 4 true leaf stage, the 6 true leaf stage and after the development of secondary stems. WUS and ACR plants showed no difference in expression levels and were pooled for further analysis. No age showed a significantly different level within PPX1 or PPX2 transcripts, though it is worth noting that PPX2 transcript levels are 100× those of PPX1 (Fig. 2.3A-B). PPO1 levels increased over the course of plant growth, with little to no detectable PPO protein in younger tissue (Fig. 2.3C). PPO2 levels remain fairly constant throughout plant growth (Fig. 2.3D).

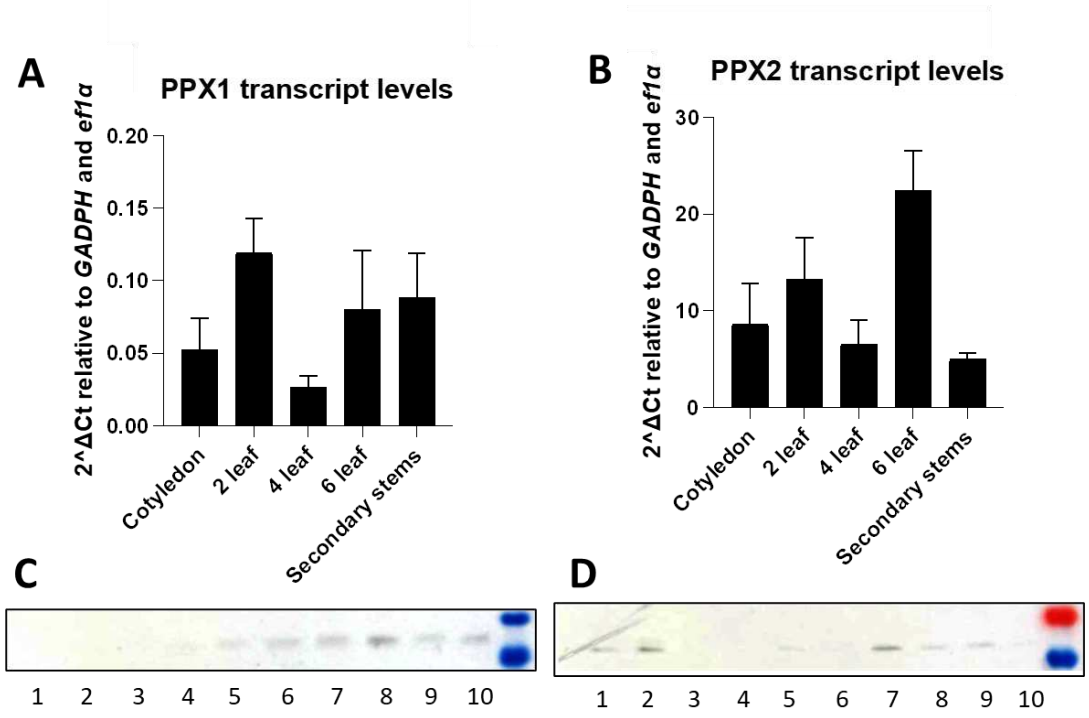

Figure 2.3: mRNA and protein levels for the two protoporphyrinogen oxidase genes in waterhemp during the five growth stages sampled. (A) Relative expression of *PPX1* compared to the average of two reference genes, no expression levels were significantly different and error bars represent standard error (n=8). (B) Relative expression (average 2^ΔCt) of *PPX2* compared to two reference genes, no expression levels were significantly different and error bars represent standard error (n=8). (C) PPO1 protein levels: 10 wells were loaded as follows: (1) ACR cotyledon, (2) WUS cotyledon, (3) ACR 2 leaf, (4) WUS 2 leaf, (5) ACR 4 leaf, (6) WUS 4 leaf, (7) ACR 6 leaf, (8) WUS 6 leaf, (9) ACR secondary stems, (10) WUS secondary stems. (D) PPO2 protein levels with the same well loading as in the previous frame.

Effect of plant development on herbicide uptake

Plants from both lines were treated with a field rate of acifluorfen at four stages: 2 true leaf stage, the 4 true leaf stage, the 6 true leaf stage and after the development of secondary stems. Plants treated pre-emergent with an equivalent dose did not germinate and were not collectable for comparison. Total herbicide uptake was the same in both lines and decreased slightly as plants matured (Fig. 2.4A), with significant difference ($p<0.01$) between the 2-leaf stage and the 6-leaf stage. Although herbicide uptake was the same, proto accumulation differed

between biotypes (Fig. 2.4B). WUS accumulated much higher levels of proto in early growth stages than ACR ($p<0.001$), but both ACR and WUS showed a trend of reduced proto accumulation in older tissue. Untreated plants accumulated an average of 0.2 µg of proto per gram fresh weight, and damage can be observed with amounts of proto as low as 2-6 µg per gram fresh weight.

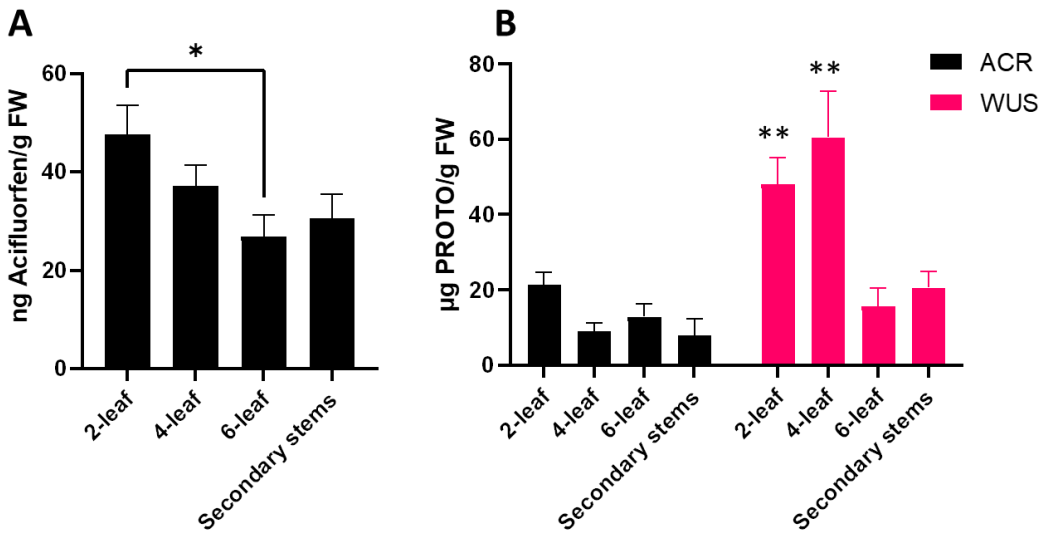

Figure 2.4: Effects of herbicide uptake on ACR (resistant) and WUS (sensitive) waterhemp. (A) Acifluorfen concentration inside tissue of plants treated at the 2-leaf through secondary stem growth stages treated with 280 g a.i./ha of the formulation Ultra Blazer. WUS and ACR did not show differential uptake, and were pooled in analysis, error bars represent standard error (n=10). The line represents the two groups that showed significant differences ($p< 0.01$). (B) Proto concentration in identically treated samples to those described above. Error bars represent standard error (n=5). Starred bars indicate a group of significant difference ($p< 0.001$).

Antioxidant capacity

The antioxidative potential in soluble extracts of untreated plants were not significantly different between sensitive and resistant biotypes, so results were pooled into 6 replicates at each plant height. Plants between the 4- and 6-leaf stages had much higher levels of soluble

antioxidants than younger plants, amounting to a 3-fold difference in ROS quenching capacity between younger and older plants (Fig. 2.5).

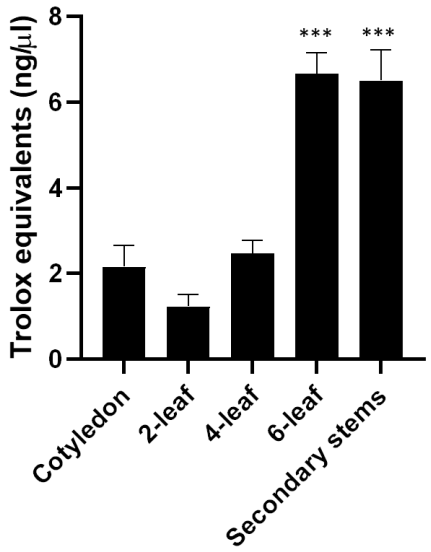

Figure 2.5: Antioxidant capacity of soluble waterhemp extracts at the 5 stages tested, measured relative to a Trolox standard. Data from ACR and WUS were not significantly different and were combined for statistical analysis, error bars represent standard error (n=6). Starred columns belong to a statistically different group ($p < 0.0001$).

The antioxidative potential in soluble extracts of untreated plants were not significantly different between sensitive and resistant biotypes, so results were pooled into 6 replicates at each plant height. Plants between the 4- and 6-leaf stages had much higher levels of soluble antioxidants than younger plants, amounting to a 3-fold difference in ROS quenching capacity between younger and older plants (Fig. 2.5).

Relationship of glutamate and related amino acids on efficacy of acifluorfen

The exogenous addition of glutamine and glutamate, but not asparagine and aspartate, increases the efficacy of acifluorfen on sensitive waterhemp at the 6-leaf stage treated with a sublethal dose of the herbicide causing approximately 10% damage (Fig. 2.6A-B). The increase

potency of acifluorfen correlated with the increase in proto levels in the presence of exogenous glutamine and glutamate. This pattern was not observed with the resistant ACR biotype (data not shown). Free glutamine and glutamate levels were measured in aqueous extracts from plants of all 5 ages described above, taken from both biotypes. There was no difference in the free pools of these amino acids in ACR and WUS and the data were pooled for further analysis. Free amino acid levels were lower in cotyledons and remained fairly stable over the rest of the stages tested (Fig. 2.6C).

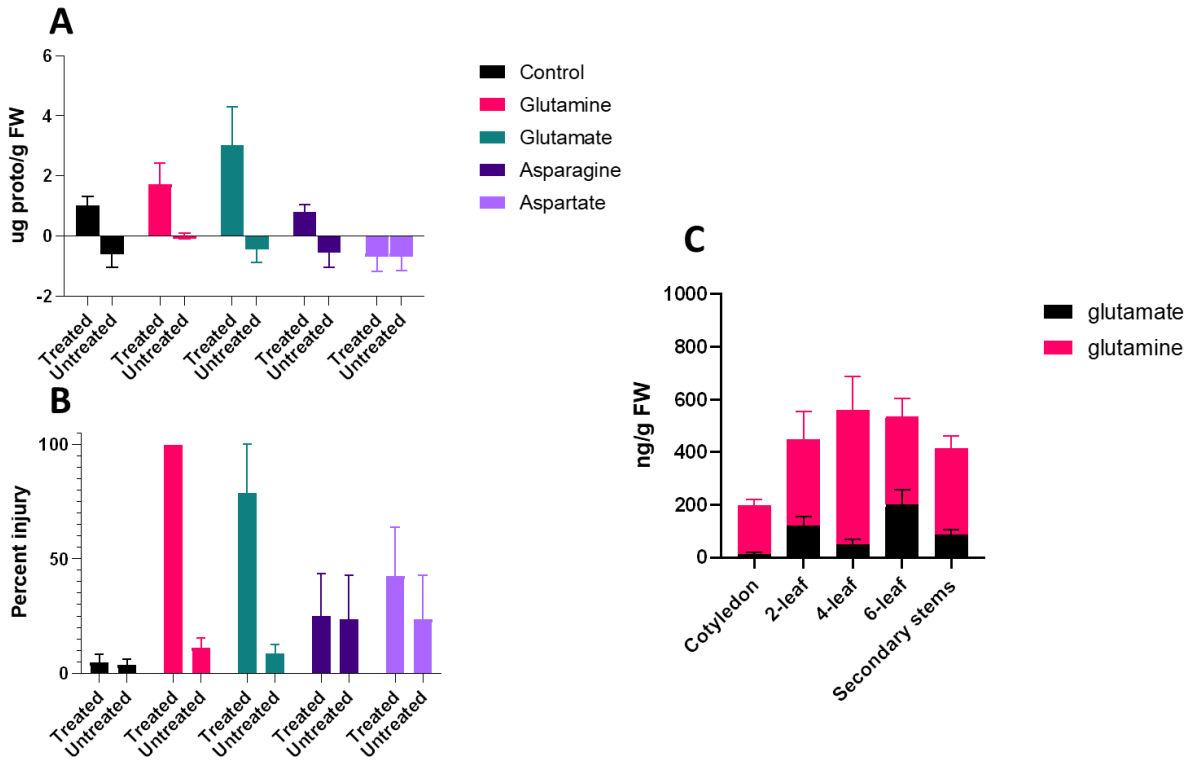

Figure 2.6: The relationship between glutamate and related amino acids, and the efficacy of acifluorfen (a PPO inhibitor) in waterhemp. (A) Proto accumulation in WUS (PPO sensitive) plants supplemented with amino acids and treated with a low dose of acifluorfen. Error bars represent standard error (n=4). (B) Percent injury in WUS (PPO sensitive) plants supplemented with amino acids and treated with a low dose of acifluorfen. Error bars represent standard error (n=4). (C) Free glutamine and glutamate levels in plants collected at the 5 growth stages studied. WUS and ACR plants did not show significant differences and were pooled for statistical analysis. Error bars represent standard error (n=10).

DISCUSSION AND CONCLUSIONS

Waterhemp and the closely related Palmer amaranth (*Amaranthus palmeri*) have evolved resistance to post emergent application of group 14 herbicides via the same ΔGly210 deletion on PPO2 [19, 21]. Waterhemp was selected as a model plant system to study the differential response of these biotypes to pre- versus post- emergent applications. While this biotype has evolved resistance in the field by selection with lactofen, it is cross-resistant to other PPO inhibitors. Acifluorfen was selected as a representative group 14 herbicide because it was more amenable to our LCMS analysis than the structurally related lactofen, but shows a similar resistance profile. [37] Our dose responses pre- and post-emergent have a similar pattern in resistance ratios to those found by Lillie, Giacomini [6] although they do not have pre-emergent data for lactofen they report a decreasing resistance ratio when comparing early and late post-emergent applications. The important distinction of these dose responses is that the phenomenon of greater control in pre-emergent applications is not a lack of resistance, but rather a dramatic shift in the effective dose.

Most investigations of resistance to PPO inhibitors are explained by reporting the presence of mutations. This can be in relation to the target site or to proteins which can metabolize an herbicide. Our investigation differs from most resistance analyses because we are not simply contrasting the response of a sensitive biotype and a resistance biotype to treatments with PPO inhibitors. Our experiments aim to explain why plants that have evolve resistance to post-emergent application of PPO inhibitors can still be controlled by pre-emergent application of group 14 herbicides.

To date investigation of protein levels for PPO1 and PPO2 during germination and early plant growth have not been done, though transcript levels can be assessed from *Arabidopsis*

thaliana transcriptomics datasets.[38] In *Arabidopsis* maximum levels of PPX1 transcript are an order of magnitude higher overall than maximum levels of PPX2 transcripts, which correlates with the higher carbon flow required for chlorophyll than heme biosynthesis in plants, respectively. When Arabidopsis is germinating all tissues show transcripts of both genes. The ratio of PPX1 to PPX2 is lower in all germinating plant tissues than in actively growing leaves, though within the seedling the ratio is higher in the emerging cotyledons than in the emerging root where the ratio is closer to the nearly 1:1 ratio of the mature root. In waterhemp we showed an inverse of transcript levels compared to the *Arabidopsis* dataset with much greater expression of PPX2 transcripts than PPX1 (Fig. 2.3A-B), although that did not necessarily translate into a much greater protein expression, as both proteins had rather low signals in crude extracts (Fig. 2.3C-D) but PPX2 was more universally expressed. While this may explain the selection pressure for resistance mutations in PPO2 in waterhemp and closely related species such as Palmer amaranth, it would not account for the greater susceptibility in younger plants. Since group 14 herbicides are light-reactive, seedlings are likely killed as they emerge from the soil. Our data agrees with previous changes in resistance ratio between sensitive and resistant plants exposed to pre-emergent application, since most of the protein in the plant at that time would carry a resistance mutation,[6] but this alone does not explain why these resistant biotypes remain sensitive to post-emergent applications.

The amount of herbicide absorbed into the tissue after application is vital for the activity of herbicides. Differences in herbicide uptake can be caused by different levels of transporters, cuticle depth, leaf hair concentrations, and possibly other less obvious sources. [39] Our data show a decrease in herbicide absorbed in the older plants, up to a possible 43% reduction from 2-leaf stage to 6-leaf stage when plants would likely be treated (Fig. 2.4A), which correlates with a

68% reduction in proto levels measured in the sensitive biotype and a 40% reduction of proto levels in the resistant biotype (Fig. 2.4B). The overall lesser proto accumulation in the resistant biotype is likely due to the resistance mutation, though the amount of proto accumulated in both resistant and susceptible is equivalent or greater than amounts shown to cause damage. [5, 28]

It is known that antioxidant levels affect the efficacy of PPO inhibitors in both plants with naturally high antioxidant levels or in plants exposed to exogenous sources of antioxidants. [28, 29] Certain crops varieties can quench ROS generated by PPO inhibitors with elevated levels of antioxidants. Difference in tolerance of various tobacco biotypes to acifluorfen and S-23142 (another PPO- inhibiting herbicide) was associated to enhanced inducibility of the antioxidant system in the tolerant biotype.[40] A similar observation was made with soybean cultivars with varying tolerance to sulfentrazone associated with their intrinsic differential tolerance to the herbicide-induced peroxidative stress.[41] Radish and common chickweed (*Stellaria media*) are very tolerant to PPO inhibitors and do not develop foliar injury because they have extremely high antioxidant content.[42, 43] However, this mechanism of tolerance to PPO inhibitors does not seem to be universal across plant species.[42, 44] The high antioxidative potential of plants at a stage of development when herbicides are applied post-emergent (6-leaf stage or later) could account for some of the differential resistance seen between pre and post emergent treatments (Fig. 2.5).

Based on early research into 5-aminolevulinic acid (ALA) [5] and the recent discovery of the interaction between glufosinate and PPO inhibitor chemistry [45], we know that increasing the carbon flow toward the tetrapyrrole pathway synergizes the activity of PPO herbicides. Early experiments with ALA were tested by supplementation, and glufosinate likely increases activity in a similar manner by increasing free glutamate levels. The hypothesis was tested by exposing

whole plants to glutamate through the roots. The activity of acifluorfen increased in WUS plants exposed to an exogenous source of glutamate and glutamine (which can be rapidly converted to glutamate by glutamine oxoglutarate aminotransferase). To determine if glutamate and glutamine are major contributors to the difference between pre and post efficacy of group 14 herbicides, we measured the amount of free glutamate and glutamine in developing plants. Data show the pool of glutamate, and easily converted glutamine, is low in emerging cotyledons and then stable at a higher level in all other tissues. This trend does not give an explanation for the increased activity of PPO inhibitors in younger tissue. The observation of free amino acids, though, may be an inaccurate representation of total carbon flow through the tetrapyrrole pathway. True measures of pathway flux should be explored more thoroughly.

In conclusion the difference in effective doses of pre-emergent and post-emergent applications of PPO inhibiting herbicides are likely due to a combination of factors. Target protein levels do not appear to contribute to the differential sensitivity between seedlings and more mature plants. On the other hand, greater herbicide absorption paired with lower antioxidative potentials observed in seedling, relative to the lower herbicide absorption and greater antioxidative capacity in the older plants could account for the different response to pre- and post-emergent treatment in both sensitive and resistant biotypes. The potential role of differential metabolic detoxification between seedlings and older plants remains to be explored.

REFERENCES

1. Oerke, E.C., *Crop losses to pests.* The Journal of Agricultural Science, 2006. **144**(01): p. 31-31.
2. Green, J.M., *Current state of herbicides in herbicide-resistant crops.* Pest Management Science, 2014. **70**(9): p. 1351-1357.
3. Bell, M.S. and P.J. Tranel, *Time requirement from pollination to seed maturity in waterhemp (Amaranthus tuberculatus).* Weed science, 2010. **58**(2): p. 167-173.
4. Jacobs, J.M., N.J. Jacobs, and S.O. Duke, *Protoporphyrinogen destruction by plant extracts and correlation with tolerance to protoporphyrinogen oxidase-inhibiting herbicides.* Pesticide biochemistry and physiology, 1996. **55**(1): p. 77-83.
5. Sherman, T.D., et al., *Physiological basis for differential sensitivities of plant species to protoporphyrinogen oxidase-inhibiting herbicides.* Plant physiology, 1991. **97**(1): p. 280-287.
6. Lillie, K.J., D.A. Giacomini, and P.J. Tranel, *Comparing responses of sensitive and resistant populations of Palmer amaranth (Amaranthus palmeri) and waterhemp (Amaranthus tuberculatus var. rudis) to PPO inhibitors.* Weed Technology, 2020. **34**(1): p. 140-146.
7. Wuerffel, R.J., et al., *Characterization of PPO-Inhibitor–Resistant Waterhemp (Amaranthus tuberculatus) Response to Soil-Applied PPO-Inhibiting Herbicides.* Weed Science, 2015. **63**(2): p. 511-521.
8. Hager, A.G., et al., *Influence of diphenylether herbicide application rate and timing on common waterhemp (Amaranthus rudis) control in soybean (Glycine max).* Weed technology, 2003. **17**(1): p. 14-20.
9. Dayan, F.E., et al., *Herbicide mechanisms of action and resistance.* 2019.
10. Matringe, M., et al., *Localization within chloroplasts of protoporphyrinogen oxidase, the target enzyme for diphenylether-like herbicides.* Journal of Biological Chemistry, 1992. **267**(7): p. 4646-4651.
11. Kenyon, W., S. Duke, and K. Vaughn, *Sequence of effects of acifluorfen on physiological and ultrastructural parameters in cucumber cotyledon discs.* Pesticide Biochemistry and Physiology, 1985. **24**(2): p. 240-250.
12. Takano, H.K., et al., *Reactive oxygen species trigger the fast action of glufosinate.* Planta, 2019. **249**(6): p. 1837-1849.
13. Becerril, J. and S.O. Duke, *Acifluorfen effects on intermediates of chlorophyll synthesis in green cucumber cotyledon tissues.* Pesticide Biochemistry and Physiology, 1989. **35**(2): p. 119-126.
14. Cornah, J.E., et al., *Measurement of ferrochelatase activity using a novel assay suggests that plastids are the major site of haem biosynthesis in both photosynthetic and non-photosynthetic cells of pea (Pisum sativum L.).* Biochem J, 2002. **362**(Pt 2): p. 423-432.
15. Watanabe, N., et al., *Dual Targeting of Spinach Protoporphyrinogen Oxidase II to Mitochondria and Chloroplasts by Alternative Use of Two In-frame Initiation Codons.* Journal of Biological Chemistry, 2001. **276**(23): p. 20474-20481.
16. Dayan, F.E. and E.A. Dayan, *Porphyrins: One ring in the colors of life.* American Scientist, 2011. **99**(3): p. 236-243.
17. Gaines, T.A., et al., *Mechanisms of evolved herbicide resistance.* Journal of Biological Chemistry, 2020. **in press**.

18. Heap, I. *The International Survey of Herbicide Resistant Weeds*. 2020 [cited 2020 April 2020]; Available from: www.weedscience.org.
19. Patzoldt, W.L., et al., *A codon deletion confers resistance to herbicides inhibiting protoporphyrinogen oxidase.* Proceedings of the National Academy of Sciences of the United States of America, 2006. **103**(33): p. 12329-34.
20. Rousonelos, S.L., et al., *Characterization of a Common Ragweed (Ambrosia artemisiifolia) Population Resistant to ALS- and PPO-Inhibiting Herbicides.* Weed Science, 2012. **60**(3): p. 335-344.
21. Giacomini, D.A., et al., *Two new PPX2 mutations associated with resistance to PPO-inhibiting herbicides in Amaranthus palmeri.* Pest Management Science, 2017.
22. Rangani, G., et al., *A novel single-site mutation in the catalytic domain of protoporphyrinogen oxidase IX (PPO) confers resistance to PPO-inhibiting herbicides.* Frontiers in plant science, 2019. **10**: p. 568.
23. Bi, B., et al., *A Novel Mutation A212T in Chloroplast Protoporphyrinogen Oxidase (PPO1) Confers Resistance to PPO Inhibitor Oxadiazon in Eleusine indica.* Pest Management Science, 2019.
24. Varanasi, V.K., C. Brabham, and J.K. Norsworthy, *Confirmation and characterization of non–target site resistance to fomesafen in Palmer amaranth (Amaranthus palmeri).* Weed Science, 2018. **66**(6): p. 702-709.
25. Obenland, O.A., et al., *Carfentrazone-ethyl resistance in an Amaranthus tuberculatus population is not mediated by amino acid alterations in the PPO2 protein.* PloS one, 2019. **14**(4).
26. Dayan, F.E., et al., *Biochemical and structural consequences of a glycine deletion in the a-8 helix of protoporphyrinogen oxidase.* Biochimica et Biophysica Acta - Proteins and Proteomics, 2010. **1804**(7): p. 1548-1556.
27. Caverzan, A., et al., *Defenses against ROS in crops and weeds: The effects of interference and herbicides.* International journal of molecular sciences, 2019. **20**(5): p. 1086.
28. Dayan, F.E., et al., *The role of antioxidants in the protection of plants against inhibitors of protoporphyrinogen oxidase.* Reactive Oxygen Species, 2019. **7**(19): p. 55–63-55–63.
29. Finckh, B.F. and K.J. Kunert, *Vitamin C and E: An antioxidative system against herbicide-induced lipid peroxidation in higher plants.* Journal of Agricultural and Food Chemistry, 1985. **33**(4): p. 574-577.
30. Dayan, F.E., et al., *Horseradish peroxidase-dependent oxidation of deuteroporphyrin IX into chlorins.* Archives of Biochemistry and Biophysics, 1998. **351**(1): p. 27-34.
31. Dayan, F.E., et al., *Thiol-dependent degradation of protoporphyrin IX by plant peroxidases.* FEBS Letters, 1999. **444**(2-3): p. 227-230.
32. Yaffe, H., et al., *LogSpin: a simple, economical and fast method for RNA isolation from infected or healthy plants and other eukaryotic tissues.* BMC research notes, 2012. **5**(1): p. 1-8.
33. Montgomery, J.S., D.A. Giacomini, and P.J. Tranel, *Molecular confirmation of resistance to PPO inhibitors in Amaranthus tuberculatus and Amaranthus palmeri, and isolation of the G399A PPO2 substitution in A. palmeri.* Weed Technology, 2021. **35**(1): p. 99-105.
34. Giacomini, D.A., et al., *Coexpression clusters and allele-specific expression in metabolism-based herbicide resistance.* Genome biology and evolution, 2020. **12**(12): p. 2267-2278.
35. Schmittgen, T.D. and K.J. Livak, *Analyzing real-time PCR data by the comparative CT method.* Nature protocols, 2008. **3**(6): p. 1101-1108.

36. Ritz, C., et al., *Dose-response analysis using R.* PloS one, 2015. **10**(12): p. e0146021.
37. Patzoldt, W.L., P.J. Tranel, and A.G. Hager, *A waterhemp (Amaranthus tuberculatus) biotype with multiple resistance across three herbicide sites of action.* Weed Science, 2005. **53**(1): p. 30-36.
38. Klepikova, A.V., et al., *A high resolution map of the Arabidopsis thaliana developmental transcriptome based on RNA-seq profiling.* The Plant Journal, 2016. **88**(6): p. 1058-1070.
39. Menendez, J., M.A. Rojano-Delgado, and R. De Prado, *Differences in herbicide uptake, translocation, and distribution as sources of herbicide resistance in weeds*, in *Retention, Uptake, and Translocation of Agrochemicals in Plants*. 2014, ACS Publications. p. 141-157.
40. Kömives, T. and G. Gullner, *Mechanisms of plant tolerance to photodynamic herbicides.* American Chemical Society Symposium Series, 1994. **559**: p. 177-190.
41. Dayan, F.E., et al., *Soybean (Glycine max) cultivar differences in response to sulfentrazone.* Weed Science, 1997. **45**(5): p. 634-641.
42. Matsumoto, H., J.J. Lee, and K. Ishizuka, *Variation in crop response to protoporphyrinogen oxidase inhibitors*, in *American Chemical Society Symposium Series*. 1994. p. 120-132.
43. Matsumoto, H., Y. Kashimoto, and E. Warabi, *Basis for common chickweed (Stellaria media) tolerance to oxyfluorfen.* Pesticide Biochemistry and Physiology, 1999. **64**(1): p. 47-53.
44. Dayan, F.E. and S.O. Duke, *Phytotoxicity of protoporphyrinogen oxidase inhibitors: Phenomenology, mode of action and mechanisms of resistance*, in *Herbicide Activity: Toxicology, Biochemistry and Molecular Biology*, R.M. Roe, J.D. Burton, and R.J. Kuhr, Editors. 1997, IOS Press: Amsterdam, Netherland. p. 11-35.
45. Takano, H.K., et al., *Glufosinate enhances the activity of protoporphyrinogen oxidase inhibitors.* Weed Science, 2020. **68**(4): p. 324-332.

CHAPTER 3: CONFORMATION OF THE INTERMEDIATES IN THE REACTION CATALYZED BY PROTOPORPHYRINOGEN OXIDASE: AN IN SILICO ANALYSIS[3]

INTRODUCTION

The porphyrin pathway plays a central role in the synthesis of many pigments fundamental to sustaining life across the biological realm [1-3]. Macrocyclic tetrapyrroles derived for this pathway have a varying degree of conjugation and can be chelated with metal dications such as the alkaline earth metal Mg^{2+}, transition metals such as Fe^{2+}, Co^{2+}, and Ni^{2+}, and group 12 element Zn^{2+}. These metals are coordinated with the pyrrole nitrogens at the center of these rings. Examples of biologically important metalloporphyrins include chlorophylls (Mg^{2+}), hemes (Fe^{2+}), vitamin B12 (Co^{2+}), and coenzyme F430 (Ni^{2+}).

Biosynthesis of porphyrins consists of 7 core enzymes that culminates in the action catalyzed by protoporphyrinogen oxidase (PPO) converting the colorless precursor protoporphyrinogen IX (protogen) into the fully conjugated, bright red pigment protoporphyrin IX (proto) [3]. PPO itself is of particular interest because mutations of the protein lead to variegate porphyria diseases in humans and in agriculture it is the protein target of the PPO-inhibiting herbicides which are seeing a resurgence of use in recent years [4, 5].

There have been many inquiries into the mechanism of the three sequential oxidation reactions which convert protogen into the fully conjugated proto. An early study of the biosynthesis of heme using isotopically labelled tetrapyrrole determined that the reaction involved hydride abstractions from three of bridging methylene groups [6]. This mechanism posited two significant mechanistic properties: the hydride ion was abstracted from the *meso* face

[3] This chapter contains published work from: Barker, A.L., H. Barnes, and F.E. Dayan, *Conformation of the Intermediates in the Reaction Catalyzed by Protoporphyrinogen Oxidase: An In Silico Analysis.* International journal of molecular sciences, 2020. **21**(24): p. 9495.

(α-H) and tautomerism around the neighboring tetrapyrrole ring resulted in the formation of a double bond (Fig. 1.1).

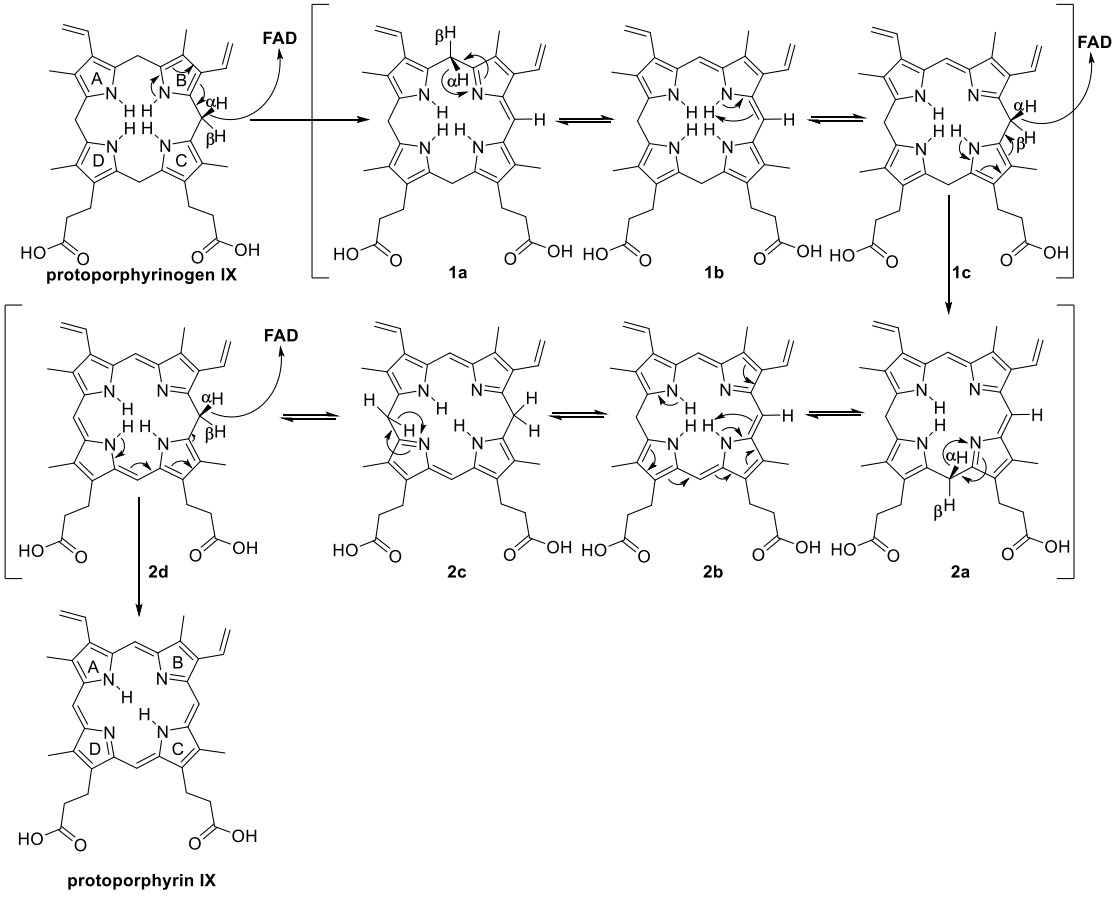

Figure 3.1. Putative reaction intermediates involved in the catalytic reaction of PPO converting protogen and proto. This figure is adapted from reaction scheme proposed by Koch et al. [7] but orienting the tetrapyrrole ring to match that of copro in its binding site in uroporphyrinogen decarboxylase (1R3Y) [8].

This mechanism required that protogen and the intermediates rotate within the catalytic domain so that the *meso* face of each methylene functionality was exposed to FAD for the next hydride abstraction to occur. However, elucidation of PPO's structure by X-ray crystallography suggested that protogen is held in a relatively fixed position within the catalytic domain by having the propionate group from ring D (Fig. 1.1) interacting with the guanidino functional group of Arg97 and maintaining the C10 carbon of protogen in close proximity to N5 of the

cofactor FAD [7]. Still, no published crystal structure of PPO has been reported with either the substrate or the product in the active site. A previous effort to bind protogen to PPO *in silico* was performed with the structure of protogen created by an extensive analysis process and a structure of PPO which was allowed to relax in a molecular dynamics simulation [9]. This method does not take into account the structure of the precursors in the pathway which are unlikely to change due to the repulsion of the hydrogen molecules in the center of the tetrapyrrole ring, and new methods with the Autodock program have simplified the analysis of flexible substrates such as protogen.

The most current understanding of PPO's reaction mechanism involves 3 subsequent hydride abstractions on C10 of protogen, the methylene bridge between pyrrole rings B and C, followed by tautomerization to regenerate the unsaturated state of C10 allowing for the next reaction [7]. Mechanistically, the first reaction is initiated by a 1:1 stoichiometric FAD as a coenzyme. The methylene functionality is prochiral because the α-H is much closer to N5 of FAD than the β-H (Fig. 3.1). Once the *meso* hydrogen is removed in the form of a hydride ion, it creates an unstable carbocation transition state at C10, which instantly rearranges in ring B as shown in intermediate 1a in Figure 3.1. The second reaction is an enamine-imine tautomerization from 1b to 1c resulting in the reformation of the methylene bridge at C10 by transfer of the proton from ring B pyrrole nitrogen. $FADH^-$ is oxidized to FAD by reaction with O_2 and the proton released from pyrrole N in the third reaction and generates H_2O_2. The second step repeats the same sequence of reactions. Oxidation of C10 by FAD, 1c and instant rearrangement of ring C, 2a followed by the enamine-imine tautomerization 2b to 2c and the subsequent reoxidation of $FADH^-$ to FAD. The third step involves the oxidation of C10 by FAD and four two electron rearrangements from ring D, 2d to yield proto.

Multiple crystal structures of PPO from differing organisms show similar folding despite a large variation in conservation of sequence: from around 90% identity between mammals to as low as 23% identity between mammalian and plant sequences (Supplementary Table S1). There are two separate isoforms of PPO in plant species which only share about 27% sequence identity, generally considered the chloroplastic and mitochondrial isoforms. Along with the mostly conserved structure, some conserved residues across phyla include the Arg97 region and the Phe353-Leu356 region [4]. One conserved feature is an unstructured loop that is not captured in any of the published crystal structures that is adjacent to the catalytic domain of the protein, located from residue 204 to 210 in the human PPO. The flexible nature of the loop and proximity to the reaction pocket could signify importance if these sequences are conserved across phyla.

We aim to better understand the reaction catalyzed by PPO by docking the substrate and product of the reaction along with relevant reaction intermediates, describe the reaction mechanism in a way that unifies previous data while taking into account the spatial limitation of the catalytic domain of PPO as well as information from substrate orientations upstream in the pathway, and to determine if sequence similarity suggests that the unstructured loop has a function in the reaction or substrate binding.

RESULTS AND DISCUSSION

Determining the initial conformation of protogen

Protogen is a very flexible tetrapyrrole because each pyrrole ring is connected to the other via unsaturated methylene bridges. There is no published crystal structure of protogen cocrystallized with any protein, and consequently it is difficult to predict the conformation of protogen in PPO. Free protogen creates a dramatically bent shape naturally because of the

repelling forces between the center hydrogen atoms. This natural shape does not fit in the catalytic domain of PPO. Furthermore, there is evidence of protein channeling or chaperoning of the intermediates in this pathway [10, 11]. Therefore we obtained a realistic starting conformation from the structure of coproporphyrinogen III (copro), which contains the same repelling hydrogens and flexible methylene bridges, cocrystallized with uroporphyrinogen decarboxylase (1R3Y) [8]. Since the only difference between copro and protogen is the presence of propionic acids instead of vinyl groups on rings A and B (Fig. 3.2), protogen was constructed from the coordinate of the optimized structure of copro. This slightly concave conformation is a particularly good starting point for docking protogen and the reaction intermediates because it fits relatively well in the catalytic domain of PPO.

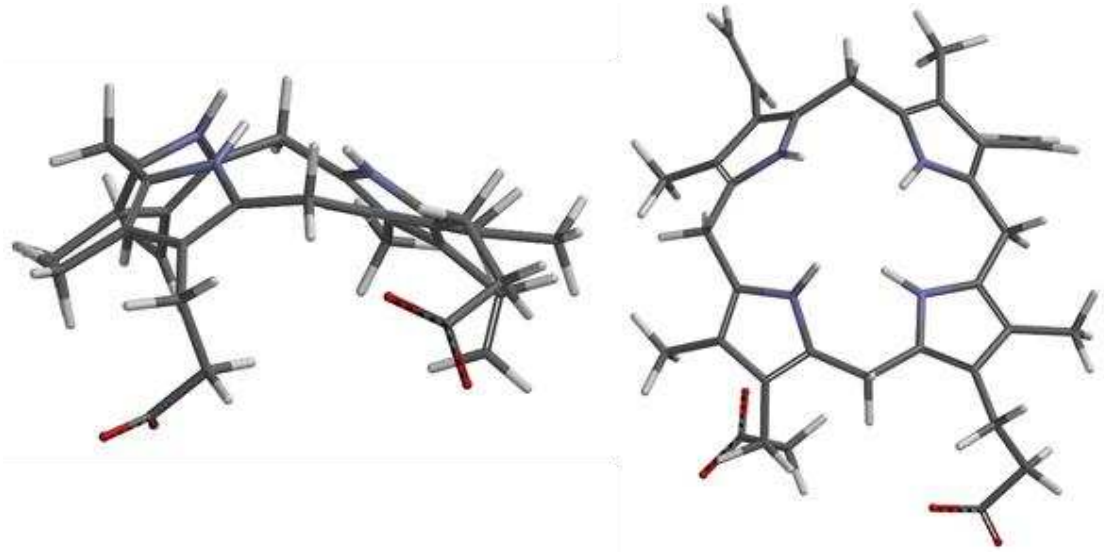

Figure 3.2. Starting conformation of geometrically optimized protogen based on the coordinates of copro in uroporphyrinogen decarboxylase (1R3Y) [8].

The structures of all the subsequent reaction intermediates were derived from this original confirmation by editing the mol2 files followed by geometric optimization with Spartan18 according to the putative reaction scheme proposed by Koch et al. [7] (Fig. 3.1).

Docking of Protogen, Tautomeric Reaction Intermediates and Proto to PPO

The reaction catalyzed by PPO involves 3 oxidative steps on the same carbon (C10) forming the methylene bridge between the B and C pyrrole rings followed by tautomeric rearrangements (Fig. 3.1). In order to dock protogen and all the relevant reaction intermediates in PPO, the docking protocol for Autodock was modified to allow flexibility of the tetrapyrrole macrocycles according to the method developed by Forli [12, 13]. The method consists of 'breaking' one of the bonds in the tetrapyrrole rings, replacing carbons at dummy atoms and applying a Lennard-Jones force between these dummy atoms to keep them proximal to each other during the docking procedure. Accordingly, we avoided bonds in partially rigid regions to reduce the complexity and calculation time without compromising accuracy. Consequently, the bond between the methylene carbon between rings C and D was selected (Fig. 3.3) since it is the most flexible bond throughout all the steps shown in Figure 3.1, due to the fact that it is the last single bond to be oxidized. This method creates a flexible ring system with an increased number of rotatable bonds to be considered during calculations.

Proto was obtained from x-ray analysis of protoporphyrin IX dimethyl ester by removing the methyl esters. The fully conjugated product of the reaction catalyzed by PPO is known to be a non-flexible planar structure and was docked in PPO without breaking the cyclic tetrapyrrole. The location of the catalytic domain was defined using a gridbox that encompassed the FAD forming the 'roof' of the cavity and, the top of α-8 helix of PPO upon which the tetrapyrrole rings are centered at the 'bottom' of the cavity, and Arg97 involved in stabilizing the rings on the right side of the cavity (Supplemental Figure S1).

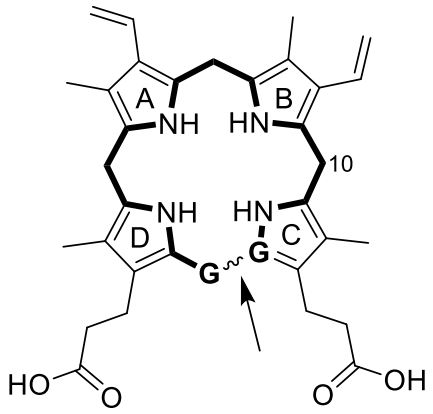

Figure 3.3. Localization of the broken bond (arrow) and respective dummy atoms (labeled **G**) selected to allow docking of the flexible ring system of the tetrapyrrole intermediates in the conversion of protogen to the last tautomer before proto. The carbon (C10) where the hydride transfers occur is labelled.

After the docking, RMSD of the clusters with best poses for each tetrapyrrole intermediate provide insight to the changes in the curvature of the tetrapyrroles during the oxidation between protogen and proto (Fig. 3.4). The RMSD for protogen is small, relative to the other reaction intermediates 1a, 1c, 2a and 2d. The low RMSD of protogen is most likely a reflection of the flexibility afforded by the fully unsaturated methylene bridges linking the pyrrole rings. In fact, the movement of the propionate side chains probably accounts for a significant portion of the RMSD. On the other hand, the increased RMSD of the reaction intermediates is due to the increased rigidity and planarity of the macromolecules as additional double bonds are introduced in the methylene bridges. The RMSD of the proto is also low. It should be noted that this refers to the coordinates of the crystal structure published by Caughey and Ibers [14]. Since proto retained its planar conformation relative to the starting conformer used for docking, little change in the shape of the tetrapyrrole ring is expected. As with protogen, a significant portion of the RMSD is probably due the movement of the propionate side chains.

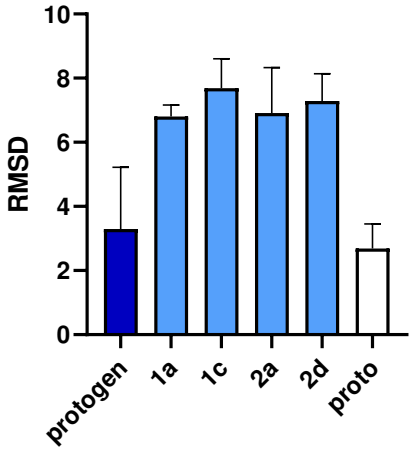

Figure 3.4. RMSD of the clusters with best poses for each tetrapyrroles relative to the conformations of the starting conformers prior to docking. Note that the starting conformers for protogen, 1a, 1c, 2a and 2d were designed using the coordinates of coproporphyrinogen bound within uroporphyrinogen carboxylase (1R3Y) [8], whereas the starting conformer of proto is based on the published planar coordinate of this molecule [14].When docked in the catalytic domain the binding energy of protogen averaged −10.59 ± 1.08 kcal/mol (Fig. 3.5). The binding energies of all reaction intermediates and proto were on average 40% greater than that of protogen, ranging from −6.00 to −7.27 kcal/mol. This is accounted for by the fact that protogen is the most flexible of the tetrapyrroles, having 4 saturated methylene bridges connecting each pyrrole rings. All subsequent tetrapyrroles are less flexible because of the introduction of an increasing number of unsaturated methylene bridges, leading to the fully conjugated and least flexible product of the reaction (proto). These binding energies agree with the paradigm of PPO-protogen > PPO-proto established in Hao et al. [9].

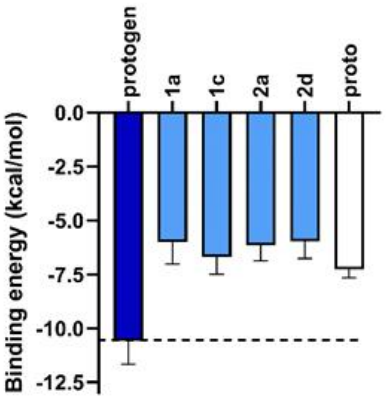

Figure 3.5. Binding energy (kcal/mol) of protogen (dark blue bars), reactions intermediates (light blue bars) and proto (white bars) to human PPO. The more negative the binding energy reflects a better fit within the catalytic domain. Dotted line represents the average binding energy of protogen.

The docking protocol allowed for the propionate groups of either ring C or D to interact with the guanidino functional group of Arg97 (Fig. 3.6), all the docked molecules from cluster 1 assumed the expected pose with the propionate group from ring D interacting with and maintaining the C10 carbon of protogen in close proximity to N5 of the cofactor FAD (Fig. 3.6) [7]. On average the propionate group was between 4.3 and 4.6 Å from Arg 97 and the C10 of protogen (and the reaction intermediates) was between 3.3 and 4.1 Å from N5 of FAD (Table 3.1).

Table 3.1. Summary of the parameters associated with the molecules docked in the expected orientation in PPO.

	Selected Docked Molecules [1]	**Distance between N5 of FAD and C10 of Tetrapyrrole (Å)**	**Distance between Propionate Group and Arg97 (Å)**
Protogen	23	4.4 ± 0.5	3.3 ± 0.8
1a	22	4.3 ± 0.7	3.5 ± 0.9
1c	12	4.3 ± 0.5	3.3 ± 0.5
2a	17	4.5 ± 0.6	3.7 ± 1.3
2d	20	4.3 ± 0.5	4.1 ± 1.7
Proto	26	4.6 ± 0.2	4.1 ± 0.8

[1] Total # of docked molecules: $n = 50$.

A key feature of the reaction postulated by Koch et al. [7] is that the oxidation of protogen to proto involves three sequential hydride abstraction from C10 of the substrate and subsequent reaction intermediate catalyzed at the N5 of FAD. Our docking study supports this by consistently positioning the α-H from the C10 of the tetrapyrroles facing the re-face of N5 of FAD. Furthermore, the average distance between N5 and α-H range from 3.6 to 3.7 Å (Table 2), which is within the known range for redox reactions catalyzed by FAD enzymes [15-21]. On the other hand, the β-H are on average 1.4 Å further from the N5 of FAD (range from 5.0–5.1 Å).

The second step requires tautomerization with an adjacent pyrrole ring and subsequent loss of a proton from the pyrrole nitrogen, to regenerate the sp3 carbon at C10 prior to the next hydride abstraction. Experiments using isotopically labeled substrates suggested that the α-Hs were preferentially removed during the oxidation of protogen into proto (Fig. 3.1) [6]. Docking of protogen and the reaction intermediates revealed that the poses with the lowest binding energy had the tetrapyrrole rings in a slightly concave conformation for optimal fit within the catalytic domain of PPO (Fig. 3.6). In this conformation, the α-Hs are closer than the β-Hs to the adjacent pyrrole bond involved in the tautomerization (Table 2), which accounts for the preferential loss of the *meso* hydrogen reported by Jones et al. [6].

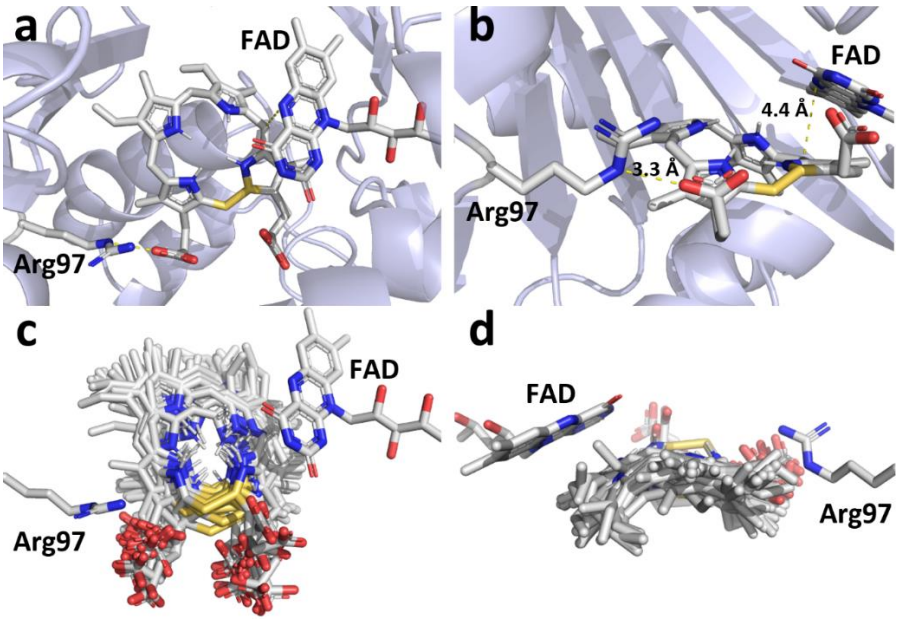

Figure 3.6. Docking of protogen to PPO using Autodock with Lennard-Jones forces. Similar results were obtained with other reaction intermediates (Supplemental Figures S3.2–S3.6). View of the docked proto with the most favorable binding energy (**a**) from above and (**b**) from the opening of the catalytic domain. All of the top docking orientation group are shown to indicate flexibility within the pocket from above (**c**) and from the back of the pocket (**d**) Yellow dotted lines represent the interactions between protogen and PPO. The average distances between the N5 of FAD and C10 of protogen and between the propionate group of ring D and the Arg97 of PPO are shown in panel (**b**). Gold bonds represent the location of the Lennard-Jones forces between two dummy atoms.

Table 3.2. Distance between Summary of the parameters associated with the molecules docked in the expected orientation in PPO.

	Distance between C10 Methylene H and N5 of FAD (Å) [1]		**Distance between Methylene H and Pyrrole N (Å) [1]**	
	α-H	**β-H**	**α-H**	**β-H**
Protogen	3.7 ± 0.8	5.1 ± 0.7	-	-
1a	-	-	3.0 ± 0.1	3.3 ± 0.1
1c	3.6 ± 0.6	5.0 ± 0.8	-	-
2a	-	-	2.9 ± 0.2	3.3 ± 0.1
2d	3.6 ± 0.6	5.0 ± 0.7	-	-

[1] Refer to Figure 3.1 for position of α-H and β-H on C10 in protogen and intermediates 1c and 2d involved in the hydride abstraction, and on the methylene carbons on intermediates 1a and 2a involved in initiating the tautomerization restoring the sp3 state of C10 prior to the next oxidation.

Hydride abstractions are involved in many enzymatic reactions [21-23]. However, the mechanisms involved in hydride transfers had never been demonstrated empirically in biological systems until the recent groundbreaking work on protochlorophyllide oxidoreductase [24]. While that study involves a tetrapyrrole molecule downstream from PPO, the enzyme being considered herein, the reaction is not identical. In the case of protochlorophyllide oxidoreductase, the cofactor is NADPH (instead of FAD), and the direction of the hydride transfer is from the cofactor to ring D of the substrate, rather than from the methylene bridge between ring B and C of the substrate to the cofactor. Nevertheless, this new understanding of hydride transfer mechanisms provides some relevant insight in the reaction catalyzed by PPO. Indeed, the participation of FAD in a wide range of redox reactions is well documented [23, 25]. In particular, the N5 of the oxidized tricyclic isoalloxazine ring system is often a site for hydride addition, converting FAD to $FADH^-$ [26].

Characterization of the Disordered Loop Crossing the Opening of PPO Binding Domain

Following the docking, an alignment was created of the top 80 related sequences to the human PPO sequence from the crystal structure used for this research to investigate the unstructured, flexible loop region near the catalytic domain, from residues 204–210. The flexibility and proximity could indicate that the loop has a function in the binding of the substrate or the release of the product. Residues that are conserved in homologous proteins between species and phyla are often associated with important function [27]. Alignment of the top 80 sequences showed a lack of homology from residue 205–209 which covers the entire sequence that is not captured in crystal structures. Furthermore, in the alignment of sequences across phyla the loop is not only not conserved at the residue level but varies in length as well (Fig. 3.7). In protein structure predictions, across all species, the region is considered a solvent exposed region and a disordered region showing no defined secondary structure. Based on these observations, it is unlikely that the region is directly involved with the binding of the substrate or the reaction carried out by PPO. Conservation of the flexible region could indicate the necessity of movement near the catalytic domain to accommodate substrate and product movement.

```
PPO C. elegans                  NMKMCYVK---DEKDIRHEIPSFMTSLQAPPP-----------------------PPPP   194
PPO Saccharomyces cerevisiae    SAKRTFKKIYYNELKHGSNTQAMIDNMRGKSRSKKTENLHQSLTGCLNDYSNAFGKDRSK   255
PPO2 Drosophila melanogaster    SVRFLMEGLFEKEQKYGGVLKGTLISRFEKNKTKDTKDGL-------------FA-ERQP   222
PPO Trichoplax sp. H2           SMKACFPQVVNYEEQYGSILAGALLDKAIPIS----------------------EVDC   223
PPO2 Danio Rerio                SVRSCFPPLYEAEQARGSIVLGMLMGSGAGPK----------------------VVPS   214
PPO2 Anolis carolinensis        SVRSCFPALFQAERAHRSVILGMTLAGGKGAP----------------------ALDS   214
PPO2 Homo sapiens               SIRSCFPSLFQAEQTHRSILLGLLLGAGR-TP----------------------QPDS   213
PPO2 Mus musculus               SIRSCFPSLFQAEQTHRSILLGLLLGAGQ-SP----------------------QPDS   213
PPO2 Oryza sativa japonica      SIRHAFPALWNLENKYGSVIAGAILSKLSTKGDSV----------┼-------KT-GGAS   226
PPO2 Arabidopsis thaliana       SMKHSFPDLWNVEKSFGSIIVGAIRTKFAAKGGKS------------------RD-TKSS   229
PPO2 Nicotiana tabacum          SMHHSFPELWNLEKRFGSVILGAIRSKLSPKNEKK------------------QG-PPKT   225
PPO Bacillus subtilis           SLMSTFPQFYQTEQKHRSLILGMKKTRPQGSG--------------------------Q   217
PPO Myxococcus Xanthus          SVAATFPMLVKMEREHRSLILGAIRAQKAQRQAAL------------------PA-GTAP   224
PPO Chlamydamonas reinhardtii   SMKAAFNRIWILEKNGGSLVGGAIKLFQERQSNPA------------------P--PRDP   289
PPO1 Arabidopsis thaliana       SMKAAFGKVWKLEQNGGSIIGGTFKAIQERKNAPK------------------A--ERDP   266
PPO1 Nicotiana tabacum          SMKAAFGKVWKLEETGGSIIGGTFKAIKERSSTPK------------------A--PRDP   277
```

Figure 3.7. Alignment of 16 representative PPO sequences from model organisms with well characterized genomes, in the region of the unstructured loop. The loop from the human structure is highlighted.

CONCLUSIONS

A novel docking model for protogen in the catalytic domain of PPO was created using a protogen structure derived from the crystal structure of a close precursor in the pathway, copro, bound to the catalytic domain of uroporphyrinogen decarboxylase. The intermediates in the pathway were created on the same backbone structure for docking, and the product proto was created based on previous crystallographic data. Binding energy for protogen was the most favorable with an average of −10.59 ± 1.08 kcal/mol, and the intermediates and product showed binding energies ~40% higher. The binding energies are consistent with the flexibility of the molecules, protogen being the most flexible and each intermediate thereafter reducing flexibility with the addition of double bonds. The docked molecules with the most energetically favorable positions all maintained an association between the propionate group of ring D and Arg98, which held the α-H of C10 within the appropriate range for redox reactions to occur with the N5 of FAD (3.6–3.8 Å). The findings here unify early experiments noting the hydride abstractions with the current understanding of the catalytic domain of PPO and known precursor conformations in the pathway. Finally, the unstructured loop near the opening to the catalytic domain was investigated for possible interaction with the substrate. A complete lack of homology, even within a phyla, indicates that no particular residue interacts with the substrate, but the conservation of the flexible region may indicate the necessity of accommodating substrate and product movement near the catalytic domain.

MATERIALS AND METHODS

Determining the initial conformation of protogen and construction of all the reaction intermediates.

Conformation of protogen was from derived from the structure of coproporphyrinogen III (copro) cocrystallized with uroporphyrinogen decarboxylase (1R3Y) [8]. This structure was extracted from the pdb file and saved as a mol2 file. As is common for ligand structures determined by protein crystallography, the atom types and bond orders of copro had to be reconstructed *in silico* using a molecular modelling and computational chemistry application (Spartan18, Wavefunction, Inc. Irvine, CA 92612). The bond angles and length were corrected by submitting the individual pyrrole rings to geometric minimization using density function theory calculations (wB97X-D 6-31*) (Supplemental Fig. S3.7). The propionic acid groups found on rings A and B of the tetrapyrrole were converted to vinyl groups to convert copro into protogen. Once protogen was constructed, all the reaction intermediates (1a, 1c, 2a, 2d) were built from this original confirmation by editing the mol2 files and submitted to geometric optimization with Spartan18. The structure of proto was obtained from the x-ray analysis of protoporphyrin IX dimethyl ester [14] deposited in The Cambridge Crystallographic Data Centre (CCDC) [28]. Spartan18 was used to remove the methyl esters and convert the propionic acids to propionate.

Docking of protogen, tautomeric reaction intermediates and proto to PPO

The crystal structure of human PPO was obtained from 3nks [29]. The atom types of FAD were corrected using Spartan 18 and the ligand was converted to its oxidized form. The electrostatic charges were calculated using density function theory calculations (wB97X-D 6-31*).

Protogen and all of the reaction intermediates were docked into the catalytic domain of PPO using a modified Autodock method using Lennard-Jones potential and dummy atoms to overcome the software's limitation (AutoDock version 4.2, Scripps Institute, San Diego CA, USA) in handling flexible ring systems (Fig. 3.3) [12, 13, 30, 31]. This was done by editing the ligand.pdbqt files. Additionally, the guanidino group of arginine 97 was designated as important in the interaction between one of the propionate groups and a grid box was used to delimitate the region of the catalytic domain according to the software [13]. The gridbox dimensions were set to 90×75×75 points with a spacing to 0.2. The box was centered on the following coordinates: x = −26.88, y = 4.47 and z = 45.17. PPO was set as a rigid structure (Supplementary Fig. S3.1). The cyclic tetrapyrroles modified to allow for flexible docking designed in the previous section were used for docking within the space defined in the gridbox. The algorithm was set to generate 50 docking poses and the top clustered was selected as optimal conformation for the docking of each ligand.

Modeling of disordered loop crossing the opening of PPO binding domain

The human PPO sequence was blasted in the NCBI database and the top 80 related sequences were selected. A second data set of 16 high quality PPO sequences spanning multiple phyla were selected to determine base homology (Supplemental Table S1). The two datasets were aligned using Clustal Omega [32]. The loop sequences from the more diverse dataset were compared from the alignment and then run through two predictive structure programs: Phyre2 [33] and PredictProtein [34].

REFERENCES

1. Battersby, A.R., *Tetrapyrroles: The pigments of life.* Natural Product Reports, 2000. **17**: p. 507-526.
2. Thunell, S., *Porphyrins, porphyrin metabolism and porphyrias. I. Update.* Scandinavian Journal of Clinical Laboratory Investigation, 2000. **60**: p. 509-540.
3. Mochizuki, N., et al., *The cell biology of tetrapyrroles: a life and death struggle.* Trends in Plant Science, 2010. **15**(9): p. 488-498.
4. Dayan, F.E., A. Barker, and P.J. Tranel, *Origins and structure of chloroplastic and mitochondrial plant protoporphyrinogen oxidases: implications for the evolution of herbicide resistance.* Pest Management Science, 2018. **74**: p. 2226-2234.
5. Wang, B., et al., *Acute hepatic porphyrias: Review and recent progress.* Hepatology Communications, 2019. **3**(2): p. 193-206.
6. Jones, C., P.M. Jordan, and M. Akhtar, *Mechanism and stereochemistry of the porphobilinogen deaminase and protoporphyrinogen IX oxidase reactions: Stereospecific manipulation of hydrogen atoms at the four methylene bridges during the biosynthesis of haem.* Journal of the Chemical Society Perkin Transactions 1, 1984: p. 2625-2633.
7. Koch, M., et al., *Crystal structure of protoporphyrinogen IX oxidase: a key enzyme in haem and chlorophyll biosynthesis.* EMBO Journal, 2004. **23**: p. 1720-1728.
8. Phillips, J.D., et al., *Structural basis for tetrapyrrole coordination by uroporphyrinogen decarboxylase.* The EMBO Journal, 2003. **22**(23): p. 6225-6233.
9. Hao, G.-F., et al., *Computational and experimental insights into the mechanism of substrate recognition and feedback inhibition of protoporphyrinogen oxidase.* PloS one, 2013. **8**(7): p. e69198.
10. Medlock, A.E., et al., *Identification of the mitochondrial heme metabolism complex.* PLoS ONE, 2015. **10**(8): p. 1-20.
11. Ferreira, G.C., et al., *Organization of the terminal two enzymes of the heme biosynthetic pathway. Orientation of protoporphyrinogen oxidase and evidence for a membrane complex.* Journal of Biological Chemistry, 1988. **263**(8): p. 3835-3839.
12. Forli, S. and M. Botta, *Lennard-Jones potential and dummy atom settings to overcome the AUTODOCK limitation in treating flexible ring systems.* Journal of Chemical Information and Modeling, 2007. **47**(4): p. 1481-1492.
13. Morris, G.M., et al., *AutoDock4 and AutoDockTools4: Automated docking with selective receptor flexibility.* Journal of computational chemistry, 2009. **30**(16): p. 2785-2791.
14. Caughey, W.S. and J.A. Ibers, *Crystal and molecular structure of the free base porphyrin, protoporphyrin IX dimethyl ester.* Journal of the American Chemical Society, 1977. **99**(20): p. 6639-6645.
15. Ismail, A., et al., *Coenzyme Q biosynthesis: Evidence for a substrate access channel in the FAD-dependent monooxygenase Coq6.* PLoS computational biology, 2016. **12**(1): p. e1004690-e1004690.
16. Lennon, B.W., C.H. Williams Jr., and M.L. Ludwig, *Crystal structure of reduced thioredoxin reductase from Escherichia coli: Structural flexibility in the isoalloxazine ring of the flavin adenine dinucleotide cofactor.* Protein Science, 1999. **8**(11): p. 2366-2379.

17. Eswaramoorthy, S., et al., *Mechanism of action of a flavin-containing monooxygenase.* Proceedings of the National Academy of Sciences, USA, 2006. **103**(26): p. 9832-9837.
18. Stirling, A.J., et al., *A key glycine in bacterial steroid-degrading acyl-CoA dehydrogenases allows flavin-ring repositioning and modulates substrate side chain specificity.* Biochemistry, 2020.
19. Lans, I., et al., *Theoretical study of the mechanism of the hydride transfer between ferredoxin–NADP$^+$ reductase and NADP$^+$: The role of Tyr303.* Journal of the American Chemical Society, 2012. **134**(50): p. 20544-20553.
20. Lans, I., et al., *Mechanism of the hydride transfer between Anabaena Tyr303Ser FNRrd/FNRox and NADP+/H. A combined pre-steady-state kinetic/ensemble-averaged transition-state theory with multidimensional tunneling study.* The Journal of Physical Chemistry B, 2010. **114**(9): p. 3368-3379.
21. Hammes-Schiffer, S., *Comparison of hydride, hydrogen atom, and proton-coupled electron transfer reactions.* ChemPhysChem, 2002. **3**(1): p. 33-42.
22. Peters, K.S., *A theory-experiment conundrum for proton transfer.* Accounts of Chemical Research, 2009. **42**: p. 89-96.
23. Walsh, C.T. and T.A. Wencewicz, *Flavoenzymes: versatile catalysts in biosynthetic pathways.* Natural product reports, 2013. **30**(1): p. 175-200.
24. Archipowa, N., et al., *Stepwise hydride transfer in a biological system: Insights into the reaction mechanism of the light-dependent protochlorophyllide oxidoreductase.* Angewandte Chemie, 2018. **130**(10): p. 2712-2716.
25. Piano, V., B.A. Palfey, and A. Mattevi, *Flavins as covalent catalysts: New mechanisms emerge.* Trends in Biochemical Sciences, 2017. **42**(6): p. 457-469.
26. Ghisla, S. and V. Massey, *Mechanisms of flavoprotein-catalyzed reactions*, in *EJB Reviews 1989*. 1989, Springer Berlin Heidelberg: Berlin, Heidelberg. p. 29-45.
27. Valdar, W.S., *Scoring residue conservation.* Proteins: structure, function, and bioinformatics, 2002. **48**(2): p. 227-241.
28. Groom, C.R., et al., *The Cambridge structural database.* Acta Crystallographica Section B, 2016. **72**(2): p. 171-179.
29. Qin, X., et al., *Structural insight into human variegate porphyria disease.* The FASEB Journal, 2011. **25**(2): p. 653-664.
30. Forli, S., et al., *Computational protein-ligand docking and virtual drug screening with the AutoDock suite.* Nature protocols, 2016. **11**(5): p. 905-919.
31. Lohning, A.E., et al., *A practical guide to molecular docking and homology modelling for medicinal chemists.* Current Topics in Medicinal Chemistry, 2017. **17**: p. 1-18.
32. Madeira, F., et al., *The EMBL-EBI search and sequence analysis tools APIs in 2019.* Nucleic acids research, 2019. **47**(W1): p. W636-W641.
33. Kelley, L.A., et al., *The Phyre2 web portal for protein modeling, prediction and analysis.* Nature Protocols, 2015. **10**(6): p. 845-858.
34. Yachdav, G., et al., *PredictProtein—an open resource for online prediction of protein structural and functional features.* Nucleic acids research, 2014. **42**(W1): p. W337-W343.

CHAPTER 4: NOVEL ARTIFICIAL INTELLIGENCE PLATFORM LEADS TO THE DISCOVERY OF NEW PROTOPORPHYRINOGEN OXIDASE INHIBITORS[4]

INTRODUCTION

Current agriculture faces new struggles against unpredictable weather pattern changes associated with climate change and managing a myriad of pests that impact crop productivity. Weeds are the most problematic pests because these undesirable plants reduce crop yields by competing for space and resources (light, nutrients, water) and cause billions of dollars in annual loss [1, 2]. Consequently, modern agricultural practices rely heavily on the use of synthetic herbicides. While herbicides have been a major contributor to the success of agriculture, they have imposed a strong selection pressure over millions of farming acres, leading to the evolution of herbicide resistance in hundreds of weed species [3]. Both target-site resistance (TSR) and nontarget-site resistance (NTSR) mechanisms have evolved to most herbicide classes [4].

Nearly three decades of silence in respect to new herbicide mechanisms of action (MoA) have left farmers in great need of new, effective tools. New weed management methods are being developed to address the current weed resistance problems, including non-chemical approaches,[5, 6] but chemical tools remain the most cost effective and no-tillage friendly [7]. Recently, there has been a flurry of reports of new modes of action to break this silence [8]. Most of these reports are from research groups within the AgChem industry. However, several startup companies have also joined the fray with novel approaches to the discovery of interesting chemistry and new mechanisms of action.

---

[4] Author information: Abigail L. Barker[*], Yael Phillip[†], Ifat Shub[†], Eyal Ben-Chanoch[‡], Franck E. Dayan[*]
[*]Department of Agricultural Biology, Colorado State University, Fort Collins CO USA.
[†]Agrematch Ltd., Plaut 10 St., Rehovot Science Park, Israel.
[‡]Agrematch Ltd., 3825 Bayside Ct, Miami FL USA.

Understanding the process by which companies discover new herbicides grants insight into the lack of new herbicide options. There are five main steps to the development of a crop protection agent, which take on average 11 years[9]: early research, when a molecule is discovered through some pipeline and its MoA and toxicity are investigated; optimization, when the molecule is taken through formulation improvements and greenhouse testing against crops and weeds; field trials, when this testing is taken to realistic conditions and large scale safety studies; development, which includes regulatory hurdles and registration of the commercial product; and finally launch, when the product is released and stewarded by the company. Due to tightening regulations on target site knowledge and lower toxicity acceptance companies are screening upwards of 160,000 molecules to find one possible target. [9] Large AgChem companies differ from startup companies (e.g., Agrematch, MoA Technology and Enko). AgChem companies still rely mostly on large scale, automated screening processes utilizing available molecule libraries. On the other hand, startup companies have developed innovative approaches to screen extremely large numbers of compounds and methods to guide them to new MoA.

Agrematch is a unique data-science product discovery and development company catering to industries that require novel compounds for their products. Agrematch's product-oriented approach utilizes compound-based data analytics, to predict early and downstream considerations which are necessary for successful product launch. Agresense, the Agrematch artificial intelligence algorithm system for rational identification of molecules with desired compound-organism interaction, utilizes unique data science concepts, biology, chemistry, and agriculture know-how to reduce the total R&D costs and risks and accelerate the time to market of sustainable and durable Ag products.

We report in this paper a new chemical class of herbicide that was discovered using the artificial intelligence algorithm developed by Agrematch. These new 4-chloro-2-pentenamides act by inhibiting protoporphyrinogen oxidase (PPO), a key enzyme in porphyrin biosynthesis [10].

MATERIALS AND METHODS

Discovery of novel structures (Agrematch innovative approach)

A database of ~1.2B compounds was screened to create a library of 50 compounds, predicted by Agresense (Agrematch Artificial Intelligence system) to have herbicidal activity, based on a unique proprietary molecular representation of the screened compounds. The iterative process of included testing the compounds identified by Agresense for their herbicidal activity in the lab and feeding back the results into the Agresense system to optimize it and to create additional iterations of compound libraries. These compounds were then analyzed by our MoA classifier algorithm to predict whether these compounds have a new MoA or belongs to an existing HRAC class.

Plant material and growth

For herbicidal activity assays, Palmer amaranth (*Amaranthus palmeri*), *Xanthium strumarium, Datura ferox, Solanum nigrum* and *Amaranthus blitoides* were planted in pots with a potting mix and grown in either growth-chamber or Net-house. All plants were watered as needed.

Cucumber seedlings (cultivar Straight eight) were planted in trays with promix and grown in the greenhouse for up to 3 weeks days to collect fresh cotyledons. These plants were discarded once the 2 true-leaf started to emerge. Palmer amaranth plants that were either

sensitive (S) or resistant (R) to PPO inhibitors due to a glycine210 deletion [11-13] were grown in the greenhouse for 4 weeks under similar conditions. All plants were watered as needed.

Herbicidal activity

For pre-emergence assays, compounds were dissolved in DMSO and diluted in water to a final concentration of 10-100 mg/L with 2% DMSO. Compounds were sprayed using a VL-SET Paasche Airbrush at a 3,000 L/ha application volume.

For post-emergence assays, compounds were dissolved in DMSO and diluted in water to a final concentration of 25-250 mg/L with 2% DMSO. Break-Thru® S-240 (EVONIK) at a final concentration of 0.05% was added. Compounds were sprayed using a VL-SET Paasche Airbrush at a 1,000 L/ha application volume. Weeds were sprayed at the 4-6 leaf stage.

For post-emergence net-house assay, 300 mg/L of compound AGR001 was dissolved in 900 mg/L xylenes, 73 mg/L ethoxylated castor oil (Kolliphor® RH 40) and 48 mg/L calcium dodecylbenzene sulfonate (Rhodacal® 60be) in water. Break-Thru® S-240 (EVONIK) at a final concentration of 0.05% was added. Weeds were sprayed using a VL-SET Paasche Airbrush at a 1,000 L/ha application volume at the 4-6 leaf stage (2-leaf stage for *D. ferox*).

Herbicidal activity was assessed and scored 7 days after application by visual inspection of the weeds in comparison to untreated controls. Activity score was in the range of 0 to 100, where 0 represents no herbicidal activity like control weeds and 100 represents the maximal herbicidal activity (i.e., total death of the weed).

Electrolyte leakage

First, time-course experiments were conducted over 40 h to measure the effect of AGR001 or AGR002 on electrolyte leakage from cucumber cotyledons using a modified method of Dayan and Watson [14]. For each compound, 36 discs (6 mm diam.) were cut from 7 to 15

day-old cucumber cotyledons and placed in a petri dish. The discs were floating over 5 mL of MES buffer (pH 6.5) with 2% sucrose with 100 µg/mL of either AGR001 or AGR002. This was done in low light intensity to prevent photodynamic damage.

Once the plates were prepared, the initial conductivity (a measure of electrolyte leakage) was measured using a FiveEasy Plus FP30 conductivity meter connected to an InLab 751-4mm microprobe (Mettler Toledo, Columbus, OH 43240). The plates were then kept in the dark at room temp for 16 h. Conductivity was measured after the dark incubation period and then the plates were moved into an LED-30L1 LED high intensity growth chamber (Percival, Perry Iowa 50220). Conductivity was measured 1, 5, 10, 24 h after exposure to light intensity (approx. 1050 µmol/m/s)

Second, dose-response curve experiments were conducted with AGR001 and GR002 at 1, 3, 10, 30, 100 and 300 µM. Control treatment consisted of DMSO alone to determine the relative potency of these molecules. Conductivity was measured as described above after 16 h dark incubation followed by 24 h exposure to high light intensity.

Third, the effect of AGR001 and AGR002 was tested on biotypes of S and R Palmer amaranth plants. For this experiment, 60 leaf discs from 4 weeks old Palmer amaranth were used. Concentrations used were 10 µM AGR001 and 100 µM AGR002, compared conductivity was compared to controls with DMSO alone.

Protoporphyrin IX accumulation

The effects of AGR001 and AGR002 on protoporphyrin IX (proto) levels were measured in cucumber cotyledons exposed to 300 µM of either compound, and compared to DMSO control after 16 h dark incubation. Proto was extracted according to [15]. Proto extraction and analysis followed a protocol described by Dayan et al. [16]. Approximately 0.2 g of cotyledonary tissue

was ground to a powder in liquid nitrogen and homogenized in 2 mL of extraction solvent (methanol:0.1 M NH_4OH, 9:1) and centrifuged at 10,000 × g for 15 min. The supernatant was saved and the pellet rehomogenized in 1 mL of extraction solvent, then centrifuged again at 10,000 × g for 15 min. Supernatants were pooled and then filtered through a 0.2-μm nylon syringe membrane filter before quantification with the LC-MS/MS system. Proto was separated in a biphenyl column (100 by 4.6 mm, 2.6 μm, 40 C) at a flow rate of 0.4 mL min^{-1} using a linear gradient of methanol (B) and 10mM ammonium acetate (A): 0 min, 50% B; 8min, 70% B; 11 min, 90% B; 13 min, 90% B; 13.5 min, 50% B; 17 min, 50% B. The MRM was optimized to 340.10 > 227.95 [17]. A standard curve generated with serial dilutions of authentic protoporphyrin IX (MilliporeSigma, St. Louis, MO) was used for quantification.

Protoporphyrinogen oxidase activity

Protoporphyrinogen oxidase was obtained by expression and purification of the *Amaranthus tuberculatus* wild type isoform as described by Dayan, Daga [18] Briefly, the cell line was cultured overnight at 37 C in 250 mL of LB with ampicillin, which was diluted into 1 L of LB with antibiotic and grown for 1 h before induction with 1 mM IPTG. After induction the culture was grown at 25 C for 5 h. Cells were harvested by centrifugation at 2,000Íg and washed with 0.1% NaCl. Cells were lysed by sonication (Model 120 Sonic Dismembrator with a Model CL-18 1/8 inch probe, Thermo Fisher Scientific, Waltham, MA, USA) in 3 x 30 s bursts with 60 s on ice in between in 50 mM sodium phosphate pH 7.5, 500 mM NaCl, 5 mM imidazole, 5% glycerol and 1ug/mL leupeptin. After lysis 1U of benzonase (Millipore Sigma, Burlington, MA, USA) and 1 mM PMSF were added. Debris were removed by centrifugation for 30 min at 2000Íg. Proteins were purified on a HisPur Ni-NTA Spin Column (Thermo Fisher Scientific, Waltham, MA, USA) as per the instructions with elution at 20 mM sodium phosphate, 300 mM

sodium chloride 250 mM imidazole, pH 7.4. Protein was desalted on a PD-10 column (GE Healthcare Bio-Sciences Corp., Piscataway, NJ, USA) equilibrated with 20 mM sodium phosphate, pH 7.5, 5 mM $MgCl_2$, 1 mM EDTA and 17% glycerol. 1 liter of culture provided approximately 6 mg of pure PPO which was stored at -20 C until use.

Protoporphyrinogen was prepared by reducing proto with sodium amalgam as described by Jacobs and Jacobs [19]. Assays were conducted with 48 ug of protein per replicate as described by Dayan et al. [18] with specific modifications for our spectrophotometer as follows: enzymatic activity was measured on an FS5 Spectrofluorometer (Edinburgh Instruments, Kirkton Campus, UK) with excitation wavelength set to 395 nm and bandwidth to 1 nm; and emission wavelength set at 633 nm and bandwidth to 10 nm. Statistical analysis was performed using the R software (v 4.1.0). Dose responses were fit using the DRC package. [20] Regression curves were imported into GraphPad Prism 9.1.1.

Docking study

All herbicide structures were downloaded as 3-D.sdf files from PubChem [21]. The two experimental compounds were build using a molecular modelling and computational chemistry application (Spartan18, Wavefunction, Inc. Irvine, CA 92612). The bond angles and length were corrected, and the atom energies were calculated by submitting all the molecules to geometric minimization using density function theory calculations (wB97X-D 6-31*). The optimized structures were saved as mol2 files along with their electrostatic charges.

The crystal structure of spinach PPO was obtained from 1sez [22]. Prior to use for docking studies, the pdb file was modified to replace the seleniomethionine residues with methionine residues. Also, the atom types of the FAD cofactor were corrected and the ligand was converted to its oxidized form using Spartan18.

All the herbicides were docked into the catalytic domain of PPO using a Autodock (AutoDock version 4.2, Scripps Institute, San Diego CA, USA) [23, 24]. Additionally, the guanidino group of arginine 98 (atom id=3782) was designated as important in the interaction between one of the propionate groups (coordinates of this proton are x = -43.390, y = -1.054 and z = 31.750). A grid box was used to delimitate the region of the catalytic domain according to the software. The gridbox dimensions were set to 38 Í 34 Í 34 points with a spacing to 0.375. The box was centered on the following coordinates: x = -40, y = -6, and z = 29. PPO was set as a rigid structure. The algorithm was set to generate 100 docking poses and the top clustered was selected as optimal conformation for the docking of each ligand.

RESULTS AND DISCUSSION

Discovery of novel structures

The iterative process of Agresense resulted in a family of compounds, AGR001-AGR014 described in this paper (Table 4.1). The log*P* values calculated by the algorithm are on the higher end of suggested values for biological relevance in regard to herbicide uptake, as the "Briggs rule" suggests ideal values are less than 3. Surprisingly, the classifier algorithm predicted these compounds to belong to HRAC group 14 (inhibitors of PPO), even though classical similarity methods showed very low similarity scores to the structure of known group 14 herbicide (Fig. 4.1A). PPO inhibitors that have been registered to date share some structural similarities to the substrate, protoporphyrinogen (protogen). Protogen is a tetrapyrrole, consisting of four pyrrole rings arranged in a ring themselves. Of the registered classes of PPO inhibitors the diphenyl ethers, *n*-phenyl-oxadiazolones, pyraflufen-ethyl and some members of the *n*-phenyl imides and *n*-phenyl-triazolinones have a two-ring structure which mimics one half of protogen. The others,

Table 4.1. Chemical names and properties of the compounds analyzed in this study

Code	Mw	logP[1]	Rotatable bonds	H-bond acceptors	H-bond donors	Chemical name
AGR001	315.24	3.48	7	2	0	(2*E*)-4-chloro-*N*-[(6-chloro-3-pyridinyl)methyl]-*N*-isobutyl-2-pentenamide
AGR002	245.79	3.31	7	1	0	(2*E*)-4-chloro-*N*,*N*-bis(isobutyl)-2-pentenamide
AGR003	315.24	3.42	7	2	0	(2*E*)-4-chloro-*N*-[(5-chloro-2-pyridinyl)methyl]-*N*-isobutyl-2-pentenamide
AGR004	329.27	3.77	8	2	0	(2*E*)-4-chloro-*N*-[(6-chloro-3-pyridinyl)methyl]-*N*-isopentyl-2-pentenamide
AGR005	305.81	2.66	7	3	0	(2*E*)-4-chloro-*N*-[(6-cyano-3-pyridinyl)methyl]-*N*-isobutyl- 2-pentenamide
AGR006	320.27	4.22	7	1	0	(2*E*)-4-chloro-*N*-[(5-chloro-2-thiophen-yl)methyl]-*N*-isobutyl-2-pentenamide
AGR007	334.30	4.50	8	1	0	(2*E*)-4-chloro-*N*-[(5-chloro-2-thiophen-yl)methyl]-*N*-isopentyl-2-pentenamide
AGR008	321.26	3.55	7	2	0	(2*E*)-4-chloro-*N*-[(2-chloro-5-thiazol-yl)methyl]-*N*-isobutyl-2-pentenamide
AGR009	271.71	3.39	7	4	0	(2*E*)-4-chloro-*N*-isobutyl-N-2,2,2-trifluoroethyl-2-pentenamide
AGR010	273.85	4.00	9	1	0	(2*E*)-4-chloro-*N*,*N*-bis(isopentyl)-2-pentenamide
AGR011	241.76	3.00	6	1	0	(2*E*)-*N*-(2-butynyl)-4-chloro-*N*-isobutyl-2-pentenamide
AGR012	255.79	3.36	6	1	0	(2*E*)-4-chloro-*N*-isobutyl-*N*-(2-pentynyl)-2-pentenamide
AGR013	285.81	3.01	8	2	0	(2*E*)-4-chloro-*N*-(4-ethoxy-2-butynyl)-*N*-isobutyl-2-pentenamide
AGR014	295.81	3.05	8	2	0	(2*E*)-4-chloro-*N*-isobutyl-*N*-[4-(2-propyn-1-yloxy)-2-butynyl]-2-pentenamide

[1]logP was calculated as the average of 5 prediction algorithm using SwissADME[29]

pyraclonil and the rest of the *n*-phenyl imides and *n*-phenyl-triazolinones have three ring structures that still roughly resemble one half to three fourths of a protogen molecule (HRAC). Half of the structures reported in this paper do a single cyclic group.

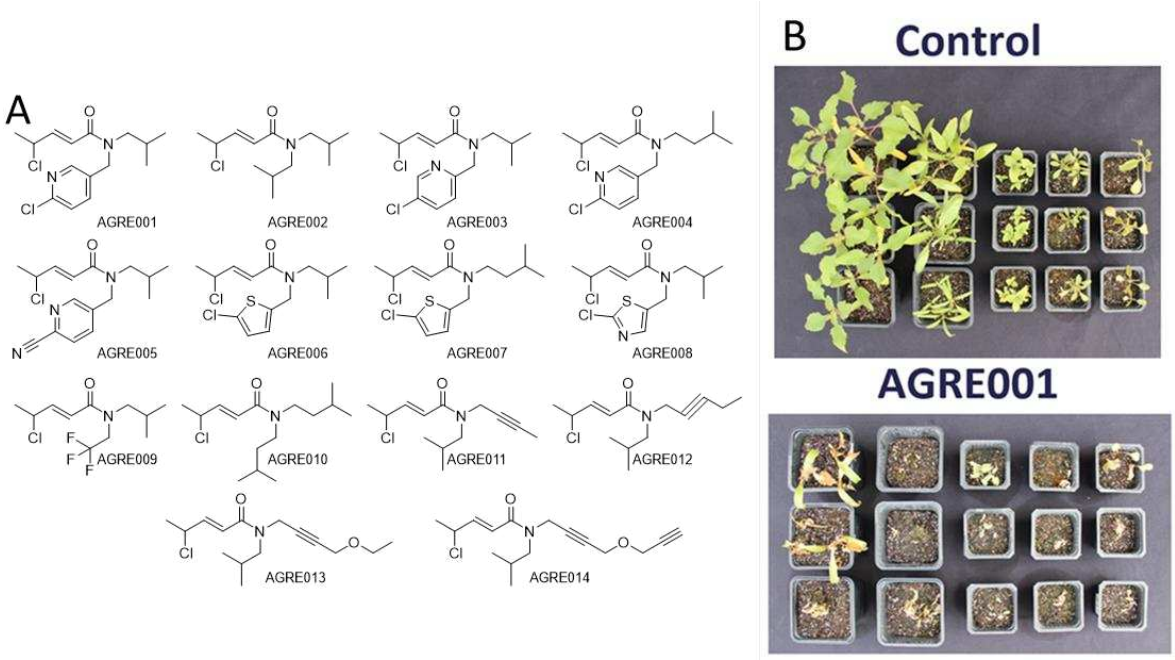

Figure 4.1. **A.** Structure of the novel 4-halo-2-pentenamides described in this paper. **B.** Herbicidal activity of AGR001 in post-emergence Net-house assay, 7 days after application of 300g/ha. From left to right: *Xanthium strumarium, Datura ferox, Solanum nigrum, Amaranthus blitoides, Amaranthus palmeri.*

Herbicidal activity

Pre-emergent and post emergent applications were tested for all 14 potential compounds. Pre-emergent activity was investigated in Palmer amaranth (Amaranthus palmeri), post emergent activity was investigated in *Xanthium strumarium, Datura ferox, Solanum nigrum, Amaranthus blitoides,* and Palmer. Post-emergent activity of AGR001 in net-house conditions is illustrated in Figure 4.1B. Despite borderline log*P* values, these compounds were herbicidal. Most tested compounds, other than AGR012 and 014 had some pre-emergent activity, with AGR001, 002 and 009 providing good control at lower rates (Table 4.2). Each of the 9 compounds tested post-emergent had good activity, though AGR001, 004 and 005 were the most active (Table 4.3).

Some of the compounds caused photobleaching, which was consistent with thee these compounds predicted activity as PPO inhibitors. AGR001 and 002 were selected as representative compounds of the structures with herbicidal activity to determine MoA.

Table 4.2. Herbicide activity at pre-emergence application on Palmer amaranth in percent control

Compounds	300g/ha	150g/ha	30g/ha
AGR001	100	90	40
AGR002	100	90	20
AGR003	100	NA	NA
AGR004	80	NA	NA
AGR005	70	NA	NA
AGR006	100	NA	NA
AGR007	80	NA	NA
AGR008	80	NA	NA
AGR009	85	80	30
AGR010	90	30	30
AGR011	90	20	0
AGR012	0	10	10
AGR013	40	NA	NA
AGR014	0	NA	NA

Mechanism of action studies

PPO inhibitors inhibiting the last common enzyme in the synthesis of heme and chlorophyll, a branch point in the tetrapyrrole pathway.[25] This causes a buildup of the substrate, protoporphyrinogen, which leaks from the plastids to the cytoplasm and is oxidized into the product of the protein, protoporphyrin IX (proto). Proto is a photodynamic red pigment

which generates reactive oxygen species (ROS). These ROS cause lipid peroxidation of the cell membranes leading to cell and plant death.[25] The activity of PPO inhibitors is quantifiable through light-dependent bleaching of tissue, light-dependent electrolyte leakage from membrane disruption, and accumulation of proto after application on plant tissue. It can also be directly observed through an enzyme assay.

Table 4.3. Herbicide activity at post-emergence application on Palmer amaranth expressed in percent control

Compounds	250g/ha	100g/ha	75g/ha	50g/ha	25g/ha
AGR001	NA	100	NA	95	90
AGR002	50	30	NA	30	NA
AGR003	100	100	NA	NA	NA
AGR004	NA	NA	100	100	NA
AGR005	NA	NA	100	90	NA
AGR007	80	NA	NA	NA	NA
AGR008	95	NA	NA	NA	NA
AGR010	50	NA	NA	NA	NA

Initial electrolyte leakage assays were performed in cucumber cotyledons. Both AGR001 and AGR002 treatments at 100 μM showed the same increase in conductivity due to cell damage after exposure to light as has been reported previous with PPO inhibitors (Figure 4.2A). [26] The second electrolyte leakage assay in cucumber cotyledons was to determine the efficacy of lower doses, showing that AGR001 is approximately ten times more active than AGR002 (Figure 2B-C). The bleaching observed in the leaf disks are typical of herbicides inhibiting PPO. To confirm that these herbicides target PPO, additional experiments measuring proto levels in plant tissues exposed to 300 μM of selected compounds. The accumulation of proto in treated tissue and not the control further supports inhibition of PPO as the MoA (Figure 4.3). A third electrolyte

leakage assay was performed on leaf disks from PPO-resistant[27] and wildtype Palmer populations (Figure 4.4). The PPO-resistant line was not sensitive to either compound, whereas the susceptible line responded to the treatments, with marked increase in electrolyte leakage.

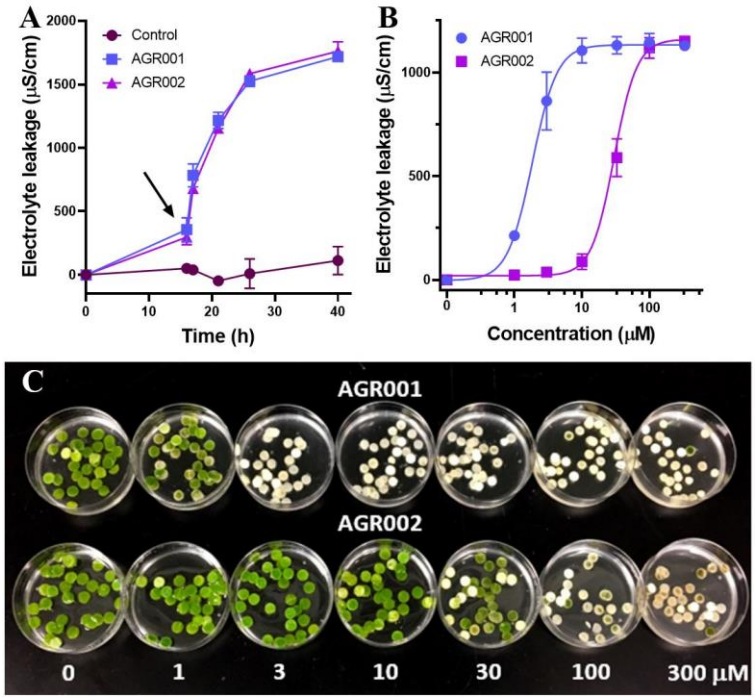

Figure 4.2. Electrolyte leakage experiments in cucumber cotyledons. A) Electrolyte leakage caused by 100 µg/mL AGR001 (light blue) or AGR002 (pink) over 40 h. The arrow indicates when the plates started exposure to high light intensity (approx. 1400 µmol/m/s). B) Dose-response curves with AGR001 (light blue) and AGR002 (pink) following 15 h dark incubation and 11 h of exposure to high light intensity. C) Bleaching of tissues at the end of the dose-response curve experiments.

Finally, the MoA of these compounds was confirmed by testing these compounds directly on purified PPO enzyme extracted from recombinant wild-type *Amaranthus tuberculatus* PPO2 heterologously expressed in *E. coli* (Table 4.4). Dose-response curves were obtained for AGR001 and 002 at concentrations ranging from 0.1 – 100 µM. Inhibition of PPO activity by AGR001 and 002 was much lower than most PPO inhibitors, requiring more than 10 µM to obtain 50% inhibition (I_{50}), whereas commercial PPO-inhibiting herbicides have I_{50} values being in the submicromal range.

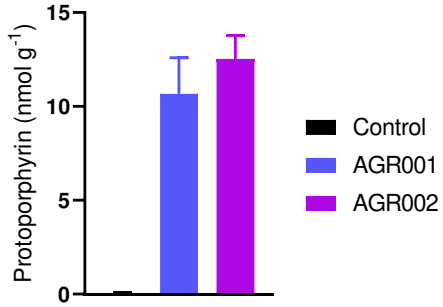

Figure 4.3. Accumulation of proto in cucumber cotyledons after 24 h exposure to 300 µM AGR001 (light blue) or AGR002 (purple) in darkness, relative to DMSO control.

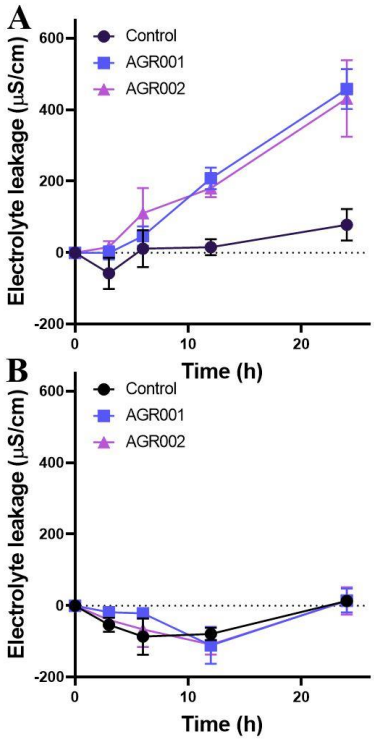

Figure 4.4. Electrolyte leakage caused by 10 mM AGR001 (light blue) and 100 mM AGR002 (purple) after 15 h dark incubation and subsequent exposure to high light intensity over 24 h on A) susceptible and B) PPO-resistant Palmer amaranth.

Table 4.4. Inhibition of purified, recombinant wild type *Amaranthus tuberculatus* PPO2

Compounds	IC50 (µM)	Activity at highest inhibiting dose (% of control)
AGR001	18.9	28.8
AGR002	NA	31.2

Docking studies

Docking studies were performed to further understand the interaction between AGR001 and AGR002 with the catalytic domain of PPO. The published binding energy of protogen and proto are -10.6 and -7.3 kcal mol^{-1}, respectively.[28] The average docking energies for AGR001 and AGR002 were -4.7 and -3.1 kcal mol^{-1}, respectively (Table 5.5). These values are lower than the binding energies of other commonly PPO inhibitors, which range from -8.8 to -5.3 kcal mol^{-1}. AGR001 and AGR002 are smaller and structurally different from all commercial PPO-inhibiting herbicides. 4-Chloro-2-pentenamides have very flexible side chains and can hold several different conformations in the active site (Figure 4.5), whereas most PPO inhibitors are more rigid multicyclic molecules that occupy a more limited number of poses and are stabilized by interactions with highly conserved residues (e.g., Arg98, Phe353 and Leu356) known to interact with the substrate in the catalytic domain. This ability of 4-chloro-2-pentenamides to assume different poses within the catalytic domain equates to an increase in entropy which may account for the low binding energies of this chemical class, and the lesser herbicidal activity.

CONCLUSION

The 4-chloro-2-pentenamides identified as putative PPO inhibitors by the Agresense AI algorithm have both pre- and post-emergent herbicidal activity on multiple weeds. Despite the lack of structural similarity with known PPO inhibitors, these compounds indeed acted by inhibiting PPO, causing the expected light-dependent loss of membrane integrity, photobleaching, accumulation of proto and inhibition of PPO. The Agresense algorithm continues to undergo refinement to predict the activity of molecules with potentially new MoAs.

Table 4.5. Docking of herbicides on catalytic domain of PPO.

Compounds	Major groups	Number of poses in group	Average docking energy kcal/mol
AGR001 A	1	18	-4.98
	2	14	-4.64
	3	13	-4.71
	4	22	-4.44
AGR001 B	1	16	-4.84
	2	25	-4.84
	3	39	-4.44
	4	6	-4.72
AGR002 A	1	29	-3.27
	2	12	-3.20
	3	13	-3.11
	4	29	-3.15
AGR002 B	2	23	-3.21
	3	42	-3.07
	4	10	-2.93
	5	12	-2.81

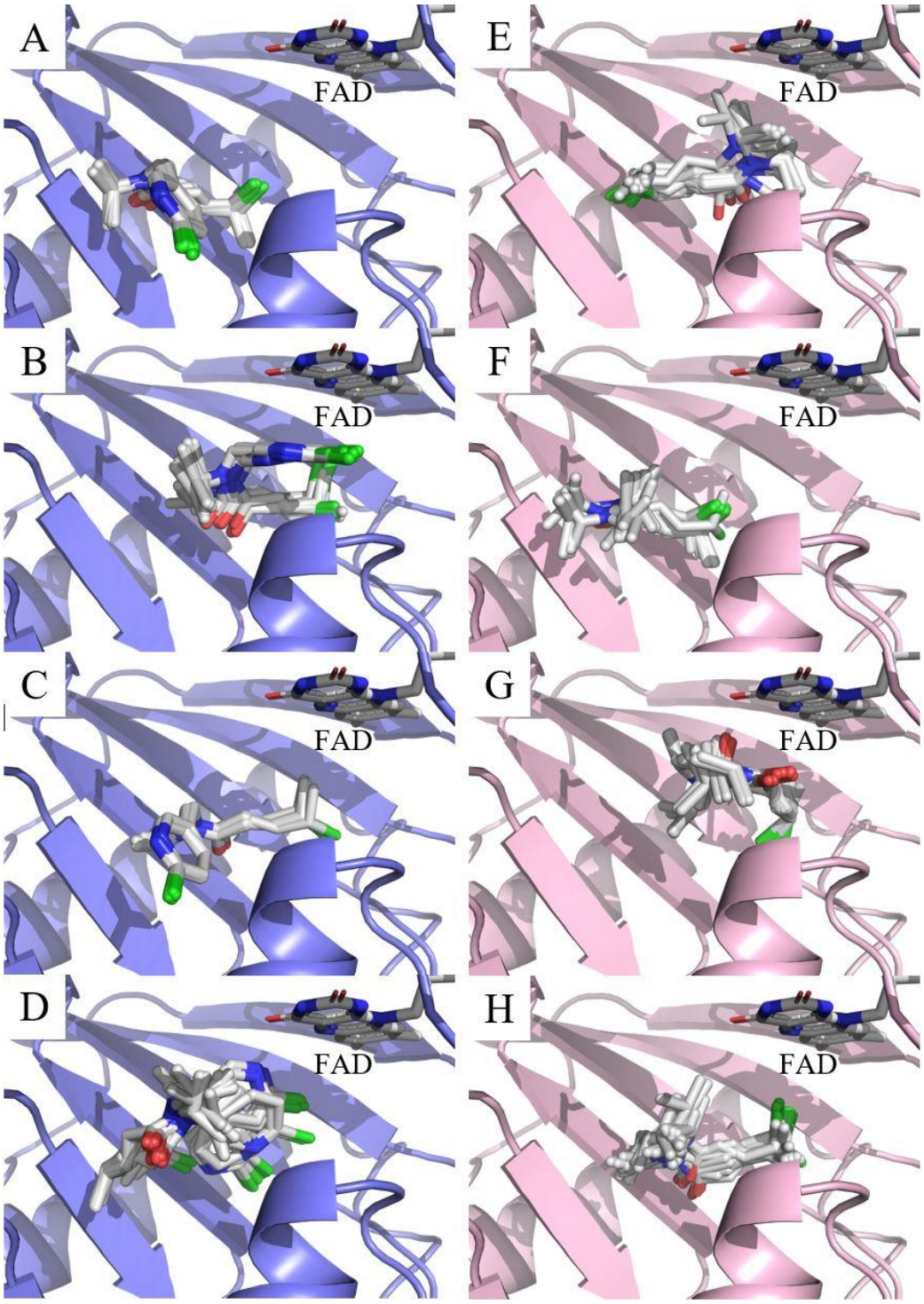

Figure 4.5. Representative docking poses of A) group 1, B) group 2, C) group 3, and D) group 4 of AGR001 (protein is in light blue), and E) group 1, F) group 2, G) group 3, and H) group 4 of AGR002 (protein is in pink) on PPO. Refer to Table 1 for number of poses in each group and average docking energies.

REFERENCES

1. Pimentel, D., R. Zuniga, and D. Morrison, *Update on the environmental and economic costs associated with alien-invasive species in the United States.* Ecological Economics, 2005. **52**: p. 273-288.
2. Soltani, N., et al., *Potential corn yield losses from weeds in North America.* Weed Technology, 2016. **30**(4): p. 979-984, 6.
3. Heap, I. *The International Survey of Herbicide Resistant Weeds*. 2020 [cited 2020 April 2020]; Available from: www.weedscience.org.
4. Gaines, T.A., et al., *Mechanisms of evolved herbicide resistance.* Journal of Biological Chemistry, 2020. **295**: p. 10307-10330.
5. Fennimore, S.A. and M. Cutulle, *Robotic weeders can improve weed control options for specialty crops.* Pest Management Science, 2019. **75**(7): p. 1767-1774.
6. Westwood, J.H., et al., *Weed management in 2050: Perspectives on the future of weed science.* Weed Science, 2018. **66**(3): p. 275-285.
7. Cooper, J. and H. Dobson, *The benefits of pesticides to mankind and the environment.* Crop Protection, 2007. **26**(9): p. 1337-1348.
8. Dayan, F.E., *Current status and future prospects in herbicide discovery.* Plants, 2019. **8**: p. 341.
9. Peters, B. and H.J. Strek, *Herbicide discovery in light of rapidly spreading resistance and ever-increasing regulatory hurdles.* Pest management science, 2018. **74**(10): p. 2211-2215.
10. Dayan, F.E. and S.O. Duke, *Protoporphyrinogen oxidase-inhibiting herbicides*, in *Haye's Handbook of Pesticide Toxicology*, R. Krieger, et al., Editors. 2010, Academic Press, Elsevier: San Diego, CA. p. 1733-1751.
11. Patzoldt, W.L., et al., *A codon deletion confers resistance to herbicides inhibiting protoporphyrinogen oxidase.* Proceedings of the National Academy of Sciences, USA, 2006. **103**: p. 12329-12334.
12. Dayan, F.E., et al., *Biochemical and structural consequences of a glycine deletion in the α-8 helix of protoporphyrinogen oxidase.* Biochimica et Biophysica Acta - Proteins and Proteomics, 2010. **1804**(7): p. 1548-1556.
13. Salas-Perez, R.A., et al., *Frequency of Gly-210 deletion mutation among protoporphyrinogen oxidase inhibitor–resistant Palmer amaranth (Amaranthus palmeri) populations.* Weed Science, 2018. **65**(6): p. 718-731.
14. Dayan, F.E. and S.B. Watson, *Plant cell membrane as a marker for light-dependent and light-independent herbicide mechanisms of action.* Pesticide Biochemistry and Physiology, 2011. **101**(3): p. 182-190.
15. Takano, H.K., et al., *Glufosinate enhances the activity of protoporphyrinogen oxidase inhibitors.* Weed Science, 2020. **68**(4): p. 324-332.
16. Dayan, F.E., et al., *Biochemical markers and enzyme assays for herbicide mode of action and resistance studies.* Weed Science, 2015. **63**(sp1): p. 23-63.
17. Moulin, M. and A.G. Smith, *A robust method for determination of chlorophyll intermediates by tandem mass spectrometry*, in *Photosynthesis. Energy from the Sun: 14th International Congress on Photosynthesis*, J.F. Allen, et al., Editors. 2008, Springer Netherlands: Dordrecht. p. 1215-1222.

18. Dayan, F.E., et al., *Biochemical and structural consequences of a glycine deletion in the a-8 helix of protoporphyrinogen oxidase.* Biochimica et Biophysica Acta - Proteins and Proteomics, 2010. **1804**(7): p. 1548-1556.
19. Jacobs, N.J. and J.M. Jacobs, *Assay for enzymatic protoporphyrinogen oxidation, a late step in heme synthesis.* Enzyme, 1982. **28**: p. 206-219.
20. Ritz, C., et al., *Dose-response analysis using R.* PloS one, 2015. **10**(12): p. e0146021.
21. Kim, S., et al., *PubChem in 2021: New data content and improved web interfaces.* Nucleic Acids Research, 2020. **49**(D1): p. D1388-D1395.
22. Koch, M., et al., *Crystal structure of protoporphyrinogen IX oxidase: a key enzyme in haem and chlorophyll biosynthesis.* EMBO Journal, 2004. **23**: p. 1720-1728.
23. Morris, G.M., et al., *AutoDock Version 4.2.* Automated Docking of Flexible Ligands to Flexible Receptors, 2012.
24. Goodsell, D.S., et al., *The AutoDock suite at 30.* Protein Science, 2021. **30**(1): p. 31-43.
25. Dayan, F.E., et al., *Herbicide mechanisms of action and resistance.* 2019.
26. Duke, S.O., et al., *Protoporphyrinogen oxidase-inhibiting herbicides.* Weed Science, 1991. **39**(3): p. 465-473.
27. Salas, R.A., et al., *Resistance to PPO-inhibiting herbicide in??Palmer amaranth from Arkansas.* Pest Management Science, 2016. **72**(5): p. 864-869.
28. Barker, A.L., H. Barnes, and F.E. Dayan, *Conformation of the Intermediates in the Reaction Catalyzed by Protoporphyrinogen Oxidase: An In Silico Analysis.* International journal of molecular sciences, 2020. **21**(24): p. 9495.
29. Daina, A., O. Michielin, and V. Zoete, *SwissADME: a free web tool to evaluate pharmacokinetics, drug-likeness and medicinal chemistry friendliness of small molecules.* Scientific Reports, 2017. **7**(1): p. 42717.

APPENDIX 1: SUPPLEMENTARY MATERIAL FOR CONFORMATION OF THE INTERMEDIATES IN THE REACTION CATALYZED BY PROTOPORPHYRINOGEN OXIDASE: AN *IN SILICO* ANALYSIS

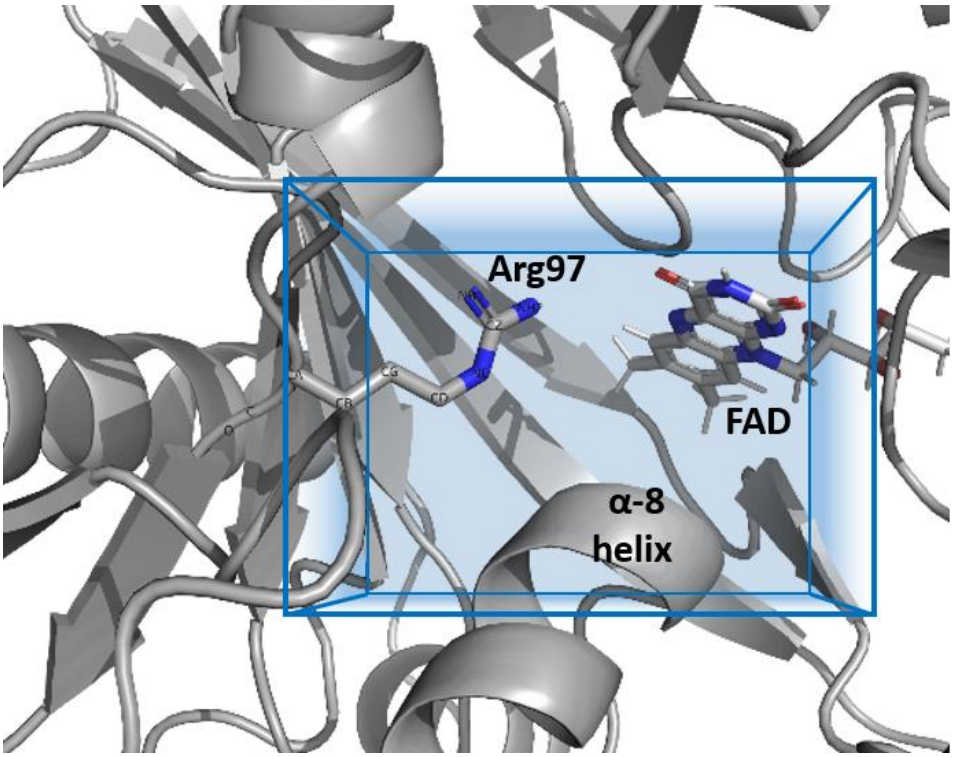

Supplemental Figure S3.1. Gridbox defining the binding domain of the tetrapyrroles in PPO, including FAD forming the 'roof' of the cavity, the top of α-8 helix of PPO upon which the tetrapyrrole rings are centered at the 'bottom' of the cavity, and arginine 97 involved in stabilizing the rings on the right side of the cavity.

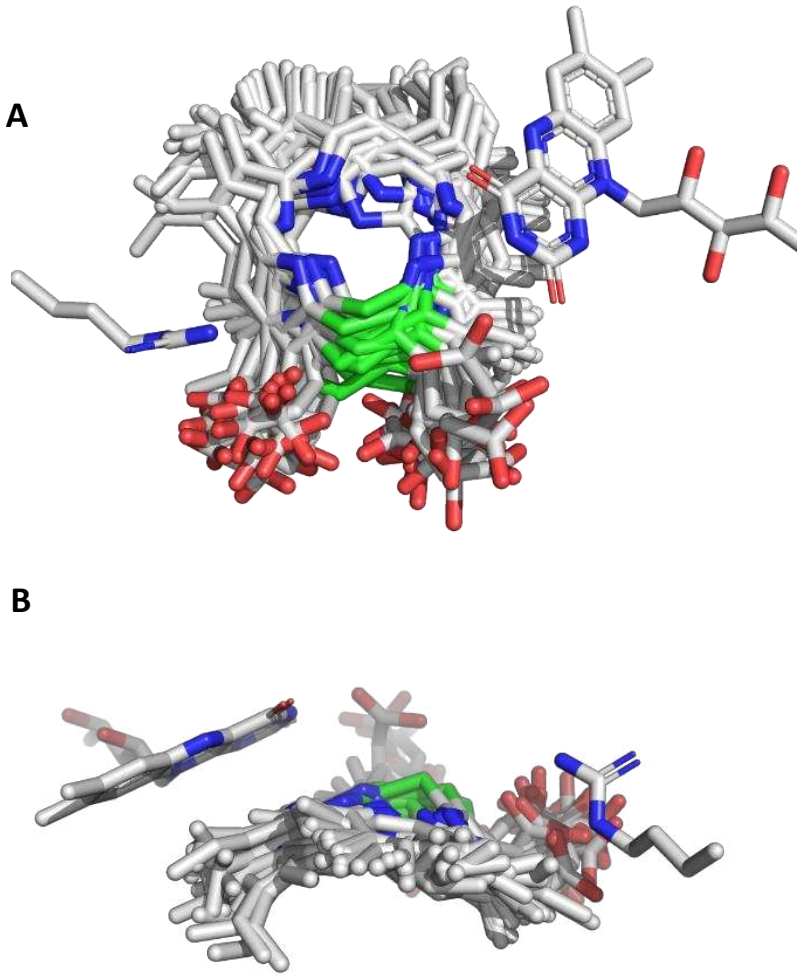

Supplemental Figure S3.2. Docking poses of the top cluster of intermediate 1a. Top = from above the catalytic domain of PPO and bottom = from inside the catalytic domain of PPO

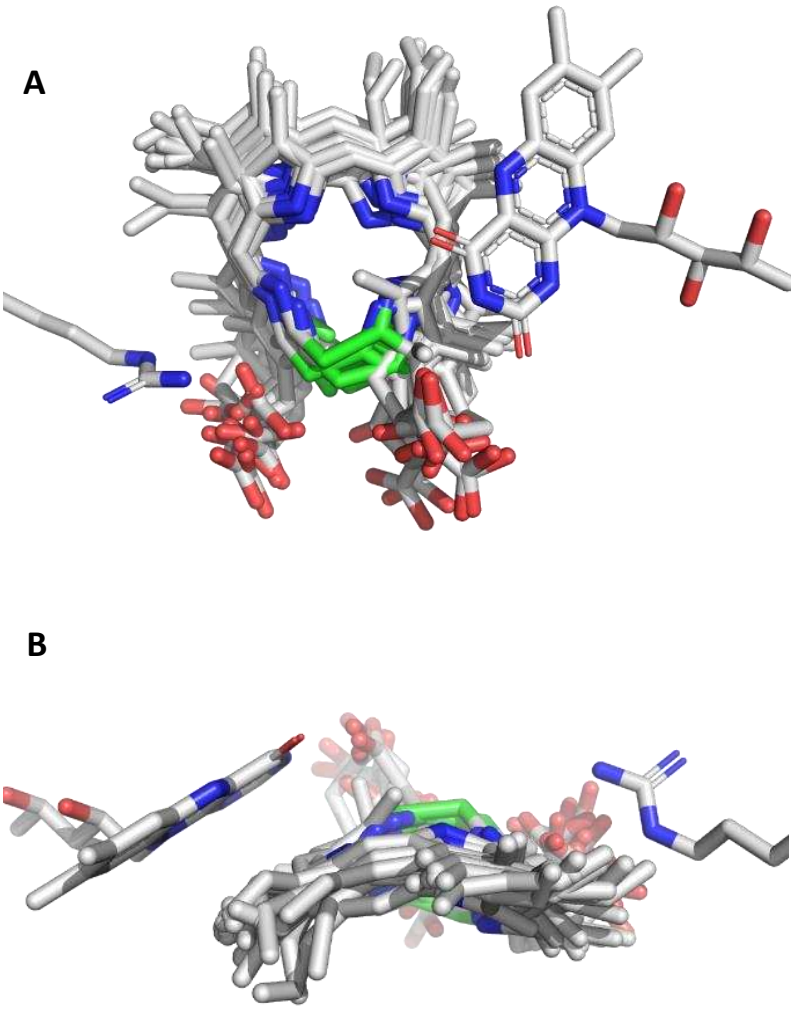

Supplemental Figure S 3.3. Docking poses of the top cluster of intermediate 1c. Top = from above the catalytic domain of PPO and bottom = from inside the catalytic domain of PPO

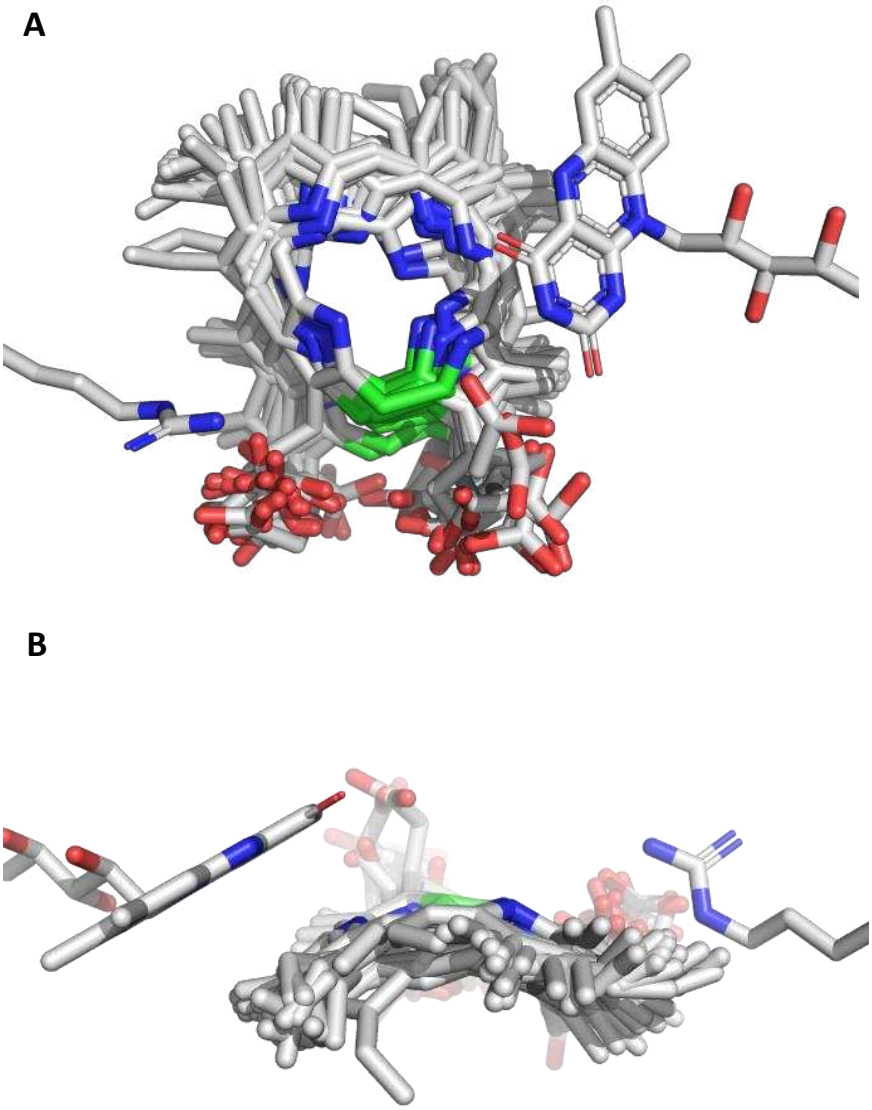

Supplemental Figure S 3.4. Docking poses of the top cluster of intermediate 2a. Top = from above the catalytic domain of PPO and bottom = from inside the catalytic domain of PPO

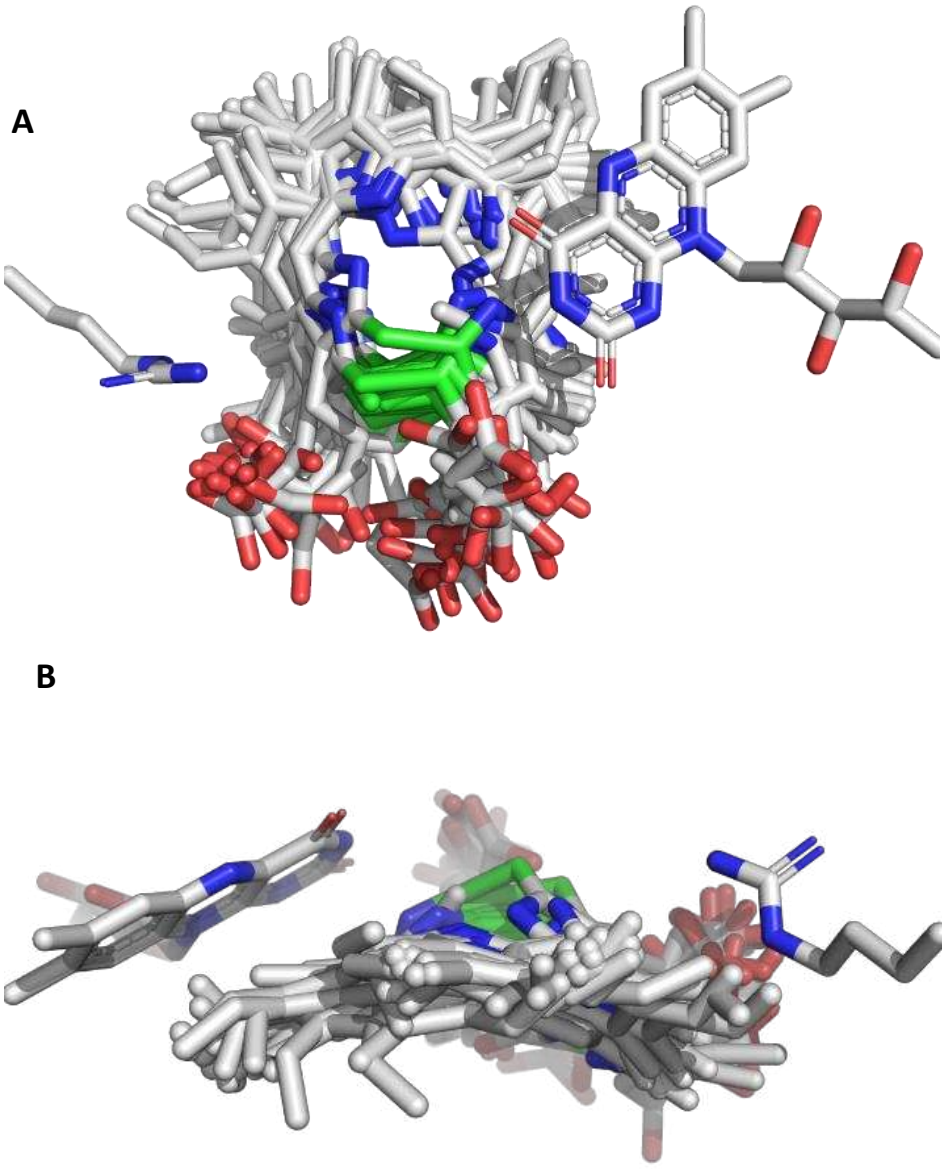

Supplemental Figure 5. Docking poses of the top cluster of intermediate 2d. Top = from above the catalytic domain of PPO and bottom = from inside the catalytic domain of PPO

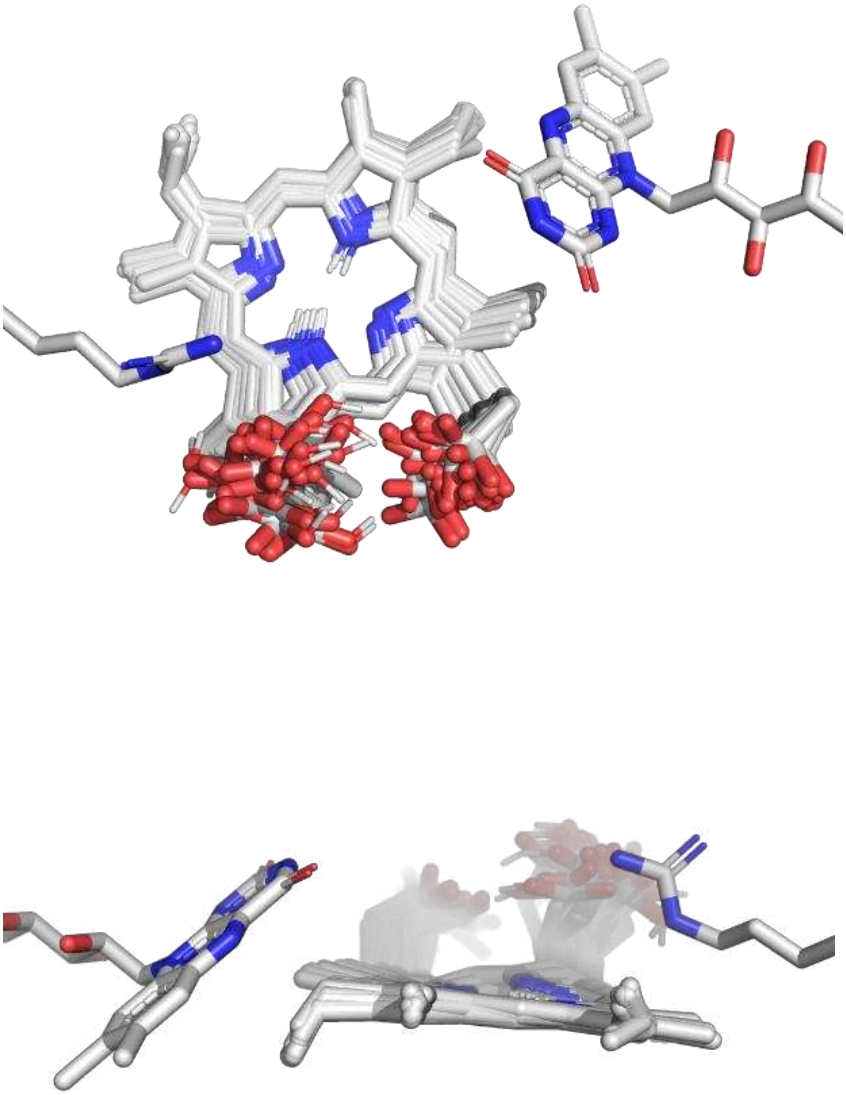

Supplemental Figure 6. Docking poses of the top cluster of intermediate proto. Top = from above the catalytic domain of PPO and bottom = from inside the catalytic domain of PPO

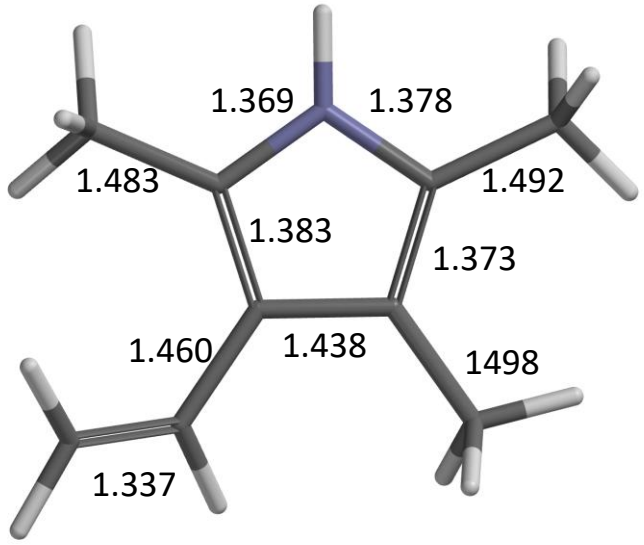

Supplemental Figure S3.7.
DFT calculation on protoporphyrinogen pyrrole 1
Equilibrium geometry with DFT wB97XD 6-31G*
Neutral molecule

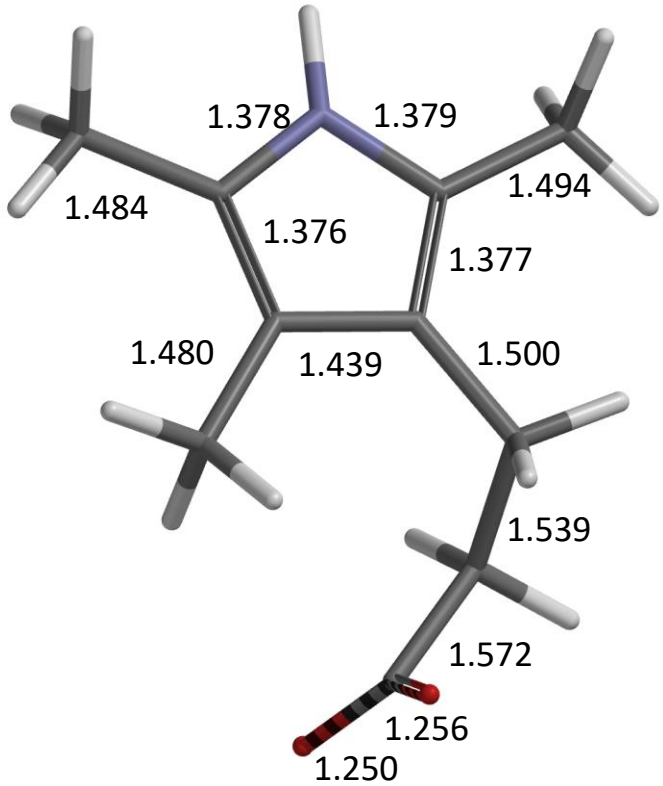

DFT calculation on protoporphyrinogen pyrrole 2
Equilibrium geometry with DFT wB97XD 6-31G*
Carrying negative -1 charge

Supplemental table S3.1. Percent identity matrix of the Clustal Omega alignment made with the file of 16 model organisms protoporphyrinogen oxidase proteins.

		1	2	3	4	5	6	7	8	9	10	11	12	13	14	15	16
1	PPO C. elegans	100	12.96	12.7	13.19	13.35	14.91	14.95	13.71	13.82	15.25	17.7	10.66	11.85	12.89	13.84	14.29
2	PPO Saccharomyces cerevisiae	12.96	100	27.33	22.88	24.58	26.11	24.09	24.09	19.87	20.73	20.26	21.88	19.26	21.7	21.67	20.35
3	PPO2 Drosophila melanogaster	12.7	27.33	100	36.01	40.43	37.96	38.48	38.04	25.56	25.11	24.72	22.81	29.48	22.37	23.94	22.65
4	PPO Trichoplax sp. H2	13.19	22.88	36.01	100	39.66	40.64	40.17	39.74	27.88	28.32	26.83	27.42	28.76	24.89	25.22	26.55
5	PPO2 Danio Rerio	13.35	24.58	40.43	39.66	100	57.89	52.85	50.74	24.16	25.28	25.11	27.15	31	25.84	23.73	24.72
6	PPO2 Anolis carolinensis	14.91	26.11	37.96	40.64	57.89	100	58.02	57.17	25.28	24.83	26.01	28.73	32.35	24.05	25.5	24.28
7	PPO2 Homo sapiens	14.95	24.09	38.48	40.17	52.85	58.02	100	88.68	24.94	26.06	24.55	25.96	30.86	25.94	27.15	25.5
8	PPO2 Mus musculus	13.71	24.09	38.04	39.74	50.74	57.17	88.68	100	24.94	24.72	25	25.96	31.08	26.39	26.93	25.72
9	PPO2 Oryza sativa japonica	13.82	19.87	25.56	27.88	24.16	25.28	24.94	24.94	100	57.75	57.26	22.3	27.45	26.57	26.85	27.29
10	PPO2 Arabidopsis thaliana	15.25	20.73	25.11	28.32	25.28	24.83	26.06	24.72	57.75	100	66.53	24.12	26.95	27.29	26.57	27
11	PPO2 Nicotiana tabacum	17.7	20.26	24.72	26.83	25.11	26.01	24.55	25	57.26	66.53	100	23.5	26.33	27.94	26.79	27.97
12	PPO Bacillus subtilis	10.66	21.88	22.81	27.42	27.15	28.73	25.96	25.96	22.3	24.12	23.5	100	27.68	27.25	30.33	29.71
13	PPO Myxococcus Xanthus	11.85	19.26	29.48	28.76	31	32.35	30.86	31.08	27.45	26.95	26.33	27.68	100	29.51	29.36	30.04
14	PPO Chlamydamonas reinhardtii	12.89	21.7	22.37	24.89	25.84	24.05	25.94	26.39	26.57	27.29	27.94	27.25	29.51	100	56.32	57.76
15	PPO1 Arabidopsis thaliana	13.84	21.67	23.94	25.22	23.73	25.5	27.15	26.93	26.85	26.57	26.79	30.33	29.36	56.32	100	75.99
16	PPO1 Nicotiana tabacum	14.29	20.35	22.65	26.55	24.72	24.28	25.5	25.72	27.29	27	27.97	29.71	30.04	57.76	75.99	100

LIST OF ABBREVIATIONS

PPO-resistant *Amaranthus tuberculatus* line ..... ACR
5-aminolevulinic acid ..... ALA
Cambridge Crystallographic Data Centre ..... CCDC
Coproporphyrinogen III ..... Copro
Flavin adenine dinucleotide ..... FAD
Glyphosate resistant ..... GR
Hours after treatment ..... HAT
Herbicide resistance action committee ..... HRAC
Mechanism of action ..... MoA
Non-target site resistance ..... NTSR
Post-emergent application ..... POST
Protoporphyrinogen oxidase ..... PPO
Protoporphyrinogen oxidase isoform 1 ..... PPO1
Protoporphyrinogen oxidase isoform 2 ..... PPO2
Gene encoding PPO1 ..... PPX1
Gene encoding PPO2 ..... PPX2
Pre-emergent application ..... PRE
Protoporphyrin IX ..... Proto
Protoporphyrinogen ..... Protogen
Reactive oxygen species ..... ROS
Target site resistance ..... TSR
PPO-sensitive *Amaranthus tuberculatus* line ..... WUS